Protein engineering to capture and kill cancer cells

Gianluca Veggiani

Department of Biochemistry

Merton College

University of Oxford

Trinity 2015

Thesis for a Doctorate of Philosophy

Abstract

The formation of protein assemblies to carry out sophisticated functions is constantly gaining attention in nano-biotechnology. However protein assemblies are often linked through non-covalent interactions, limiting the stability of the complexes and the resilience to forces. Force resistance is crucial for magnetic isolation of circulating tumour cells (CTCs), when a specific protein interaction must withstand the forces pulling a captured cell in the magnetic field. CTCs are present in the blood of cancer patients at very low frequency, making their isolation extremely challenging. However, CTC isolation provides an important approach to enable cancer prognosis and personalised therapy. By optimizing the nanotechnology of the antibody-magnetic bead linkage, the membrane fluidity of the cancer cells, and the affinity of the antibody binding we developed a new approach to minimize the level of tumour markers required to immunomagnetically capture cancer cells. To improve the sensitivity of cancer cell detection even further, a peptide-peptide covalent ligation system was used to generate self-assembled polymers of affibodies (an antibody-like scaffold). Affibody polymers allowed the establishment of multivalent interactions with cell-surface tumour markers, greatly improving the recovery of tumour cells expressing low levels of cancer biomarkers.

However, those polymers had a mixture of lengths and there was no control over polymer sequence. Using orthogonal sequential isopeptide bond formation, we synthesized sequence-controlled proteins chains and used these immuno-assemblies as potent inducers of apoptosis of cancer cells. The approaches presented in this thesis show the importance of generating covalent protein polymers for cell isolation and killing, potentially opening up new directions for cancer biotechnology.

Authorship Declaration

I declare that all work performed in this thesis is my own, with the exceptions noted below. This thesis has not been submitted for any other degree at the University of Oxford or any other institution.

Sections performed by other persons:

Chapter 3:

- Analysis of the effect of cholesterol and methyl-β-cyclodextrin on isolation of BT474 cells, performed by Dr. Jayati Jain.

Chapter 4:

- Assessment by SDS-PAGE of SpyLigase-dependent isopeptide bond formation between KTag and SpyTag.
- Validation via mass spectrometry of the covalent nature of the bond formed between KTag and SpyTag.
- Effect of temperature on SpyLigase reaction.

The listed experiments were all performed by Dr. Jacob Fierer.

Chapter 5:

- Analysis of the SnoopTag-SnoopCatcher reaction features was performed by Mr. Tomohiko Nakamura (visiting scientist from LOC Development Department, R&D Division, Medical Business Unit, Sony Corporation, Japan).

Publications arising from this thesis are detailed below:

- Veggiani G, Nakamura T, Brenner M, Gayet R, Yan J, Robinson C, Howarth M; *Programmable polyproteams built using twin peptide superglues*; Manuscript submitted.

- Fierer JO*, Veggiani G*, Howarth M; *SpyLigase peptide–peptide ligation polymerizes affibodies to enhance magnetic cancer cell capture*; PNAS; E1176–E1181; 2014.

  *authors contributed equally to this work
- Veggiani G, Zakeri B, Howarth M; *Superglue from bacteria: unbreakable bridges for protein nanotechnology;* Trends in Biotech; 32(10): 506-512; 2014.
- Jain J, Veggiani G, Howarth M; *Cholesterol loading and ultrastable protein interactions determine the level of tumor marker required for optimal isolation of cancer cells*; Cancer Res; 73(7):2310–2321; 2013.

Acknowledgements

I would like to thank Professor Mark Howarth for his guidance, patience and for having always pushed me to overtake my limits.

I express my gratitude to my funding bodies, Merton College and MRC, for their exceptional support and having granted me the chance to study at Oxford.

Thanks to the Sherratt lab members for having been always so kind to me. Especially thanks to Kasia Kate, Kasia Z, Rachel, Florence, Pawel, Rogelio and Kuba that have simply been perfect companions during my DPhil. Thanks to Manisha, Carl, Io Nam and Fikret to be always so entertaining and available in improving my days. Thanks to Canna to simply be unconventionally funny.

I greatly appreciated the help and support of my fellow lab members, Mike F, Dejan, Khalil and Raphael. Thanks to Tomo who helped me a lot and taught me a few important Japanese sentences. In particular I want to thank Karl, Can and Sam who always made my days in the lab and in Oxford extremely entertaining and for being, rather than colleagues, awesome friends.

Thanks to Jacob, for having been and keeping being, despite the distance, a good, supportive, funny and amazing friend.

I obviously want to thank Chris and Eric. They simply have been my family in Oxford, they helped me in my troubles, shared with me my joys and constantly pushed me to give my best.

Thanks to Silvia that shared with me another life experience, and always supported me, contributing to make me a better man.

Finally I would like to thank my family that always believed in me and helped me to reach my goals.

Abbreviations

A_{280}	Absorbance at 280 nm
Ab	Antibody
AFM	Atomic force microscopy
APC	Antigen Presenting Cells
BCA	Bicinchoninic acid
BCCP	Biotin Carboxyl Carrier Protein
BirA	Biotin ligase
BiTE	Bi-specific T-cell engager
bp	base pair
BSA	Bovine Serum Albumin
CD	Circular Dichroism
CD3	Cluster of differentiation 3
CD45	Cluster of differentiation 45, common leucocyte marker
CETC	Circulating Epithelial Tumour Cells
CFSE	Carboxyfluorescein succinimidyl ester
CTCs	Circulating Tumour Cells
Da	Dalton
DEP	Dielectrophoresis
DISC	Death-inducing signalling complex
DMEM	Dulbecco's modified Eagle's medium
DMSO	Dimethyl sulfoxide
DR5	Death Receptor 5
DTT	Dithiothreitol
EC_{50}	Half maximal effective concentration

EDTA	Ethylenediaminetetraacetic acid
EGFR	Epidermal Growth Factor Receptor
EMT	Epithelial to mesenchymal transition
EpCAM	Epithelial Cell Adhesion Molecule
Fab	Fragment antigen-binding
FACS	Fluorescence Activated Cell Sorting
Fc	Fragment crystallisable
FCS	Fetal Calf Serum
FDA	Food and Drug Administration
FITC	Fluorescein isothiocyanate
HB	Herringbone
HER2	Human Epidermal Growth Factor Receptor 2
hr	Hour
Hu4D5	Humanized 4D5 antibody
IGF1R	Insuling Growth Factor 1 Receptor
IgG	Immunoglobulin
IPTG	Isopropyl-β-D-thiogalactopyranoside
kb	kilobases
K_d	Equilibrium dissociation constant
kDa	kilodaltons
LB	Luria Bertani broth
mAb	Monoclonal antibody
MBP	Maltose Binding Protein
MHC	Major histocompatibility complex
MMP	Matrix Metalloproteinase

MS	Mass spectrometry
NCL	Native Chemical Ligation
Ni-NTA	Nickel-nitrilotriacetic acid
OD_{600}	Optical density at 600 nm
PAF	Paraformaldehyde
PAFC	Photoacoustic Flow Cytometry
PAGE	Polyacrylamide gel electrophoresis
PCR	Polymerase chain reaction
PDB	Protein Data Bank
PBS	Phosphate buffered saline
PE	Phycoerythrin
PEI	Polyethylenimine
PMSF	Phenylmethylsulfonyl Fluoride
QM/MM	Quantum mechanics/molecular mechanics
SD	Standard deviation
SDS	Sodium dodecyl sulfate
SUMO	Small Ubiquitin-like Modifier
TBS	Tris buffered saline
TMAO	Trimethylamine N-oxide
TRAIL	TNF-related apoptosis-inducing ligand
TRC	T-cell receptor
TRITC	Tetramethylrhodamine
UAA	Unnatural amino acid
Vh	Variable heavy chain
Vl	Variable light chain

Zif268	Zinc finger transcription factor
Z-VAD-FMK	Z-Val-Ala-Asp-fluoromethylketone, pan-caspase inhibitor

Table of contents

Chapter 1 : Introduction

1. Circulating Tumour Cells

Cancer metastasis account approximately for the 90% of cancer-associated mortality (Soerjomataram et al., 2012; Torre et al., 2015; Weigelt et al., 2005; Wittekind and Neid, 2005). Cancer cell dissemination and subsequent formation of secondary tumours at distant organs is a complex multistage process that requires cancerous cells to (i) escape from the primary tumour and intravasate into the circulation, (ii) migrate in the bloodstream, (iii) extravasate and colonize distant tissues (Geiger and Peeper, 2009; Wittekind and Neid, 2005) (Figure 1).

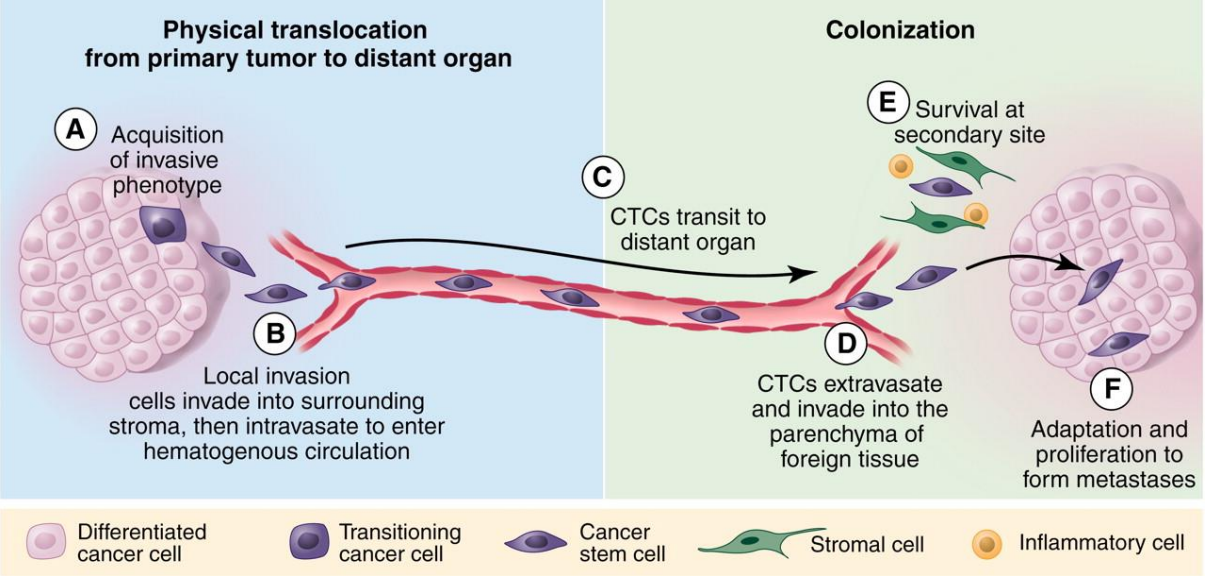

Figure 1. The metastatic cascade. Representation of the metastatic process from Chaffer and Weinberg, 2011, reprinted with permission from AAAS. The cancer metastasis processes can be divided in two major phases: (i) physical translocation of cancer cells from the primary tumour followed by (ii) spread and colonization of secondary sites. To initiate the metastatic cascade a cancer cell has to (A) acquire an invasive phenotype and remodel the tumour microenvironment, (B) invade the surrounding stroma and enter into the bloodstream. Cancer cells that migrate into the circulation (C) (called circulating tumour cells, CTCs) can (D) extravasate at distant organs, where tumour cells need to escape immune surveillance, (E) adapt to the new microenvironment and proliferate to establish secondary tumours.

Studies utilizing *in vivo* video microscopy clearly described the circulation of cancer cells in the bloodstream, as circulating tumour cells (CTCs), as a necessary

phenomenon for the formation of metastasis (Cameron et al., 2000; Naumov et al., 2002).

Despite the existence of CTCs being postulated for the first time in 1869 by Thomas Ashworth, who observed cancer cells in the blood of a man with metastatic cancer (Ashworth T. R., 1869), CTCs are yet poorly understood.

However, since CTCs can be found in the peripheral blood of patients even at the pre-malignant stage (Hüsemann et al., 2008), researchers and clinicians had begun to look at CTCs as a useful real-time “liquid biopsy” for cancer prognosis and therapy tailoring (Hayes et al., 2006; Panchapakesan et al., 2010; Toss et al., 2014). In fact, the amount of CTCs in the bloodstream closely correlates with increased metastatic burden, disease severity, and decreased time to relapse (Aggarwal et al., 2013; Lim et al., 2015; Pantel and Alix-Panabières, 2013).

Studies demonstrated that the concentration of CTCs in the peripheral blood of cancer patients is extremely low, ranging between 1–10 cells per billion of blood cells, representing a critical issue for any analytical system (Hou et al., 2011).

In addition to CTCs low frequency, the absence of well defined CTC molecular signatures and cancer’s intrinsic heterogeneity strongly hampered, so far, the translation of CTC detection systems to the clinic. Although cell-surface epithelial-specific markers are widely use to detect CTCs (Deng et al., 2008; Lacroix, 2006; Pantel et al., 2009), with the epithelial cell adhesion molecule (EpCAM) considered the "gold standard" for CTC detection (Khan et al., 2011; Pantel and Alix-Panabières, 2010; Schulze et al., 2013), numerous studies reported that CTC markers expression may change over time as a consequence of the epithelial-to-mesenchymal transition (EMT) (Barriere et al., 2014; Gorges et al., 2012).

Epithelial-to-mesenchymal transition is a complex reversible cellular program which results in loss of cell-cell adhesion, cell polarity and gain of invasive stem-like phenotype (Thiery et al., 2009; Thompson and Haviv, 2011; Zhang et al., 2013a). During this process epithelial markers commonly used to isolate CTCs can be totally absent, therefore preventing cell isolation (Grover et al., 2014; Kallergi et al., 2011).

However, despite the complexity of CTC detection, CTCs have been isolated from several epithelial tumours, including prostate, bladder, gastric, liver, lung, colon and breast cancer (Aggarwal et al., 2013; Bidard et al., 2013; Hou et al., 2012; Hu et al., 2013; Sun et al., 2011), suggesting the elevated clinical potential of CTC analysis.

1.1 Methods to isolate and detect CTCs

1.1.1 Affinity-based methods

Affinity-based methods rely on the ability of binding the cell-type of interest through the use of antibodies or other binding molecules (e.g. aptamers) specific for cell surface markers. Affinity-based enrichment of CTCs can be performed either via positive or negative selection.

1.1.1.1 Positive selection of CTCs

Positive selection of CTCs exploits binding agents that specifically recognize antigens expressed on the surface of tumour cells. However, the major bias of this approach is represented by the lack of a universal and highly specific CTC marker. The ideal biomarker, in fact, should be expressed at high levels on the surface of CTCs but not on other cell types (e.g. leucocytes, endothelial cells, mesenchymal cells, erythrocytes) and its expression should never change during the circulation of the cells in the bloodstream. Since their lack of expression on normal blood cells

(Pantel and Alix-Panabières, 2013), epithelial markers have been widely used to detect CTCs, but several studies reported that the expression of epithelial antigens on CTCs can be dynamic, posing a serious concern about their efficacy for CTCs isolation (Gires and Stoecklein, 2014).

However, since positive selection of CTCs has the advantage of being easy to perform and extremely specific, ensuring to enrich cells with high purity, this approach is widely use to isolate CTCs.

Some of the main markers used for the positive selection of CTCs are listed below.

1.1.1.1.a Epithelial cell adhesion molecule

The epithelial cell adhesion molecule EpCAM is a glycoprotein involved in the formation of calcium-independent homophilic cell adhesion (Litvinov et al., 1994), as well as in cell signaling, migration, proliferation, and differentiation (Maetzel et al., 2009; Trzpis et al., 2007). Since this glycoprotein is expressed in a broad range of epithelial tissues and carcinoma, EpCAM is the most used marker to isolate CTCs (Man et al., 2011a). However, increasing evidences suggest that CTC heterogeneity (Millner et al., 2013) and transient expression of epithelial marker compositions (Yu et al., 2013) limit the sensitivity of EpCAM-based CTC enrichment, resulting in false negative results. Therefore, the usefulness of EpCAM as CTCs marker is currently being reconsidered (Grover et al., 2014).

Among the methods that isolate CTCs via positive selection, of particular interest is the CellSearch™ system. CellSearch™ (Veridex, Janssen diagnostics) is currently the only CTC detection system approved by the FDA for the detection and analysis of CTCs from patients with breast, prostate and colorectal cancers (Balic et al., 2012). The CellSearch™ system consists of an automated device able to isolate

CTCs from 7.5 mL of blood simply by applying to the sample ferrofluid nanoparticles coated with antibodies against EpCAM. CTCs are magnetically isolated and stained with a cockatail of antibodies for cytokeratins 8, 18 and 19 (markers of epithelial cells) and CD45 (a common marker for white blood cells) to detect contaminant leucocytes. Enriched samples are then analyzed using a semi-automated microscope for CTCs identification and enumeration. Clinical investigations with CellSearch™ showed that a CTCs count equal or greater than 5 cells per 7.5 mL of blood correlates with poor prognosis (de Bono et al., 2008). Although CellSearch™ is characterized by a good sensitivity, with the ability of detecting CTCs in about 70% of patients with metastatic breast cancer (Riethdorf et al., 2007), the main limits of this technology are its dependence on EpCAM expression for CTC isolation and the abundant presence of contaminant leucocytes (~800 leucocytes/CTC) even after CTC enrichment (Sieuwerts et al., 2009).

1.1.1.1.b The human epithelial growth factor receptor 2

The human epithelial growth factor receptor 2 (HER2) is a transmenbrane tyrosine kinase receptor that belongs to the ErbB receptor family involved in cell growth and differentiation (Yarden, 2001). HER2 is overexpressed and/or amplified in about 30% of all breast cancer patients (McCann et al., 1991) and correlates with poor prognosis (Hynes and Stern, 1994). The receptor exist in the plane of the membrane as a monomer and upon ligand binding forms homodimers and heterodimers, resulting in the phosphorylation of its cytoplasmic tyrosine kinase domain, promoting cell proliferation (Yarden, 2001). HER2 has been used as marker for CTC detection in several studies, including in clinical trials to assess the efficacy of cancer therapies for metastatic breast cancer patients (Smerage et al., 2014; Stebbing et al., 2013).

1.1.1.1.c The human epithelial growth factor receptor 1

The human epithelial growth factor receptor 1 (EGFR) is a tyrosine kinase receptor belonging to the ErbB receptor family (Herbst, 2004).

Binding of EGFR to its cognate ligands (e.g. epidermal growth factor, EGF), induces receptor dimerization, leading to the transphosphorylation of the intracellular kinase domain of EGFR and subsequent activation of signalling cascades mainly involved in cell growth, differentiation and migration (Citri and Yarden, 2006). EGFR overexpression and/or mutations are the cause of aberrant signalling pathways responsible for the pathogenesis and progression of different cancer types, including non-small lung cancer (NSLC) (Normanno et al., 2006). EGFR-based CTCs isolation has been used to recover cells from colorectal, breast and gastric cancer (Dragovich and Campen, 2009; Lankiewicz et al., 2008; Payne et al., 2009). Interestingly, CTCs-expressing EGFR have been detected more frequently in patients affected by early stage carcinomas rather than in the blood of metastatic patients (Zieglschmid et al., 2007), thus representing a good target for CTC early detection.

1.1.1.1.d Mesenchymal markers

During the metastatic cascade, tumour cells undergo several phenotypic changes that allow cells to assume more invasive and stem-like properties (Książkiewicz et al., 2012).

Epithelial-to-mesenchymal transition is associated with downregulation of the epithelial antigen expression and upregulation of mesenchymal markers (Zeisberg and Neilson, 2009). As a consequence of this change, isolation of CTCs based on targeting epithelial marker could fail to detect CTCs that have undergone EMT (Gorges et al., 2012; Yu et al., 2013).

Therefore, mesenchymal markers are emerging as a useful target for the identification of CTCs that have undergone EMT (Kallergi et al., 2011; Li et al., 2013). In particular, elevated levels of N-cadherin, a calcium-dependent cell adhesion molecule (Shih and Yamada, 2012), and vimentin, a member of the intermediate filament protein family (Clarke and Allan, 2002), are associated with increased tumour cell invasiveness and poor cancer prognosis (Clarke and Allan, 2002; Zhao et al., 2008), so both these EMT markers are currently being investigated in a clinical trial (NCT02025413).

1.1.1.2 Negative selection of CTCs

Since positive selection of CTCs is biased by the need of knowledge about the expression of CTC cell surface markers, negative selection approaches represent a valuable alternative for CTC isolation.

In negative selection, after lysis of red blood cells, leucocytes are immunomagnetically depleted from the blood using antibodies against CD45 (a common marker of leucocytes). Although this technique surpasses the requirement for specific markers expression on CTCs, it is affected by a low purity of CTC isolation (0.97%), making the molecular analysis of isolated cells more challenging (Liu et al., 2011). Furthermore, since not all CD45-negative cells in the blood are tumour cells (e.g. circulating endothelial cells) (Blann et al., 2005), the negative selection of CTCs could lead to false positive results. Moreover, by exploiting this method it is possible to deplete from the blood CTC-associated macrophages (Lustberg et al., 2014) resulting in false-negative results.

1.1.2 Detection of CTCs based on physical properties

In addition to biochemical features, CTCs differ from normal blood cells in intrinsic physical features, including cell size, deformability and electrical properties (Harouaka et al., 2013).

Isolation of CTCs on the basis of their size difference with normal blood cells represent an attractive strategy that surpasses the limit of affinity-based methods for specific tumour markers.

In fact, since tumour cells are generally larger than hematopoietic cells (≥10-15 μm) (Harouaka et al., 2013), different devices for the antigen-independent enrichment of CTCs have been developed (Hou et al., 2013; Lin et al., 2010; Ntouroupi et al., 2008; Sollier et al., 2014). However, some CTCs can have similar deformability to that of leucocytes and a smaller size than that of white blood cells (Hou et al., 2013; Stott et al., 2010; Zhang et al., 2012a). Also, size-based CTC enrichment methods usually correlate with low purity of isolated cells (1-10%), which can make challenging the molecular analysis of captured CTCs (Harouaka et al., 2013).

Other methods that detect CTCs on the basis of their physical properties are photoacoustic flow cytometry (PAFC) and dielectrophoresis (DEP).

Photoacoustic flow cytometry, based on the detection of laser-induced acoustic waves upon *in vivo* irradiation of specific blood vessels (Galanzha and Zharov, 2012), offers the advantage of performing CTC detection *in vivo*, allowing analyis of larger blood volumes than conventional methods and avoiding sample manipulation (Galanzha and Zharov, 2013).

Dielectrophoresis, the movement of particles in a non-uniform electric field, is highly influenced by specific cell properties such as surface area, size, conductivity

and volume (Pohl and Crane, 1971). Therefore, by modulating the frequency of the electric field applied to a cell sample, it is possible to fractionate different cell types (Pohl and Crane, 1971). By taking advantage of cell electrical properties, ApoCell developed a continuous flow dielectrophoretic device, ApoStream™, for the antibody-independent isolation of cancer cells from blood (Gupta et al., 2012).

1.1.3 Isolation of CTCs with microfluidic devices

Among the methods used for CTCs isolation, microfluidic technologies are recently becoming popular (Gach et al., 2014; Kang et al., 2012; Nagrath et al., 2007; Yoon et al., 2013). Microfluidic devices enable minimal manipulation of complex biological fluids with negligible damage to the cells and high isolation efficiency. The main advantages of microfluidic platforms over batch purification techniques rely on (i) separating cells without blood fractionation, (ii) the high level of standardization, and (iii) the miniaturized size of these platforms.

The Herringbone (HB)-Chip enabled isolation of CTCs by flowing unprocessed blood into a chip containing 8 herringbone channels whose surface was coated with anti-EpCAM antibodies. The HB-Chip isolated CTCs from the blood of patients with prostate and lung cancer with high efficiency (93%), but low purity (14%) (Stott et al., 2010).

Another chip-based technology is exemplified by the CTC-iChip which combines either positive or negative CTC selection and size-based filtration strategies, so maximizing removal of erythrocytes and leucocytes (Ozkumur et al., 2013). More recently, the CTC-Cluster, a microfluidic device for the antibody-independent physical isolation of CTC clusters has been developed (Sarioglu et al., 2015). The significance of CTC clusters has not been fully established, but their

presence in the blood of cancer patients is associated with increased metastatic potential and reduced survival (Yu et al., 2014).

The CTC-Cluster microfluidic device enabled the isolation with high frequency CTC clusters from the blood of patients with melanoma, breast and prostate cancer, paving the route for the physiological understanding of CTC-based clusters (Sarioglu et al., 2015).

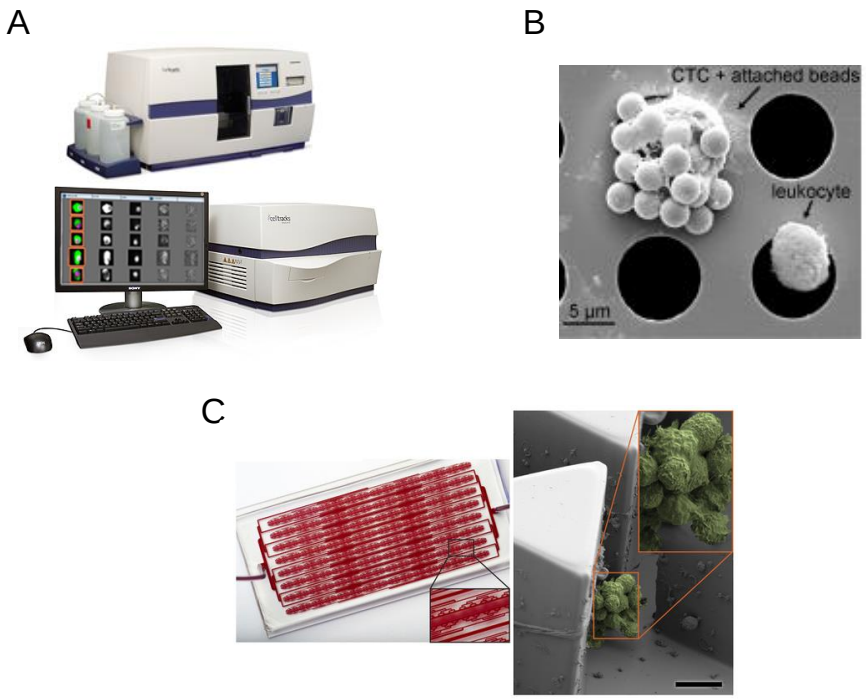

Figure 1.1. CTCs isolation technologies. A) The automated FDA-approaved CellSearch™ system (permission obtained). B) Scanning electron microscopy (SEM) of a CTC isolated by a combination of affinity-based and filtration system (Lee et al., 2013, permission obtained). C) The CTC-Cluster microfluidic device allows the isolation of CTC clusters from unprocessed whole blood (Sarioglu et al., 2015, permission obtained).

1.2 Methods to analyze isolated CTCs

Numerous techniques have been applied to define CTCs at the molecular level. Analysis of the cellular morphology coupled with immunostaining and fluorescence *in situ* hybridization (FISH) is a common strategy (Babayan et al., 2013; Maheswaran et al., 2008; Nagrath et al., 2007). However, conventional microscopic analysis is time-

consuming and cannot be used for the systematic examination of samples in the clinic.

PCR-based methods and microarrays are extremely sensitive, but require minimal contamination of isolated CTCs with leucocytes (Ignatiadis et al., 2008; Yu et al., 2011a).

Isolated viable CTCs can be expanded in cell culture and analyzed *in vitro* by Epithelial Immuno SPOT (EPISPOT) to detect the secretion of specific proteins (Alix-Panabières, 2012). The invasive potential of cell culture-expanded isolated viable CTCs can be determined *in vitro* by the ability of CTCs to digest a fluorescently labelled cell adhesion matrix (Friedlander et al., 2014). However, both the EPISPOT and the invasion assay require the expansion of isolated CTCs in cell culture. Cultured CTCs could undergo biological changes during expansion and significant modification of their molecular features and therefore could be no longer representative of the phenotype of CTCs *in vivo* (Kolostova et al., 2015).

Since every mentioned strategy is characterized by advantages and drawbacks, a combination of different analytical techniques could encompass CTCs heterogeneity, potentially unraveling CTC biology.

1.3 Bio-nanotechnology for CTC isolation

The ability to selectively isolate viable CTCs from whole blood with minimal perturbation of their phenotype is emerging as an important requirement for understanding CTC biology (Li et al., 2015; Sarioglu et al., 2015). Up till now the majority of the efforts to develop CTC isolation methods has been addressed to improve capture performance and specificity, without focusing on preserving the CTC fitness.

Bio-nanomaterials represent a promising tool for improved capture efficiency, purity, throughput and retrieval of viable CTCs with minimal cellular perturbation, but their development is still in its infancy.

Cancer cells and epithelial cells are characterized by unique adhesion preferences for nanostructured surfaces (Chen et al., 2012). On the contrary, the majority of blood cells, including leucocytes and erythrocytes, are non-adhesive (Chen et al., 2012). Therefore, by specifically tuning the topography of surfaces used to capture CTCs, it is possible to improve the specificity and efficiency of CTC isolation with minimal effect on their phenotype (Chen et al., 2013). Among these nanostructured surfaces, nanopillars/nanowires (Hong et al., 2014; Wang et al., 2014), nanofibers (Zhao et al., 2013), nanoroughened surfaces (Chen et al., 2013) and nanocomposite materials (Yoon et al., 2013) have been extensively investigated.

Nanostructured surfaces are useful to support cell adhesion (Smith et al., 2009), but to control the interaction between the cells and nanotopographic materials, the use of protein engineering approaches to precisely tailor the scaffold properties are highly desirable.

Adhesive properties of CTCs for patterned surfaces has been used for their capture, but tailoring nanostructures with binding agents through engineered interactions enhanced capture efficiency (Lu et al., 2015a; Xie et al., 2014).

Another example of combining protein engineering and nanotechnology to capture of CTCs is provided by the work of Maeda and colleagues (Maeda et al., 2009). Maeda et al. developed nano-sized bacterial magnetic particles tailored with both biotin carboxyl carrier protein (BCCP) to enable *in vivo* biotinylation for nanoparticles decoration via streptavidin-coated quantum dots and protein G to precisely immobilize anti-EpCAM antibodies. The obtained nanocomposite enabled

the simultaneous isolation and labelling of lung cancer cell lines with high efficiency and specificity.

2. Peptide tags and protein engineering

Peptide tags are useful tools to precisely control and modify protein function. Since peptides are characterized by a small size, peptide tags can be easily inserted into the protein of interest with minimal disruptive potential, representing a useful tool for biotechnology (Huh et al., 2003; Terpe, 2003). However, the small surface area of peptides and their general lack of structural order strongly affect their interaction with protein partners, resulting in the generation of weak and reversible bonds (London et al., 2010).

The “slippery” nature of the peptide-protein interaction hampers the use of peptide tags especially in applications where the peptide-protein linkage must last for a long time, survive harsh conditions or withstand physical forces (e.g. magnetism) (Chivers et al., 2010; Jain et al., 2013; McCloskey et al., 2003a). Nonetheless, since peptides can be easily fused to proteins via established molecular biology techniques, allowing the introduction into the protein of interest of a highly diverse set of functionalities, peptides are widely used by protein engineers.

2.1 Peptide tags forming non covalent interactions with their partners

Epitope tags (e.g. HA, myc, FLAG tags) rely on the specific binding of antibodies to their cognate peptides and are widely used for protein purification and detection (Brizzard and Chubet, 2001).

By exploiting the interaction between the imidazole ring in the Histidine side chain and bivalent nickel or cobalt ions, the polyhistidine-tag (ranging from 2 to 10

consecutive Histidine residues, most commonly 6, was develop for routine protein purification and detection (Hengen, 1995; Zhao et al., 2010).

S*trep*-tag II is an eight residues long peptide tag able to bind to core streptavidin (a truncated version of streptavidin) (Pähler et al., 1987) and to *Strep*-Tactin (an engineered streptavidin variant) (Voss and Skerra, 1997) with a dissociation constant around 1 µM (Voss and Skerra, 1997). *Strep*-tag II reversibly binds to the same binding pocket as streptavidin's natural ligand, biotin, enabling dissociation of the peptide tag by competition with D-biotin (Schmidt and Skerra, 2007).

Another peptide tag based on the biotin/streptavidin interaction is the AviTag, a 15 amino acid peptide that can be fused to proteins of interest for the enzymatic and site-specific *in vivo* and *in vitro* biotinylation, mediated by the *E. coli* biotin ligase BirA, allowing subsequent streptavidin or avidin labelling (Beckett et al., 1999; Chen et al., 2005).

Proteolytic digestion of the bovine RNase A with subtilisin, a serine protease from *Bacillus subtilis* (Siezen and Leunissen, 1997), and subsequent optimization of the obtained fragments enabled the generation of a peptide tag named S-Tag that can bind to its protein partner (S-protein) with pH-tunable affinity ($K_d \geq 10^{-9}$ M) (Kim and Raines, 1993).

2.2 Peptide tags for covalent protein-protein ligation

Biotechnology is often limited by weak reversible interactions. Therefore, to enlarge the range of applications of engineered proteins, highly specific and covalent interactions are desirable. The main covalent bioconjugation methods and their applications are discussed below.

2.2.a Native chemical ligation

Native chemical ligation (NCL) allows the chemo-selective conjugation of two unprotected polypeptides (Dawson and Kent, 2000). The bioconjugation reaction is extremely specific and involves the formation of an amide bond between a C-terminal α-thioester group and a N-terminal Cysteine, with internal Cysteine residues unable to hinder the reaction (Lu et al., 1996).

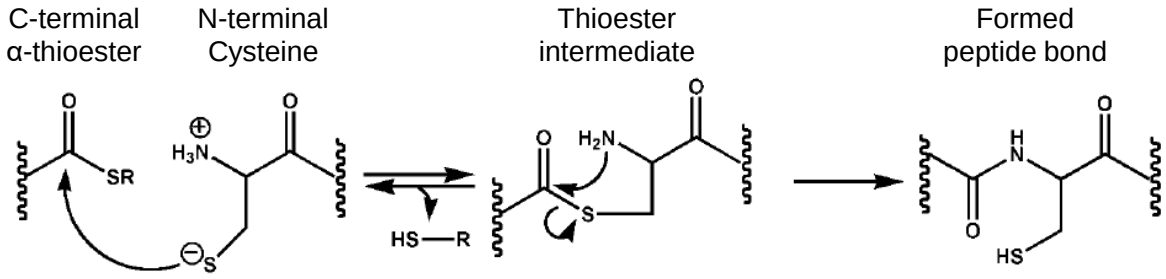

Figure 1.2. Native chemical ligation reaction mechanism. The thiol group of an N-terminal Cysteine residue attacks the carbonyl group of a C-terminal α-thioester polypeptide, forming a thioester intermediate. The thioester intermediate spontaneously rearranges by an intramolecular S-N acyl shift, resulting in the formation of a peptide bond.

Since the reaction occurs under mild conditions and is traceless, only leaving a Cysteine residue at the ligation site, NCL has been used for protein cyclization (Berrade and Camarero, 2009), labelling (Busch et al., 2008) and to fully synthesize proteins by joining together peptides produced by solid phase synthesis (Dawson et al., 1994). However, NCL is affected by the need to avoid Isoleucine, Valine or Proline residues at the C-terminus of the polypeptide carrying the α-thioester group (Hackeng et al., 1999), the need of reducing agents in the reaction mixture and the presence of the reactive groups at specific protein termini.

2.2.b Split inteins

Inteins are non-coding protein segments inserted into protein precursor that undergo self-excision during post-translational maturation of the host protein (Mills et al., 2014). During protein splicing, inteins are excised and the remaining flanking

ends (N- and C-exteins) are joined together by a peptide bond. The auto-catalytic excision of inteins does not require any cofactor, but it is dependent on the correct folding of these non-coding protein segments (Saleh and Perler, 2006).

The splicing mechanism is initiated by an N-S acyl shift of a nucleophile residue of the N-extein (Cysteine, Serine or Threonine), resulting in the formation of a thioester intermediate, followed by a nucleophilic attack at the C-extein to obtain a branched thioester intermediate. Cyclization of an Asparagine at the C-terminus of the intein enables the release of the intein from the host protein, linking the exteins via a thioester bond, converted to a peptide bond after S-N acyl shift (Figure 1.3) (Saleh and Perler, 2006). Naturally occurring split inteins have been exploited to link together polypeptide chains, but their cross-reactivity restricted their application in multi-fragment ligation (Dassa et al., 2007). Although engineered split inteins circumvented this limit, enlarging the number of splicing pairs, this technology is still characterized by some issues. The inteins splicing reaction is based on the formation of thioester intermediates, a reactive species that can react with several nucleophilic groups on proteins, potentially leading to unwanted side products (Siebold and Erni, 2002). Moreover, since the splicing reaction could be dependent on the presence of catalytically important Cysteine residues, the redox status of the environment is important (but not for Ser/Thr-dependent inteins). Furthermore, inteins must be located at the termini of proteins, limiting their application in the generation of non-linear protein conjugates (Lockless and Muir, 2009).

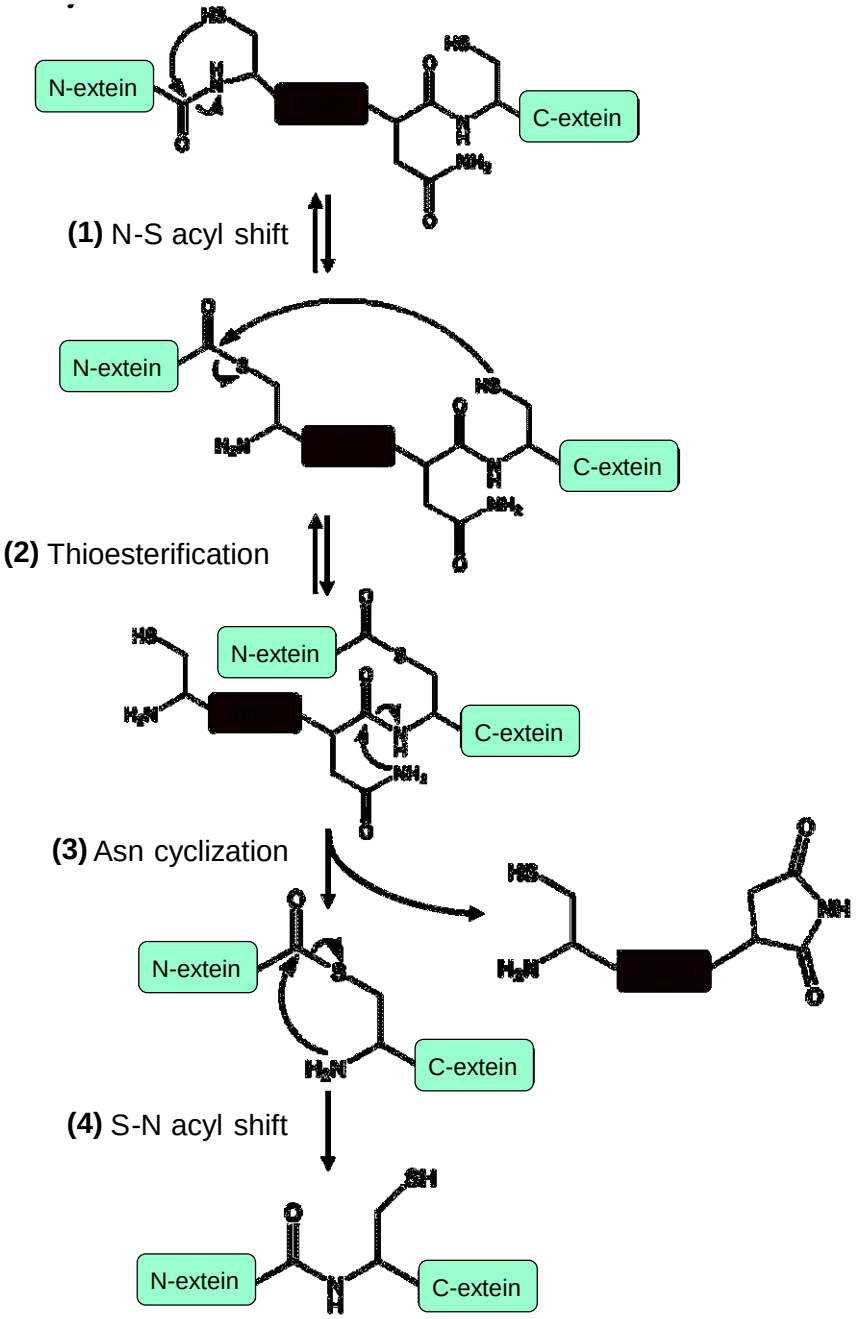

Figure 1.3. Inteins-mediated protein splicing. A thioester intermediate is obtained by N-S acyl shift of the N-extein (1), followed by a nucleophilic attack of the C-extein to the N-terminal thioester, obtaining a branched intermediate (2). Subsequent Asparagine cyclization releases the intein (3), promoting the formation of an amide bond between the two extein fragments via S-N acyl shift.

2.2.c Unnatural amino acids

Unnatural amino acids (UAAs) enabled the expansion of the genetic code and the incorporation of unique chemical functionalities into target biomolecules (Wang et al., 2001). For incorporation of unnatural amino acids an orthogonal aminoacyl-tRNA-synthetase engineered to accept only the desired tRNA and a unique codon that designates the unnatural amino acid are required (Wang et al., 2001). Since this method allows the introduction of minimally obtrusive, orthogonally reactive groups, unnatural amino acids have been exploited for several applications, including covalent protein bioconjugation (Hancock et al., 2010), antibody and enzyme engineering (Kim et al., 2012; Ravikumar et al., 2015) and *in vivo* protein imaging (Prescher and Bertozzi, 2005) (Figure 1.4).

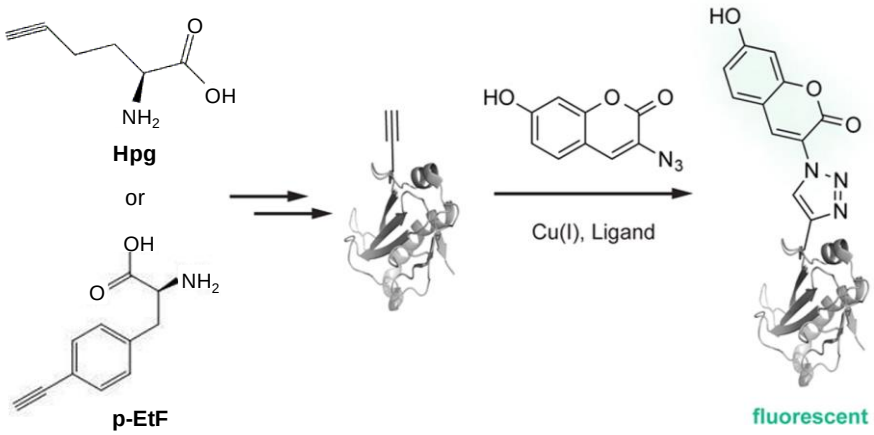

Figure 1.4. Unnatural amino acids used for azide-alkyne cycloaddition. L-homopropargylglycine (Hpg) and p-ethynylphenylalanine (p-EtF) are usually incorporated into proteins as Methionine and Phenyalanine analogs respectively. Alkyne-bearing unnatural amino acids and azide-functionalized ligands combine to form an aromatic triazole linkage (Adapted from Lang and Chin, 2014, permission obtained).

However, the use of unnatural amino acids is far from perfect: incorporation of multiple UAAs per protein is complex and leads to limited protein yields due to reduced protein stability and/or inefficient translation, limiting the ubiquitous application of this technology (Brustad and Arnold, 2011).

2.2.d Covalent interactions between proteins/peptides and small molecules

Another approach to exploit covalent interactions for biotechnology is represented by the combination of genetically encoded polypeptides with the vast functional diversity offered by synthetic chemistry.

Fluorescein Arsenical Helix Binder (FlAsH), is a small domain containing the tetracysteine CCXXCC motif able to form a covalent bond with the biarsenical labeling reagents FlAsH-EDT2 and ReAsH-EDT2 (Griffin et al., 1998) (Figure 1.5).

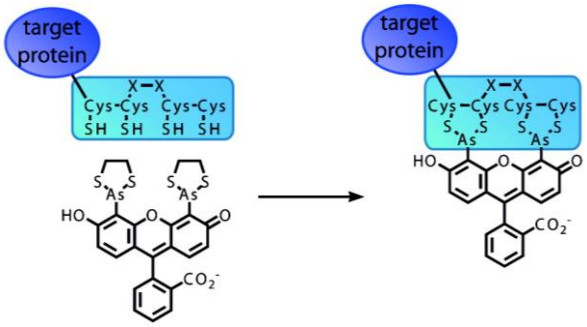

Figure 1.5. Representation of the FlAsH tag technology. FlAsH tag contains a tetracysteine core able to form a covalent bond with biarsenical ligands (Jing and Cornish, 2011, permission obtained).

This approach takes advantage of the affinity of proteins containing closely spaced pairs of Cysteine residues for organoarsenicals (Kalef and Gitler, 1994). Since the FlAsH-EDT2 and ReAsH-EDT2 reagents are membrane-permeable and increase in fluorescence upon binding with proteins containing the CCXXCC motif, the FlAsH tag has been used for live cell imaging (Griffin et al., 1998), but it also found application in protein purification (Thorn et al., 2000). This method requires only the fusion of a small peptide to the protein of interest and to use biarsenical reagents, but the FlAsH system is redox sensitive and it is promiscuous as FlAsH-EDT2 can bind to endogenous Cysteine-rich proteins (Stroffekova et al., 2001).

SNAP-tag is an engineered O^6-alkylguanine-DNA-alkyltransferase (hAGT) that specifically forms a covalent bond with O^6-benzylguanine derivatives (Gautier et al.,

2008). Although SNAP-tag is widely used for imaging purposes as well as for generating antibody-based diagnostic tools (Hussain et al., 2013), the large size of the tag (~20 kDa) could disrupt the folding of the fusion partner.

Another protein tagging system that allows covalent conjugation with small molecules is represented by the HaloTag. HaloTag is an optimized mutant of a *Rhodococcus* haloalkane dehalogenase able to form a covalent bond with alkyl-halide derivates (Los et al., 2008) (Figure 1.5).

Although HaloTag has been used for cell imaging (Los et al., 2008) as well as for protein purification and studying protein-protein interactions (Daniels, D. L. et al., 2014), the large size of the tag (~33 kDa) represents a limitation of this technology.

2.2.e Isopeptide bond-based covalent bioconjugation

Another method to irreversibly lock together proteins and peptide is provided by isopeptide bonds. An isopeptide bond is an amide bond formed off the main protein chain, connecting a side chain to a side chain or a side chain to the protein's backbone. Isopeptide bond formation can be catalyzed by enzymes such as transglutaminases (Zemskov et al., 2012), ubiquitin ligases (Martin and Raines, 2010), sortases (Spirig et al., 2011) or can occur autocatalytically as first observed in the in the bacteriophage HK97 (Wikoff et al., 2000).

2.2.e.1 Enzyme-catalyzed isopeptide bonds

Transglutaminases (TGases) are a class of enzymes that catalyze the formation of an isopeptide bond between the ε-amine of a Lysine residue and the γ-carbonyl amide group of a Glutamine residue (Griffin et al., 2002). TGases promote the formation of cross-linked protein polymers important for the homeostasis of the epidermis, blood clotting and wound healing (Lorand and Graham, 2003).

Transglutaminases have been used for covalent protein bioconjugation, and for the preparation of antibody-drug conjugates (Dennler et al., 2014). As isopeptide bond formation occurs under mild conditions and without the need of cofactors, transglutaminases are desirable enzymes for covalently link proteins, but they are characterized by limited specificity, reducing their application in biotechnology (Griffin et al., 2002).

Sortases are transpeptidases found in Gram-positive bacteria that catalyze the covalent anchoring of surface proteins to the cell wall and to other proteins (Marraffini et al., 2006). Sortases cleave the peptide bond between a Threonine and a Glycine residues of a target motif (LPXTG in the case of Sortase A from *Staphylococcus aureus*) via nucleophilic attack by a catalytic Cysteine residue, forming an acyl–enzyme intermediate (Figure 1.6) (Ritzefeld, 2014). A second nucleophilic attack is subsequently performed by the α-amino group of a penta-Glycine peptide on the thioester intermediate, thus completing the transpeptidation reaction (Figure 1.6) (Ritzefeld, 2014).

Since Sortase-medated site-specific conjugation is easy and requires only the modification of the target polypeptides with the LPXTG and the oligo-Glycine penta-peptides, Sortases have been highly exploited for protein conjugation and circularization (Popp et al., 2007, 2011), as well as for cell surface labelling (Swee et al., 2015). However Sortase A-mediated protein modification has some flaws: the reaction requires millimolar concentration of Ca^{2+} (Popp et al., 2007) limiting the use of this enzyme *in vivo*. Other disadvantages are the reversibility of the acyl–enzyme intermediate which prevents the reaction from reaching completion (Ling et al., 2012), and the need for the LPXTG and the oligo-Glycine penta-peptides to be at

specific locations in the proteins of interest (Popp et al., 2007; Williamson et al., 2012, 2014).

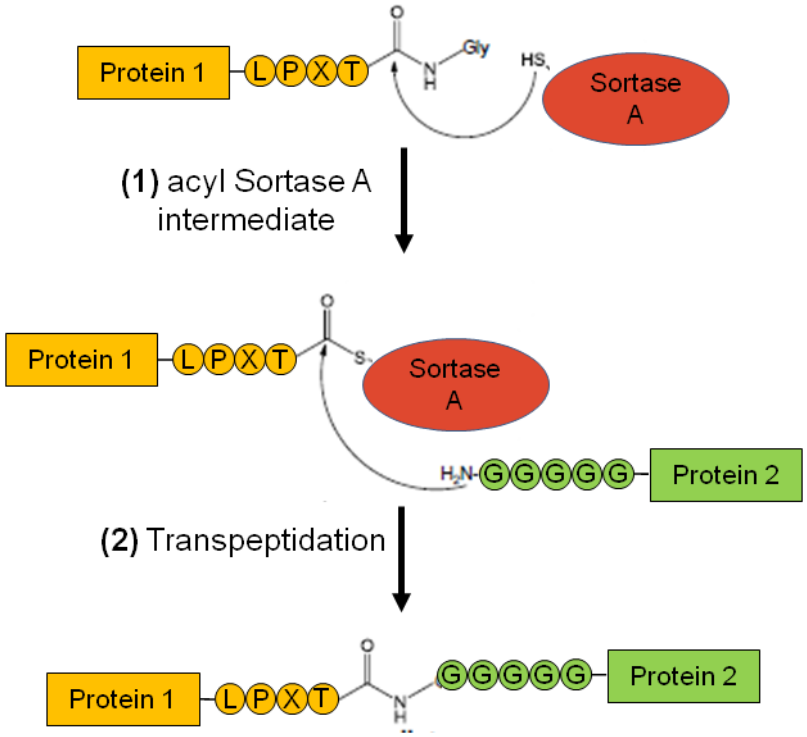

Figure 1.6. Sortase A-mediated ligation mechanism. The sulfhydryl group of the catalytic Cysteine residue of Sortase A performs a nucleophilic attack on the Threonine-Glycine amide bond of the LPXTG recognition sequence, forming a tetrahedral intermediate that is then converted to acyl-enzyme intermediate (1). The Sortase A transpeptidation reaction is completed by the nucleophilic attack of the amino group of a Glycine on the thioester of the acyl-enzyme intermediate (2). The schematic representation of the reaction was adapted from Tsukiji and Nagamune, 2009 (permission obtained).

2.2.e.2 Site-specific protein conjugation via spontaneously occurring isopeptide bonds

Analysis of the crystal structure of the major pilin protein of *Streptococcus pyogenes*, Spy0128, revealed the presence of two self-catalyzed intramolecular isopeptide bonds cross-linking a Lysine side chain to an Asparagine side chain (Figure 1.7) (Kang et al., 2007).

Further crystallographic and sequence comparison analysis identified similar isopeptide bonds in other cell surface proteins of Gram-positive bacteria

characterized by a CnaA or a CnaB domain (Budzik et al., 2008; Krishnan et al., 2007; Nelson et al., 2007), suggesting that intramolecular isopeptide bonds are formed in specific protein folds (Symersky et al., 1997). The folding of the domain containing the isopeptide bond is important as the Lys-Asn/Asp-Glu/Asp reactive residues need to be in optimal proximity, surrounded by an hydrophobic environment involved in protonation of the reactive Glutamate/Aspartate and deprotonation of the reactive Lysine, favouring the autocatalytic amide bond formation (Kang et al., 2007).

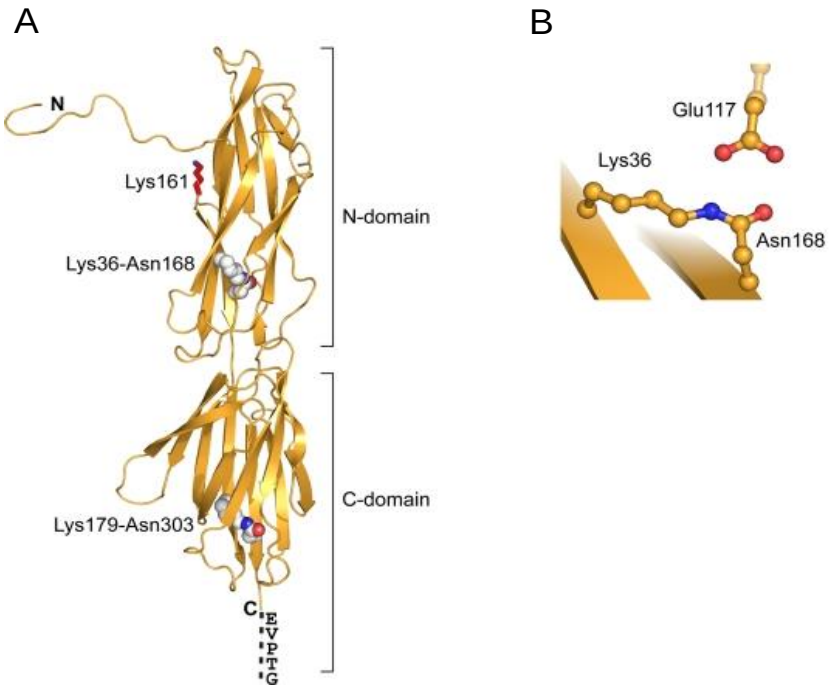

Figure 1.7. Spy0128 contains two intramolecular isopeptide bonds. A) Cartoon of Spy0128 domains. Residues forming the isopeptide bond are shown as spheres, the Lysine residue involved in the intersubunit linkage of pilus proteins is shown in stick mode red-coloured. The Sortase target motif EVPTG is represented as a dotted line at the end of Spy0128 C-terminal domain. B) Structure of the isopeptide bond of Spy0128 N-terminal domain. The figure was adapted from Kang and Baker, 2009 (permission obtained).

Quantum mechanics/molecular mechanics (QM/MM) simulations suggest the first step is direct nucleophilic attack of the Lysine ε-amino group on the Asparagine/Aspartate γ-carbonyl forming a tetrahedral intermediate.

The second reaction steps involves two concerted proton transfers, mediated by the catalytic Glutamate acting as proton shuttle, to release one ammonia or water molecule (Figure 1.8) (Kang and Baker, 2011).

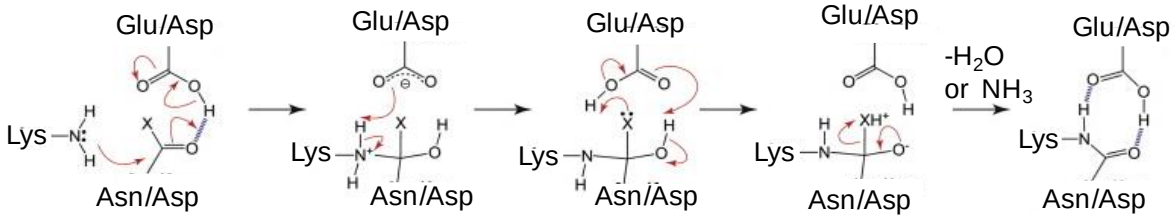

Figure 1.8. Proposed isopeptide bond formation reaction mechanism. Inverse protonation of the reactive Glutamate/Aspartate facilitates Lysine's nucleophilic attack on Asparagine/Aspartate carbonyl group, leading to the formation of a tetrahedral intermediate. A second nucleophilic attack results in release of water or ammonia and formation of the amide bond. The figure was adapted from Kang and Baker, 2011 (permission obtained).

Isopeptide bonds confer resilience to extreme chemical (pH 2), thermal (100°C) and mechanical stress (800 pN), as well as to proteolysis (Kang and Baker, 2011), so isopeptide bond-containing proteins provide new opportunities for biotechnology.

Splitting proteins into inactive fragments that can reassemble and regain function has been widely used to study protein-protein interactions (Shekhawat and Ghosh, 2011). Splitting isopeptide bond containing proteins has the potential to provide a chemoselective covalent bioconjugation system.

The Spy0128 protein is composed of two domains containing two spontaneously occurring intramolecular isopeptide bonds (Kang et al., 2007). By splitting the N-terminal and C-terminal domains of Spy0128, Zakeri et al. obtained two peptide-protein pairs able to form, simply upon mixing, an isopeptide bond (Zakeri and Howarth, 2010). Splitting the N-terminal domain of Spy0128 enabled the generation of the peptide tag isopeptag-N, containing the reactive Lysine, and its protein partner pilin-N bearing the reactive Asparagine and Glutamate (Zakeri and Howarth, 2010). Analogously, the C-terminal domain of Spy0128 was engineered to

develop the isopeptag/pilin-C peptide-protein pair (Figure 1.9) (Zakeri and Howarth, 2010).

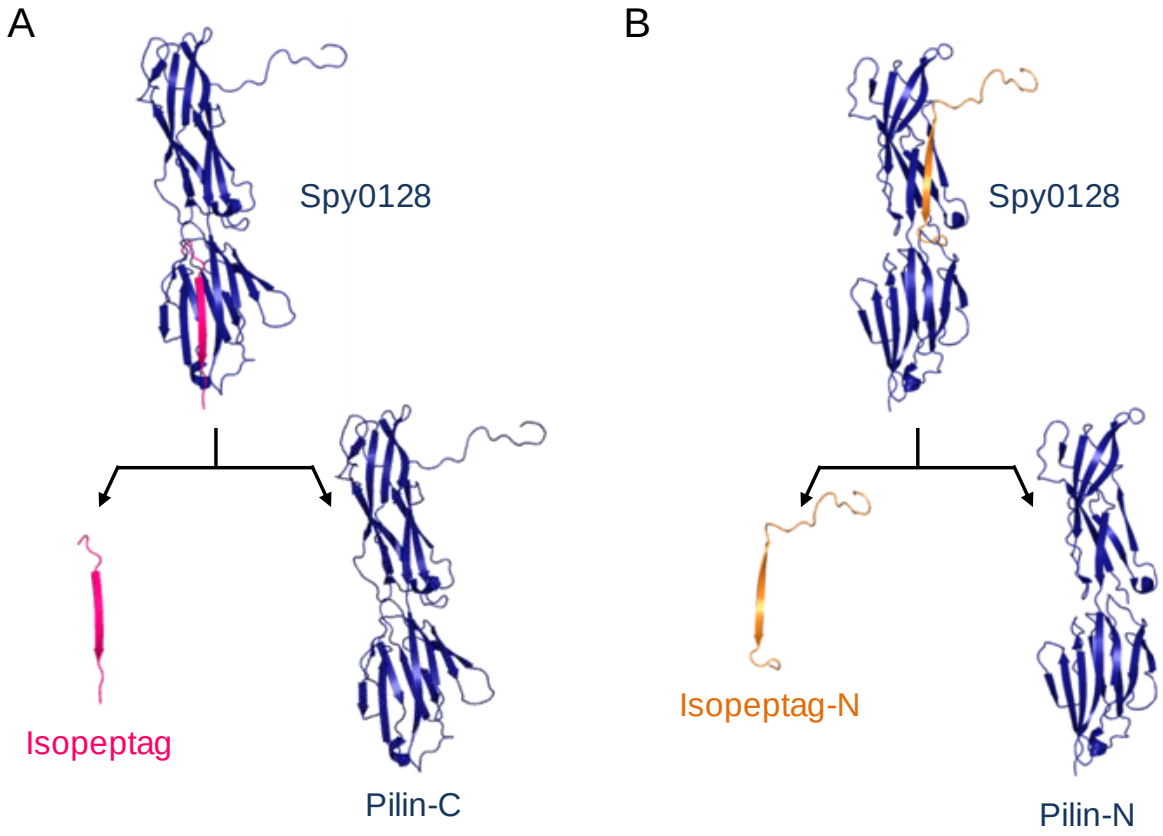

Figure 1.9. Cartoon of isopeptag/Pilin-C and isopeptag-N/Pilin-N construction. A) The C-terminal domain of the pilin Spy0128 (PDB 3B2M) was dissected, obtaining the protein domain Pilin-C and its complementary peptide tag Isopeptag. B) Similarly, by splitting the N-terminal domain of Spy0128 (PDB 3B2M), Pilin-N and Isopeptag-N were generated.

Both the systems enabled site-specific protein conjugation via isopeptide bond formation *in vitro* under a broad range of conditions, with the isopeptag/pilin-C pair able to irreversibly lock together proteins even *in vivo* (Zakeri and Howarth, 2010). Although these ligation systems provided an interesting tool for bioconjugation, the slow reaction rate, the inability to reach reaction completion and the large size of the protein domains (~35 kDa) are major limits of this technology.

Therefore, to generate a new peptide tag-protein pair with improved features, Zakeri and colleagues split and engineered another isopepite bond-containing protein domain (Zakeri et al., 2012).

The immunoglobulin-like collagen adhesion domain (CnaB2) of the fibronectin-binding protein FbaB from *Streptococcus pyogenes* contains an intramolecular isopeptide bond between Lysine 31 and Asparagine 117 (Amelung et al., 2011). The CnaB2 domain was split and engineeried into a 13 residue long peptide tag, named SpyTag, and the complementary protein domain SpyCatcher (Figure 1.10) (Zakeri et al., 2012).

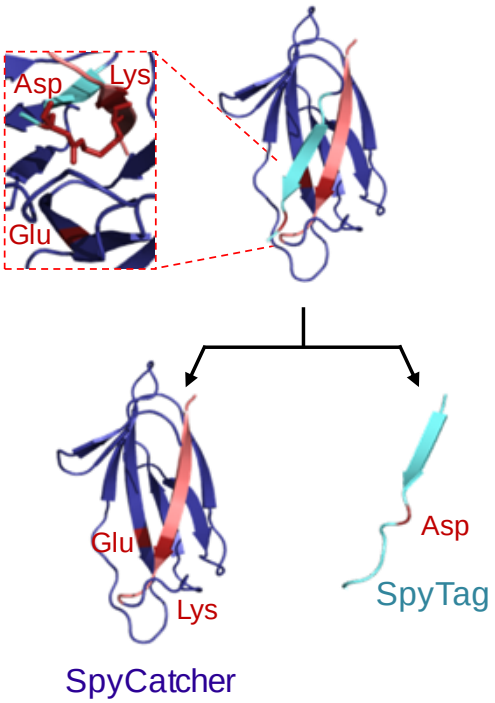

Figure 1.10. Generation of SpyTag and SpyCatcher. The CnaB2 domain (PDB 2X5P) was dissected into a protein domain (SpyCatcher) and a peptide tag (SpyTag). Residues involved in the isopeptide bond formation are coloured in red. Inset shows the isopeptide bond's structure.

SpyTag-SpyCatcher spontaneously form an isopeptide bond upon mixing with a rate constant of 1.4 x 10^3 $M^{-1}s^{-1}$ (Zakeri et al., 2012). The SpyTag-SpyCatcher reaction occurs under a broad range of temperatures, pH values, buffers and even in presence of non-ionic detergents. Moreover, as neither SpyTag nor SpyCatcher contain Cysteine residues, this system is independent from the redox status of the environment (Zakeri et al., 2012). SpyTag is a short peptide and enables the formation of the isopeptide bond when fused at the N-terminus, C-terminus and even internally to the target protein (Zakeri et al., 2012). SpyTag-SpyCatcher have been used for various applications in bio-nanotechnology,

including enzyme cyclization (Schoene et al., 2014), generation of hydrogels for stem cell culture (Sun et al., 2014), vaccine development (Liu et al., 2014) and biofilm engineering (Nguyen et al., 2014).

3. Thesis objectives

The main goals of this thesis were the development of new biochemical approaches enabling the immunomagnetic isolation of cancer cells and the assembly of controlled protein conjugates for cancer cell killing.

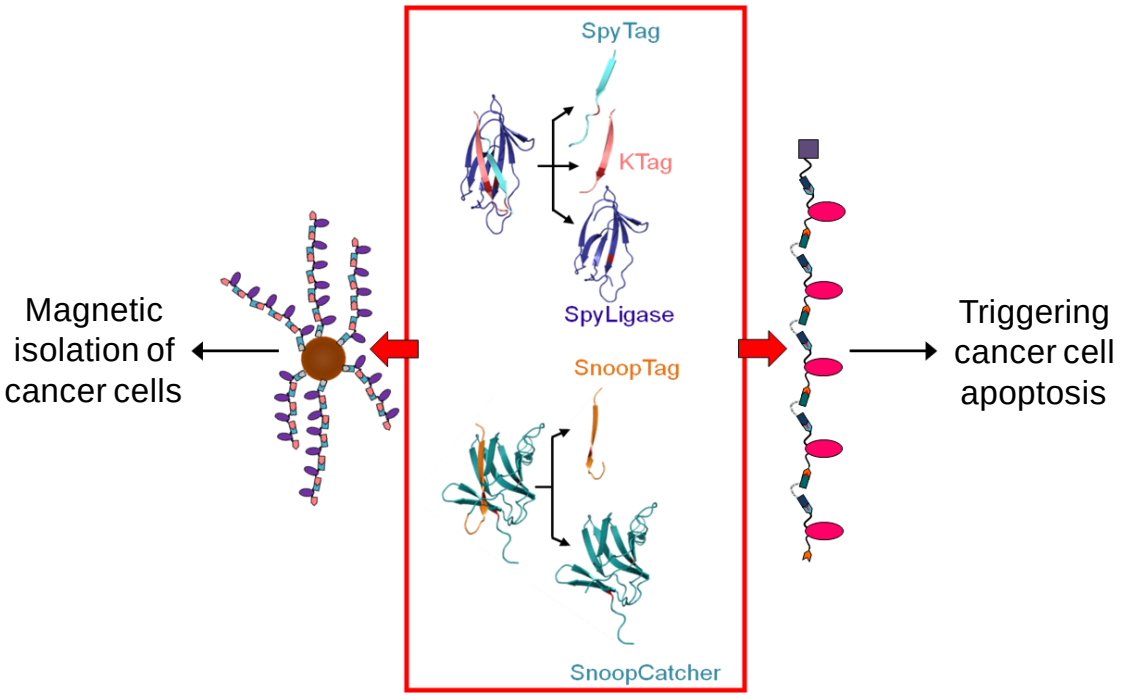

Figure 1.11. Schematic representation of the thesis objectives. Engineering of protein domains containing intramolecular isopeptide bonds allowed the development of orthogonal protein domain-peptide tag pairs to control protein polymerization. Affibody polymers obtained using SpyLigase have been applied to increase the isolation efficiency of tumour cells. Polymerization of affibody and nanobodies via specific and sequential formation of amide bonds enabled the development of precisely controlled multimeric chains to induce cancer cell apoptosis.

Through the analysis of (i) the expression levels of the target antigen, (ii) the strength of the antibody-antigen interaction, (iii) the nature of the antibody-magnetic

bead connection and (iv) the properties of the cell membrane, I intended to identify the molecular requirements to enhance capture cancer cells capture.

To further improve the isolation of tumour cells, I investigated the effect of multivalent interactions by using self-assembled affibody polymers created through a peptide-peptide covalent ligation system.

With the aim of generating controlled protein polymers, a new peptide tag-protein pair able to form an isopeptide bond was developed. I investigated the biochemical features of the SnoopTag-SnoopCatcher reaction and exploited this conjugation system, in combination with SpyTag-SpyCatcher, to synthesize with molecular precision protein polymers. I aimed to use the synthesized assemblies to precisely coordinate the clustering of cell surface receptors for potent apoptosis induction of cancer cells.

Chapter 2 : Methods

2.1 Cloning

All PCR and site-directed mutagenesis reactions were performed using KOD Hot Start DNA Polymerase (Roche) in a C1000™ Thermal Cycler (Bio-Rad). Constructs were all transformed into chemically competent *E. coli* DH5α (Life Technologies). All DNA primers were ordered from Life Technologies. All mutations and constructs were verified by sequencing

2.1.1 Insert amplification and ligation

A typical amplification reaction contained 1x KOD Hot Start DNA Polymerase buffer, 1.5 mM $MgSO_4$, 0.4 mM dNTPs, 3% DMSO (v/v) (Sigma), 0.4 µM forward and reverse primers, 20 ng DNA template, 0.02 U/µL of KOD Hot Start DNA polymerase (Novagen), and MilliQ water to a total volume of 50 µL. Typical cycling conditions were: initial denaturation step for 5 min at 95°C, 25 cycles of denaturation for 30 s at 95°C, annealing for 30 s at 55°C, elongation at 68°C for 40 s, followed by a final elongation step at 68°C for 5 min, before samples cooling to 10°C. Annealing temperature was optimized case by case, whereas the length of the elongation step generally was 1.5 kb/min.

PCR products were analyzed by loading 5 µL of the amplified reaction on an agarose gel (0.7-2% w/v, depending on the size of the DNA fragment) containing 0.01% (v/v) ethidium bromide (Sigma), and running the samples for 45 min at 130 V. Gels were imaged using the Gel Imager Universal Hood II (Bio-Rad) and analyzed with Image Lab Software 3.0 (Bio-Rad).

Vector and PCR product digestion was performed using the appropriate restriction enzymes (New England Biolabs) according to the manufacturer's

instructions. Digested vectors and inserts were purified by agarose gel extraction using the QIAquick Gel Extraction Kit (Qiagen).

Typical ligation reactions were performed at a 5:1 vector-to-insert ratio in 1x T4 DNA Ligase buffer (NEB), 20 U/µL T4 DNA Ligase (NEB), MilliQ water to a final volume of 20 µL. Reactions were incubated at 25°C for 1 h prior to transformation into chemically competent *E. coli* DH5α.

2.1.2 Inverse PCR, SLIM and QuickChange

Inverse PCR (Kaluz et al., 1999), QuickChange (Stratagene) and Site-directed ligase-indipendent mutagenesis (Chiu et al., 2004) reactions were typically assembled by combining 1x KOD Hot Start DNA Polymerase buffer, 2.5 mM $MgSO_4$, 0.4 mM dNTPs, 3% DMSO (v/v) (Sigma), 0.4 µM forward and reverse primers, 20 ng DNA template, 0.02 U/µL of KOD Hot Start DNA polymerase (Novagen), and MilliQ water to a total volume of 25 µL. For SLIM PCR, four DNA primers at 0.4 µM were used. Cycling conditions were: initial denaturation step for 5 min at 95°C, 25 cycles of denaturation for 30 s at 95°C, annealing for 30 s at 55°C, elongation at 68°C for 4 min, followed by sample cooling at 10°C. Annealing temperatures and elongation times were optimized case by case. PCR products were analyzed by agarose gel and methylated DNA template was digested by incubating the reaction mixtures with 1 µL DpnI (NEB) at 37°C for 2 h. For inverse PCR, after DpnI digestion, samples were purified using the GeneJET™ Plasmid Miniprep Kit (Fisher) and ligation was performed by incubating 10 µL of the PCR product at 25°C for 1 h with 1x T4 DNA Ligase buffer (NEB), 20 U/µL T4 DNA Ligase (NEB), 10 U/µL T4 polynucleotide kinase (NEB) and MilliQ water to a final volume of 20 µL. Reactions were transformed into chemically competent *E. coli* DH5α.

2.1.3 Cloning of affibodies

pET28a-KTag-AffiHER2-SpyTag (N-terminal KTag-spacer-Affibody against HER2- His_6-SpyTag), based on $Z_{HER2:342}$ (Orlova et al., 2006) was cloned by inverse PCR with 5'-GGGTAAAAGAGCTATCTCCCAGTAAGCGTTCCTCATTTCTTTGTTGAATTTGTTGTCCACGCC and 5'-AACTTAAACAATCAACAGAAAAGGGCTTTCATAAGGTCGTTATACGATGACCCAAGCCAAAGCGCTACC, using as template pET28a-KTag-AffiEGFR-SpyTag (cloned by Dr. Jacob Fierer, Howarth laboratory). To reduce immunoglobulin binding of the affibody scaffold, the N23T S33K mutations were introduced in the affibody framework (Feldwisch et al., 2010) by inverse PCR using pET28a-KTag-AffiEGFR-SpyTag as a template with 5'-GGGTAAAAGAGCTATCTCCCAGTAAGCGTTCCTCATTTCTTTGTTGAATTTGTTGTCCACGCCCGG and 5'-AACTTAACCAATCAACAGAAAAGGGCTTTCATAAGGAAATTATACGATGACCCAAGCCAAAGCGCTAAC to make pET28a-KTag-AffiHER2-SpyTag_2.

pET28a SnoopTag-AffiEGFR-SpyTag (N-terminal His_6-SnoopTag-spacer-Affibody against EGFR-spacer-SpyTag), based on $Z_{EGFR:1907}$ (Friedman et al., 2008) was generated by inverse PCR from pET28a SnoopTag-AffiHER2-SpyTag (cloned by Tomohiko Nakamura, Howarth laboratory) using 5'-CCTAATCTGAATGGATGGCAGATGACCGCTTTTATTGCCTCTCTTGTTGATGACCCAAGCCAAAGCGC and 5'-GAGGTTTCGTATTTCCTCCCATGCAGCCCACATTTCTTTGTTGAATTTGTTGTCCACGCC. pET28a SnoopTag-AffiIGF1R-SpyTag, containing an affibody against human IGF1R (Li et al., 2010a) was generated by inverse PCR with the primers 5'-

TAAATCGAAAACAGTCTACCGCATTTATTTCTAGCCTTGAAGATGACCCAAGCCA AAGCGCTAACC and 5'-GATTCGGTAATGCCAGGATTTCGATTGCAGCATAGAAACCTTCTTTGTTGAATTT GTTGTCCACGCCCG from pET28a SnoopTag-AffiHER2-SpyTag.

2.1.4 Fab cloning

The KTag/SpyTag-fused anti HER2 Fab was obtained by assembling the murine 4D5 MMP_SpyTag Vh chain and the humanized hu 4D5 KTagGY Vl chain. The murine 4D5 MMP_SpyTag Vh (was cloned into pOPINVh, using 4D5 Vh as template, cloned by Dr. Jayati Jain, Howarth laboratory), via SLIM PCR using 5'-GCCTCCGGTACCAGCTACGCAACCCATC, 5'-GATGGGTTGCGTAGCTGGTACCGGAGGCGCCCACATCGTGATGGTGGACGCCT ACAAGCCGACGAAG, 5'- CAACGATAGGGGCACAACACCAGAGCCTCC and 5'-GCCCACATCGTGATGGTGGACGCCTACAAGCCGACGAAGGGAGGCTCTGGTGT TGTGCCCCTATCGTTG. Going from the N-terminus, 4D5 MMP_SpyTag Vh chain contains a signal sequence (cleaved in the endoplasmic reticulum), SpyTag, GSG linker, MMP-9 cleavage site (VVPLSLR), VH domain, CH1 domain and a His_6 tag.

The hu 4D5 KTagGY Vl chain (N-terminal signal sequence, VL domain, Cκ domain, and KTagGY) was produced in two steps from Fab0.11 (Cho et al., 2003a). KTag was fused at the C-terminus of the light chain using the forward 5'-TGGGTTGCGTAGCTGGTACC and the reverse 5'-ACAGGGCGAGTGCGGTAGTGGTGCTACCCATATTAAATTCTCAAAACGTGATTA ATAAGTTTAAACGATCA. The obtained PCR product was digested with KpnI and PmeI, and subcloned into pOPINVl (Nettleship et al., 2008). This construct was used as template to add GY at the C-terminus of KTag using 5'-

GCTACCCATATTAAATTCTCAAAACGTGATGGTTATTAATAAGTTTAAACGATCAA AACGATCAAACATCACCATCAC and 5'-GTGATGGTGATGTTTGATCGTTTTGATCGTTTAAACTTATTAATAACCATCACGTT TTGAGAATTTAATATGGGTAGC.

2.1.5 Cloning of anti-DR5 nanobody tailored with SnoopTag and SpyTag

Nanobodies are single domain antibody fragments deriving from the variable region of camelid's heavy chain-only antibodies (VHH) (Siontorou, 2013). pET28a SnoopTag-NanoDR5-SpyTag (N-terminal SnoopTag-spacer- 4E6 nanobody against human DR5-spacer-SpyTag- His_6) based on the 4E6 nanobody (Huet et al., 2014) was synthesized, with a periplasmic leader peptide for expression in the periplasm of *E. coli*, via GeneArt® Gene Synthesis (Life Technologies). To express SnoopTag-antiDR5-SpyTag in the cytoplasm of *E. coli*, the periplasmic leader peptide was removed via QuickChange with 5'-TTAAGAAGGAGATATACCATGAGCGGTAAACTGGGTGATATTG and its reverse complement.

2.1.6 Cloning of MBP-SpyCatcher

pET28a MBP-SpyCatcher was obtained by fusing SpyCatcher with a Gly/Ser spacer at the C-terminus of MBP, through overlap extension PCR (Higuchi et al., 1988). MBP was amplified from pET28a SpyTag-MBP (Zakeri et al., 2012) with the forward primer 5′-ATCTCATATGGGCAGCAGCCATCATCATCATCATCAC and the reverse primer 5′-GTATCAACCATGGCACCACTACCGCCCGAACCCGAGCTCGAATTAGTCTGCG. The forward primer 5′-GTTCGGGCGGTAGTGGTGCCATGGTTGATACCTTATCAGGTTTATCAAGTGAGC

AAG and the reverse primer 5′-TACTAAGCTTCTATTAAATATGAGCGTCACCTTTAGTTGCTTTGCCATTTACAG were used to amplify SpyCatcher from pDEST14-SpyCatcher (Zakeri et al., 2012).

The two resulting PCR products were mixed and amplified again using the SpyCatcher forward primer and the MBP reverse primer, digested with NdeI and HindIII, and subcloned into pET21. To increase the affinity of MBP-SpyCatcher for amylose, MBP residues 172, 173, 175 and 176 were deleted (Telmer and Shilton, 2003) and the A312V and I317V mutations (Walker et al., 2010) were introduced by Tomohiko Nakamura (Howarth laboratory), generating MBPx-SpyCatcher. To further decrease the MBP dissociation from amylose resin, Tomohiko Nakamura (Howarth laboratory) generated a tandem fusion of MBPx-SpyCatcher to give pET21 2x MBPx-SpyCatcher.

2.1.7 Cloning of MBP-KTag-Zif-DA

To test whether KTag can form an isopeptide bond with SpyTag in presence of SpyLigase, MBP-KTag-Zif-DA (N-terminal His_6- MBP- spacer- KTag- spacer- Zif268 zinc finger- unreactive SpyTagDA) was generated. SLIM PCR was performed using as DNA template MBP-SpyTag-Zif-DA (N-terminal His_6- MBP- spacer- SpyTag- spacer- Zif268 zinc finger- unreactive SpyTagDA, cloned by Dr. Jacob Fierer, Howarth laboratory) with 5- ACCACTACCGCCCGAACCCGAGCTCG, 5’-ATCACGTTTTGAGAATTTAATATGGGTAGCACCACTACCGCCCGAACCCGAGCTCG, 5'- AGCGGCGGGAGCGGAGAACGC and 5’-GCTACCCATATTAAATTCTCAAAACGTGATAGCGGCGGGAGCGGAGAACGC.

2.2 Protein expression and purification

2.2.1 Protein expression from bacteria

pDEST14 constructs (SpyCatcher, and SpyLigase) were expressed in *E. coli* BL21 DE3 pLysS (Stratagene), while pET28a and pET21 constructs (affibody fusions, SnoopCatcher, MBP fusions) were expressed in *E. coli* BL21 DE3 RIPL (Agilent). Colonies were grown up overnight at 37 °C in LB containing 0.5 mg/mL kanamycin for pET28a vectors and 0.1 mg/mL ampicillin for pET21. The overnight cultures were diluted 1:100 in LB containing 0.8% glucose (v/v) with the appropriate antibiotic, grown at 37 °C, 200 rpm to OD_{600} 0.5-0.6 and induced with 0.4 mM IPTG at 30°C, 200 rpm for 4 h.

For SnoopTag-NanoDR5-SpyTag expression, to facilitate disulfide bond formation, nanobody was expressed in *E. coli* BL21 DE3 previously transformed with a plasmid for the expression of the Erv1p sulfhydryl oxidase and the disulfide bond isomerase DsbC (Veggiani and de Marco, 2011). Cultures were inoculated at 37 °C in LB containing 34 µg/mL chloramphenicol and 0.5 mg/mL kanamycin and grown overnight. Overnight cultures were diluted 1:100 in LB containing 0.8% glucose (v/v) with the appropriate antibiotic, grown at 37 °C, 200 rpm to OD_{600} 0.4 and Erv1p/DsbC expression induced by adding 0.5% arabinose (w/v). The temperature was lowered to 30°C, cultures were grown at 200 rpm for 45 min and nanobody expression was achieved by adding 0.4 mM IPTG to the cultures and growing bacteria at 30°C, 200 rpm for 4 h. Cells were harvested by centrifugation at 4,000xg for 20 min and pellets stored at -80°C.

2.2.2 Protein expression from mammalian cells

HEK 293T cells were grown in three T-175 flasks (Corning) containing 20 mL D10 medium at 37°C with 5% CO_2 until cell confluency reached ~90%. The D10 cell medium contained Dulbecco's Modified Eagle Medium (DMEM), 10% fetal calf serum (Sigma), 50 U/mL penicillin and 50 µg/ml streptomycin (Sigma). After reaching 90% confluency, cells were transferred into a roller bottle (Greiner) in 250 mL D10 medium and grown at 37°C for three days. Transfection mixture was prepared by mixing 1.15 mg polyethyleneimine (branched, 25 kDa, Sigma) with 320 µg endotoxin-free DNA (160 µg 4D5 MMP_SpyTag Vh and hu 4D5 KTagGY Vl) in DMEM serum-free with 50 U/mL penicillin and 50 µg/mL streptomycin, and incubated at 25°C for 20 min. Medium in the roller bottle was replaced with 200 mL DMEM serum-free with 50 U/mL penicillin and 50 µg/mL streptomycin and transfection mixture was added to cells. 25 mM 4-(2-Hydroxyethyl)piperazine-1-ethanesulfonic acid (HEPES) (Sigma), 3.8 mM valproic acid (Sigma) and 4 mM glutamine (Life Technologies) were added to transfection. The roller bottle was then incubated at 37°C for four days and secreted Fab was collected by harvesting the culture supernatant.

2.2.3 Ni-NTA purfication of His_6-tagged proteins

Purification of His_6-tagged proteins expressed in bacteria was performed by resuspending the cell pellet on ice in Ni-NTA binding buffer (50 mM Tris Base, 300 mM NaCl, pH 7.8) containing 10 mM phenylmethylsulfonylfluoride (PMSF) (Sigma) and EDTA-free mixed protease inhibitors (Roche). Resuspended cells were sonicated on ice for three times at 40% pulse for 1 min, with 1 min between each pulse, using the Sonics Vibra-Cell sonicator (Ultrasonic Processor). Cell debris was spun at 17,000 g, 4°C for 20 min. Supernatant was collected and loaded onto Ni-NTA

resin (Qiagen) previously washed with MilliQ water and equilibrated with Ni-NTA binding buffer. The mixture was incubated at 4°C for 30 min with end-over-end rotation (Stuart Equipment) and then centrifuged at 1,000 rpm for 3 min to collect the resin.

For purification of Fabs secreted from mammalian cells, four days after transfection the culture supernatant was collected, spun at 4,000 rpm for 30 min and filtered using 0.2 µm sterile filters (Nalgene) to remove cell debris. 25 mL 10× PBS (1.4 M NaCl, 27 mM KCl, 100 mM $Na_2HPO_4•H_2O$, 20 mM KH_2PO_4 pH 7.4), $MgCl_2$ to the final concentration of 100 µM, 10 mM phenylmethylsulfonylfluoride (PMSF) (Sigma) and EDTA-free mixed protease inhibitors (Roche) were added to 250 mL of filtered supernatant. The processed supernatant was aliquoted into six 50 mL tubes, and 0.1 mL slurry Ni-NTA resin (Qiagen), previously rinsed with MilliQ water and equilibrated with Ni-NTA binding buffer, were added to each tube. The mixture was incubated at 4°C for 16 h with end-over-end rotation (Stuart) and then centrifuged at 1,000 rpm for 3 min to collect the resin.

After binding of His_6-tagged proteins to Ni-NTA matrix, the resin was rinsed with 10 mL Ni-NTA binding buffer, transferred to a Polyprep column (BioRad) and sequentially washed with Ni-NTA binding buffer containing 10 mM imidazole and Ni-NTA binding buffer containing 30 mM imidazole. Protein elution was performed with Ni-NTA binding buffer containing 100 mM imidazole and Ni-NTA binding buffer containing 200 mM imidazole collecting 0.5 mL fractions. Protein purity was assessed by SDS-PAGE, and eluate was dialyzed at 4°C against 4L of PBS (140 mM NaCl, 2.7 mM KCl, 10 mM $Na_2HPO_4•H_2O$, 2 mM KH_2PO_4 pH 7.4), changing buffer three times.

For BiCatcher (SpyCatcher fused to SnoopCatcher, cloned by Tomohiko Nakamura) and 2x MBPx-SpyCatcher purification, after elution from Ni-NTA, the buffer was exchanged by dialysis into 20 mM Tris HCl pH 8.0. After Ni-NTA purification, SnoopTag-fused affibodies were dialyzed in 20 mM 2-(N-morpholino)ethanesulfonic acid (MES) pH 5.8.

2.2.4 Anion exchange chromatography

After elution from Ni-NTA, 2x MBPx-SpyCatcher eluate was exchanged into 20 mM Tris HCl pH 8.0 by dialysis and loaded onto a 1mL quaternary high performance (Q-HP) column (GE Healthcare) at the flow rate of 1 mL/min. Protein elution was performed by applying a 10 column volume (i.e. 10 mL) linear gradient of 0–0.15 M NaCl, followed by an extra elution step performed with a 10 mL linear gradient of 0.15–0.35 M NaCl at the flow rate of 1.5 mL/min, using 20 mM Tris·HCl pH 8.0 as the running buffer. 0.5 mL fractions were collected, protein purity assessed by SDS-PAGE and purified 2x MBPx-SpyCatcher was dialyzed into TBS (50 mM Tris 50 mM NaCl pH 8.0), concentrated using a Vivaspin centrifugal concentrator 5 kDa cutoff (GE Healthcare) and stored at −80 °C. 2x MBPx-SpyCatcher purification was performed using an ÄKTA purifier 10 (GE Healthcare).

For BiCatcher purification, Ni-NTA eluate was exchanged into 20 mM Tris HCl pH 8.0 by dialysis, and mixed with 0.5 mL of slurry Q-HP resin (GE Healthcare), previously rinsed with MilliQ water and equilibrated with 20 mM Tris HCl pH 8.0. The mixture was incubated at 4°C for 30 min with end-over-end rotation and resin was collected via centrifugation at 1,000 rpm for 3 min.

After protein binding, the resin was rinsed with 10 mL 20 mM Tris HCl pH 8.0, transferred to a Polyprep column (BioRad) and BiCatcher was eluted with a linear

gradient of 0.2–0.5 M NaCl and collecting 0.5 mL fractions. Collected fractions were dialyzed into TBS, concentrated using a Vivaspin centrifugal concentrator 5 kDa cutoff (GE Healthcare) and stored at −80 °C.

2.2.5 Cation exchange chromatography

Ni-NTA purified SnoopTag-affibody fusions were dialyzed in 20 mM MES pH 5.8 at 4 °C and mixed with 0.5 mL slurry sulfopropyl high performance (SP-HP) resin (GE Healthcare). After incubation at 4 °C for 30 min with end-over-end rotation, the mixtures were spun at 1,000 rpm for 3 min, the resin rinsed with 10 mL 20 mM MES pH 5.8 and transferred to a Polyprep column (BioRad). Protein elution was performed by applying a linear gradient of 0.2–0.5 M NaCl and collecting 1 mL fractions. The eluted fractions were concentrated using a Vivaspin centrifugal concentrator with a 5 kDa cutoff (GE Healthcare), dialyzed into TBS and stored at −80 °C.

2.2.6 Quantification of protein concetration

Protein concentration was either determined by using the micro Bicinchoninic Acid (BCA) assay kit (Thermo Scientific) according to the manufacturer's instructions or by measuring the A_{280} with the ND-1000 Nanodrop (NanoDrop) and the extinction coefficient predicted by ExPASy ProtParam.

2.3 Polyacrylamide gel electrophoresis

SDS-PAGE was performed on Tris-glycine gels using an XCell SureLock (Life Technologies). Protein samples were mixed with 6× SDS loading buffer (0.23 M Tris-HCl, pH 6.8, 24% v/v glycerol, 120 µM bromophenol blue, 0.23 M SDS) and heated at 95 °C for 5 min using a Bio-Rad C1000 thermal cycler. Tris-glycine gels were

typically run at 200 V for 1 h at room temperature in Tris-glycine running buffer (25 mM Tris·HCl, 192 mM glycine, and 0.1% SDS, pH 8.2).

SDS-PAGE was also performed on Tris-acetate gels. Samples were mixed with 5× loading buffer (150 mM Tris-Acetate pH 7.0, 10% SDS, 25% sucrose, 0.2% bromophenol blue), loaded unboiled onto the gels and run using an XCell SureLock (Life Technologies) at 150V for 90 min at room temperature in Tris-acetate running buffer buffer (50 mM Tricine, 50 mM Tris·HCl, and 0.1% SDS, pH 8.2).

To evaluate the molecular weight of the protein bands, PageRuler™ Pre-stained protein ladder (Fermentas) or the HiMark™ Pre-stained protein markers (Thermo Scientific) were loaded onto the gel alongside the samples. Gels were stained with InstantBlue Coomassie stain (Triple Red Ltd.), de-stained in MiliQ water three times, imaged by a ChemiDoc™ XRS+ Imager (Bio-Rad), and analyzed with the Image Lab Software 3.0 (Bio-Rad).

2.4 Circular dichroism

2.4.1 Far-UV analysis of SpyLigase

Far-UV CD spectra of SpyLigase in 40 mM Na_2HPO_4, 20 mM citric acid pH 5.0 containing 1.5 M Trimethylamine N-Oxide Dihydrate (TMAO, Sigma) (PCT buffer) were recorded using a Jasco J-815 spectropolarimeter. Samples at 0.5 mg/mL were analyzed in a 0.5 mm path-length quartz cuvette, recording spectra between 205 and 260 nm at 4, 12, 25 and 37°C and collecting data at 0.2 nm intervals. Three scans/samples were recorded, averaged and smoothed with a Savitzky-Golay filter (Savitzky and Golay, 1964) using Jasco J-815 Spectra Manager software.

2.4.2 SpyLigase thermal unfolding

SpyLigase in PCT buffer at 0.5 mg/mL was analyzed in a 0.5 mm path-length quartz cuvette by heating the samples with ramping from 4°C to 90°C at 2°C/min. Three spectra/sample were recorded between 215 and 250 nm, averaged and smoothed with a Savitzky-Golay filter (Savitzky and Golay, 1964) using the Jasco J-815 Spectra Manager software.

2.5 SpyLigase Ligation reactions

2.5.1 Analysis of SpyTag and KTag topology for SpyLigase reaction

To test whether KTag can form an isopeptide bond with SpyTag in the presence of SpyLigase, when KTag is placed at the C-terminus, N-terminus or internal to a protein, 10 µM SUMO-KTag (C-terminal KTag), KTag-MBP (N-terminal KTag) or MBP-KTag-Zif-DA (N-terminal His_6- MBP- spacer- KTag- spacer- Zif268 zinc finger-unreactive SpyTagDA) was mixed with 10 µM SpyTag-MBP and 40 µM SpyLigase in PCT buffer. Similarly, to test the influence of SpyTag topology on SpyLigase reaction, 10 µM SpyTag-MBP (N-terminal SpyTag), SUMO-SpyTag (C-terminal SpyTag) or MBP-SpyTag-Zif-DA (internal SpyTag) was incubated with 10 µM SUMO-KTag in the presence of 40 µM SpyLigase in PCT buffer. Moreover, to evaluate whether SpyTag and KTag can form an amide bond even when both are internal to a protein, MBP-KTag-Zif-DA and MBP-SpyTag-Zif-DA each at 10 µM were incubated with 40 µM SpyLigase. All the reactions were incubated for 16 h at 4°C, stopped by addition of 6× SDS loading buffer, followed by sample boiling and analysis on 10 and 16% SDS-PAGE.

2.5.2 Affibody and Fab polymerization

38 µM KTag-AffiEGFR-SpyTag was incubated with 100 µM SpyLigase for 24 h at 4°C in PCT buffer. For Fab polymerization, 50 µM SpyTag-Fab-KTag was mixed with 150 µM SpyLigase and incubated at 4°C for 24 h. As a negative control, both affibody and Fab were incubated with the inactive SpyLigase EQ mutant using the same conditions described above. Reactions were stopped by addition of 6× SDS loading buffer followed by sample boiling and analysis on 8 and 16% SDS-PAGE.

2.5.3 Time course of affibody polymerization

5 µM KTag-AffiEGFR-SpyTag was incubated with 20 µM SpyLigase in PCT buffer at 4°C for 0.5, 1, 2, 4, 6, 8, 12, 24, 48 h. Reactions were stopped at the desired time-point by addition to the samples of 6× SDS loading buffer and sample boiling. Samples were loaded onto 16 and 8% SDS-PAGE. The polymerization rate was determined by quantifying, via densitometry, the band corresponding to KTag-AffiEGFR-SpyTag. Polymerization rate was expressed as [100-(100x(affibody mixed with SpyLigase/affibody alone)].

2.5.4 Affibody polymerization on magnetic beads

Polymerization of affibodies on magnetic beads was performed in two steps: initially SpyCatcher was coupled to magnetic particles, then affibodies were polymerized on beads coated with SpyCatcher for precise anchoring.

For coupling of SpyCatcher on the magnetic beads, Dynabeads M-270 Amine (2.8 µm diameter superparamagnetic polystyrene beads having primary amino functionalities on their surface, 2×10^9 beads/mL, Life Technologies) were washed three times with 1 mL PBS containing 0.1 M $NaHCO_3$ pH 8.0 (coupling buffer). The heterobifunctional reagent sulfosuccinimidyl 6-(3'-[2-pyridyldithio]-propionamido)

hexanoate (sulfo-LC-SPDP, Thermo Scientific) in coupling buffer was added to beads at a final concentration of 2.5 mM and incubated on a ThermoMixer comfort (Eppendorf) at 25°C for 1 h with 1,000 rpm shaking. Magnetic beads were then placed onto a magnet (MagRack 6, GE Healthcare), the excess of sulfo-LC-SPDP removed and beads washed thrice with 1 mL of PBS. After washing, beads were resuspended at 2 × 10^9 beads/mL in 200 µM Cys-SpyCatcher (N-terminal His_6-Cysteine- SpyCatcher), for disulfide-mediated attachment, and incubated for 16 h at 25°C with 1,000 rpm shaking. Beads were washed three times with 1 mL of PBS containing 0.5% bovine serum albumin (BSA) and 0.1% Triton-X-100, resuspended in PBS containing 3% BSA and 0.05 % sodium azide at 2 × 10^9 beads/mL, and incubated for 1 h at 25°C with 1,000 rpm shaking. Beads were washed three times with 1 mL PBS, resuspended at 2 × 10^9 beads/mL in PBS containing 0.5% BSA and 0.05% sodium azide, and stored at 4°C. For affibody polymerization on magnetic particles, SpyCatcher-coated beads were washed three times with 1 mL PBS, resuspended at 2 × 10^9 beads/mL in PBS containing 8.3 µM KTag-AffiEGFR-SpyTag or KTag-AffiHER2-SpyTag and incubated for 2 h at 25°C with 1,200 rpm shaking. After incubation, beads were placed on a magnet and uncoupled affibody removed. Beads were split into two vials, washed thrice with PBS, resuspended at 2 × 10^9 beads/mL in PCT buffer and KTag-AffiEGFR-SpyTag or KTag-AffiHER2-SpyTag was added at the final concentration of 76 µM. To polymerize affibodies on beads, SpyLigase at the final concentration of 200 µM was added (polymeric beads); for monomeric beads (beads coated with an affibody monolayer) 200 µM SpyLigase EQ was added. Beads were incubated on a ThermoMixer comfort (Eppendorf) for 72 h at 4°C with 1,200 rpm shaking. To assess polymerization, beads were washed three

times with PBS, resuspended in 6× SDS loading buffer containing 100 mM dithiothreitol, heated at 95°C for 5 min and loaded onto 8 and 14% SDS-PAGE.

2.6 Isopeptide bond reconstitution reactions

The pilus-associated adhesin RrgA D4 domain was split by Raphaël Gayet (a lab member) into two molecular partners, obtaining the protein domain RrgACatcher and the peptide tag RrgATag. RrgATag was optimized by removing its last 3 C-terminal amino acids, generating SnoopTag. To optimize reaction with SnoopTag, at first the G842T point mutation was introduced into RrgACatcher (RrgACatcher G842T), followed by the additional point mutation D848G to obtain SnoopCatcher (containing both G842T and D848G point mutations).

To test whether the introduced point mutants enhanced reactivity with SnoopTag-MBP (SnoopTag fused at the N-term of MBP), 10 µM RrgACatcher (RrgACatcher WT), RrgACatcher G842T or SnoopCatcher were mixed with 10 µM SnoopTag and incubated for 1 h at 25°C in PBS. After incubation, reactions were stopped by addition of 6× SDS loading buffer, heated to 95°C for 5 min and loaded, alongside with all the proteins in isolation, onto a 16% SDS-PAGE. Each reaction was performed in triplicate.

Isopeptide bond formation efficiency was quantified by densitometry analyzing the intensity of the band corresponding to RrgACatcher WT, RrgACatcher G842T and SnoopCatcher. The percentage of reacted Catchers was calculated as 100x[1-(Catcher band intensity in the presence of SnoopTag)/(Catcher band intensity in the absence of SnoopTag)] and fold change in reactivity was calculated as [(% reacted Catcher)/(% reacted RrgACatcher WT)].

To test the effect of temperature on the SnoopTag-SnoopCatcher reaction, 10 µM SnoopTag-MBP was mixed with 10 µM SnoopCatcher in PBS in a final volume of 50 µL. Reactions were incubated for 20 min at 4, 12, 25, 37 and 42°C in a C1000™ Thermal Cycler (Bio-Rad). After incubation, reactions were stopped as described above and analysed using a 16% SDS-PAGE. % of reacted SnoopCatcher was calculated, by densitometry, as 100x[1-(SnoopCatcher band intensity in the presence of SnoopTag)/(SnoopCatcher band intensity in the absence of SnoopTag)]. Each condition was tested in triplicate.

To evaluate sensitivity to buffer composition, SnoopTag-MBP and SnoopCatcher, both at 10 µM, were incubated for 30 min at 25°C in PBS, PBS containing Triton-X100 1% (v/v), NP-40 0.5% (v/v), Tween-20 1% (v/v) or 100 mM DTT. Reactions were stopped and analyzed by SDS-PAGE as previously described.

To test SnoopTag/SnoopCatcher orthogonality to SpyTag/SpyCatcher, 10 µM SnoopTag-MBP and 10 µM SnoopCatcher or SpyCatcher were incubated for 16 h at 25 °C in PBS, before SDS-PAGE. Similarly 10 µM SpyTag-MBP and 10 µM SnoopCatcher or SpyCatcher were incubated as above.

2.7 Solid phase synthesis of protein polymers

2.7.1 General procedure

40 µL of slurry amylose resin (NEB) was applied to a 1 mL poly-prep column (Bio-Rad), rinsed with 1 mL MilliQ water and equilibrated with 1 mL TBS (50 mM Tris HCl pH 8.0 with 50 mM NaCl). As the first protein building block of the chain, 320 pmol MBP-SpyCatcher in TBS in a final volume of 80 µL was added to the resin and incubated at 25°C for 1 hour with 700 rpm shaking on a ThermoMixer comfort (Eppendorf). Unreacted protein was removed from the column by gravity flow and

resin washed with 1 mL Wash Buffer (50 mM Tris HCl pH 8.0 with 500 mM NaCl). 3 nmol SnoopTag-Affi-SpyTag (Affibody anti-HER2) in TBS in a final volume of 80 µL was added to the resin and incubated at 25°C for 1 hour with 700 rpm shaking. Unreacted SnoopTag-Affi-SpyTag was removed from the column by gravity flow and resin washed with 1 mL Wash Buffer. 4 nmol BiCatcher in TBS with 1.5 M TMAO was added to the resin and incubated at 25°C for 2 h with 700 rpm shaking. Unreacted BiCatcher was removed from the column by gravity flow and resin washed with 1 mL Wash Buffer. Chains were produced by sequential addition of SnoopTag-Affi-SpyTag and BiCatcher, according to the conditions described above. Chains were eluted, after resin washing, by applying onto the column 40 µL TBS containing 50 mM D-maltose (Sigma) and incubating the solution at 25°C for 10 min with 700 rpm shaking. Chains were collected by spinning the column in a 1.5 mL tube for 10 s at 17,000 g, mixed with 6× SDS loading buffer, heated at 95°C for 5 min and loaded, alongside monomer controls in isolation, onto 8 and 16% SDS-PAGE.

2.7.2 Analysis of chains extension using different attachments to the resin

To improve protein polymer recovery, different attachments to the resin were tested. 320 pmol MBP-SpyCatcher, MBPx-SpyCatcher (MBP bearing A312V and I317V mutations and residues 172, 173, 175 and 176 deletion) or 2x MBPx-SpyCatcher (tandem repeat of MBPx fused to SpyCatcher) were added to 40 µL of slurry amylose resin previously equilibrated with TBS. After resin incubation with he protein at 25°C for 1 hour with 700 rpm shaking on a ThermoMixer, unreacted proteins were removed from the column by gravity flow and resin washed with 1 mL Wash Buffer. Chain extention was performed by sequential addition of SnoopTag-

Affi-SpyTag and BiCatcher as described above, until a polymer 6 units long was obtained. Chains were eluted and analyzed after each step as previously described.

For biotin/streptavidin-based attachment, 40 µL of slurry monomeric avidin resin (Thermo Scientific) was applied to a 1 mL poly-prep column, rinsed with 1 mL MilliQ water and equilibrated with 1 mL TBS. As the first building block for chains extension, 4 µM biotinylated-SpyCatcher in TBS in a final volume of 80 µL was added to the resin and incubated at 25°C for 1 hour with 700 rpm shaking on a ThermoMixer comfort. Unreacted biotinylated-SpyCatcher was removed by gravity flow and resin washed with 1 mL Wash Buffer. Protein polymer formation was achieved by sequential addition of SnoopTag-Affi-SpyTag and BiCatcher as described above, until a polymer 10 units long was obtained. After resin washing with 1 mL of Washing buffer, chains were eluted by incubating 40 µL 1 mM D-biotin in TBS at 25°C, 700 rpm shaking for 4 h. Chains were collected and analyzed by SDS-PAGE as previously indicated.

2.7.3 Analysis of the best buffer for BiCatcher incorporation in the chains

To identify the best conditions for BiCatcher coupling to the nascent chain, 20 µL of slurry amylose resin (NEB) was applied to a 1 mL poly-prep column (Bio-Rad), rinsed with 1 mL MilliQ water and equilibrated with 1 mL TBS. 320 pmol MBP-SpyCatcher in TBS in a final volume of 40 µL was added to the resin and incubated at 25°C for 1 hour with 700 rpm shaking on a ThermoMixer comfort. Unreacted MBP-SpyCatcher was removed from the column by gravity flow and resin washed with 1 mL Wash Buffer. 3 nmol SnoopTag-Affi-SpyTag (Affibody anti-HER2) in 40 µL TBS was added to the resin and incubated at 25°C for 1 hour with 700 rpm shaking. Unreacted protein was removed from the column by gravity flow and resin washed

with 1 mL Wash Buffer. 4 nmol BiCatcher (having an helical linker connecting SpyCatcher to SnoopCatcher) was added to the resin in TBS, TBS containing 0.1 M $NaHCO_3$ pH 9.0, TBS containing 0.1 M $NaHCO_3$ pH 10.0 or TBS containing 1.5 M TMAO and incubated for at 25°C for 1 hour with 700 rpm shaking. After removal of unreacted BiCatcher and resin wash, assembled trimers were eluted and analyzed by 16% SDS-PAGE as described in section 2.7.1.

2.7.4 Analysis of chains extension using BiCatcher variants

To improve BiCatcher incorporation into the nascent chain, BiCatcher variants (cloned by Tomohiko Nakamura, a laboratory member) were used (see Appendix for sequence alignments). 20 µL of slurry amylose resin was applied to a 1 mL poly-prep column, rinsed with 1 mL MilliQ water and equilibrated with 1 mL TBS. MBP-SpyCatcher immobilization and SnoopTag-Affi-SpyTag addition were performed as previously described (section 2.7.1). After resin washing, 4 nmol BiCatcher, BiCatcher long linker or BiCatcher helical linker in 40 µL TBS were added to the resin and incubated for 2 h at 25°C with 700 rpm shaking. Unreacted proteins were removed by gravity flow and resin was washed with 1 mL of Washing buffer. Trimers were eluted and analyzed as reported in section 2.7.1.

2.7.5 Generation of decamer

To make a 10 unit long chain (a decamer), polymerization was performed as described in section 2.7.1. To ensure stable attachment to amylose resin, 2x MBP-SpyCatcher was used as the first protein building block in place of MBP-SpyCatcher. BiCatcher helical linker was added to the extending chain in TBS with 1.5 M TMAO to maximize protein conjugation. Conditions for SnoopTag-Affi-SpyTag incorporation in

the chain were left unchanged. After each step, chains were eluted as described in section 2.7.1 and analyzed by SDS-PAGE on 10 and 4% Tris-acetate gels.

2.7.6 Characterization of decamer

To analyzed the properties of decamer, size exclusion chromatography, mass spectrometry and temperature-stability tests were performed.

For size exclusion chromatography, decamer (generated as described above) was loaded on a Superdex 200 GL 10/300 column (24 mL bed volume) (GE Healthcare) previously equilibrated with 50 mM Tris HCl containing 0.5 M NaCl and calibrated using gel filtration standards (BioRad). Gel filtration of decamer was performed, using an ÄKTA purifier 10 (GE Healthcare), by eluting the sample at 0.4 mL/min using 50 mM Tris·HCl containing 0.5 M NaCl pH 8.0 as the running buffer.

For mass spectrometry (MS), decamer was concentrated to ~5 µM and buffer exchanged into 250 mM ammonium acetate using an Amicon Ultra 0.5 mL centrifugal filter with a 100 kDa cut-off (Millipore). MS was performed using a first generation Synapt High Definition Mass Spectrometry (HDMS) Quadrupole Time of Flight mass spectrometer (Waters). After mass spectra were smoothed and peak-centered, masses were assigned using MassLynx v4.1 (Waters).

To test stability to storage, decamer (prepared as described in section 2.7.2) in TBS containing 0.1 NaN_3, 1 mM PMSF, 1 mM EDTA and EDTA-free mixed protease inhibitors in a final volume of 40 µL was incubated at 25°C for 24 and 96 h. At each time point samples were spun at 4°C, 17,000 g for 30 min, before supernatant was collected and analyzed on 8% SDS-PAGE. To evaluate the thermal stability of decamer, protein chains at 3 µM in 150 mM ammonium acetate in a final volume of 30 µL were incubated in a Bio-Rad C1000 Thermal Cycler at 25, 37, 50, 60 or 70°C,

ramping at 3°C/s. Following heating for 3 min, samples were cooled down to 10°C, spun at 17,000 g for 30 min and supernatant was analyzed by SDS-PAGE on a 8% Tris-glycine gel.

2.7.7 Combinatorial assembly of protein polymers

40 µL of slurry amylose resin (NEB) was applied to an AcroPrepTM Advance 1 mL 96-well plate with a 0.45 µm GHP (hydrophilic polypropylene) membrane (Pall). Resin was rinsed with 1 mL MilliQ water and equilibrated with 1 mL TBS. As the first protein building block of the chain 160 pmol 2x MBPx-SpyCatcher in TBS in a final volume of 80 µL were added to the resin and incubated at 25°C for 1 hour with 1,000 rpm shaking on a ThermoMixer comfort. Unbound protein was removed by centrifugation at 1,000 rpm at 25°C for 1 min and resin was washed by applying 1 mL/well of Wash buffer followed by centrifugation at 1,000 rpm at 25°C for 1 min. 2.4 nmol SnoopTag-AffiIGF1R-SpyTag, SnoopTag-AffiEGFR-SpyTag, SnoopTag-SpyTag-AffiHER2×3 or SnoopTag-antiDR5-SpyTag was added to the resin in 40 mM Na_2HPO_4 and 20 mM citric acid pH 5.0 and incubated at 25 °C for 1 h with 1,000 rpm shaking. Unreacted protein was removed by centrifugation at 1,000 rpm at 25 °C for 1 min and resin was washed with 1 mL Wash Buffer. 2.8 nmol BiCatcher helical linker in TBS containing 1.5 M TMAO in a final volume of 80 µL was incubated at 25 °C for 2 h with 1,000 rpm shaking. Following removal of BiCatcher's excess by centrifugation at 1,000 rpm at 25°C for 1 min, resin was washed by applying 1 mL/well of Wash buffer and spinning the 96-well plate at 1,000 rpm at 25°C for 1 min. Chains were assembled by sequential addition of SnoopTag/SpyTag monomers and BiCatcher. All the synthesized chains were extended up to 10 units. The position of affibody in chains formed by combination of SnoopTag-antiDR5-SpyTag and

SnoopTag/SpyTag-tagged affibodies was systematically varied (see Chapter 5, Figure 5.14). Protein polymers were eluted by adding 20 µL/well of TBS containing 100 mM D-maltose and incubating the 96-well plate at 25°C for 10 min with 1,000 rpm shaking. Eluted chains were collected by placing the 96-well plate on top of 96-well round-bottom polystyrene plate (Corning) and centrifuging at 25 °C, 1,000 rpm for 1 min. Collected polymers were analyzed as previously described and protein concentration was determined by using the micro bicinchoninic acid (BCA) protein assay kit (Pierce) according to the manufacturer's instructuions.

2.8 Mammalian cell culture

2.8.1 Cell lines

MDA-MB-453, MDA-MB-231 and MDA-MB-468 were from ATCC, A431, BT474 and MCF7 were from Cancer Research UK, Lincoln's Inn Fields (CR-UK). LBL 721.221 were a kind gift of Tim Elliott (University of Southampton). All cells were grown in DMEM with 10% fetal calf serum (FCS) (Sigma), 50 U/mL penicillin and 50 µg/mL streptomycin (Sigma) (D10 buffer) and were passaged for fewer than 6 months. Insulin (Sigma) was added to BT474 cells at 5 µg/mL.

2.8.2 Mycoplasma testing

To test for the presence of Mycoplasma in cultured cell lines, 1 mL cell culture supernatant from each cell line was collected and spun for 3 min at 1,700 g to pellet cellular debris. The obtained supernatant was transferred to 1.5 mL tube and spun for an extra 10 min at 17,000 g to sediment Mycoplasma. The supernatant was discarded and the obtained pellet (not visible) was resuspended with 50 µL MilliQ water and mixed thoroughly. After heating samples for 3 min at 95°C, Mycoplasma presence was assessed by PCR with 5′-GGGAGCAAACAGGATTAGATACCCT and

5′-TGCACCATCTGTCACTCTGTTAACCTC, using Taq DNA Polymerase (NEB). Cycling conditions used were: initial denaturation at 94°C for 0.5 min, followed by 35 cycles of denaturation at 94°C for 2 min, annealing at 60ºC for 2 min, and elongation at 72°C for 1 min. Samples were finally heated for 1 cycle at 94°C for 0.5 min, 60°C for 2 min, and 72°C for 5 min, before sample cooling to 10°C. As a positive control, the PCR template from the EZ-PCR Mycoplasma test (Biological Industries) was used. Amplified products were detected by loading onto an ethidium bromide-stained 2% agarose gel and imaged using the ChemiDoc™ XRS+ Imager (BioRad).

2.9 Flow cytometry

To determine the expression levels of HER2, EpCAM and EGFR on different cell lines, cells were harvested by trypsinization for 5-15 min at 37°C, 5%CO_2 and resuspended in D10 buffer at 2.5 x 10^6 cells/ml. 125,000 cells/sample were used.

For HER2 and EpCAM expression, cells were incubated for 30 min at 25°C with 10 µg/mL biotinylated anti-HER2 Fab 0.35 and 10 µg/mL mouse anti-human EpCAM (eBioscience, clone 1B7) in PBS containing 1% BSA and 0.1% NaN_3 (FACS-A buffer). For assessement of EGFR expression, cells were incubated for 10 min at 25°C with 10 µg/mL mouse anti-human EGFR antibody (Millipore, clone 528).

Antibodies excess was removed by centrifugation at 1,300 rpm for 3 min, followed by sample washing with 100 µL of FACS-A buffer for three times.

To detect EGFR and EpCAM expression, 100 µL/sample of 1:100 goat anti-mouse IgG phycoerythrin (PE) conjugated (Invitrogen) in FACS-A buffer was added. For HER2 expression, 100 µL/sample of 1:100 streptavidin-PE was used. Cells were incubated with secondary antibodies or with streptavidin for 10 min on ice. After cells spinning at 1,300 rpm, 4°C for 3 min and washing with 100 µL of FACS-A buffer three

times, samples were resuspended in 300 µL of ice cold FACS-A buffer and analyzed on a FACScalibur flow cytometer with CellQuest Pro version 5.2.1 (Becton Dickinson).

2.10 Immunomagnetic isolation of cells

2.10.1 Cell beading general procedure

Cells were grown in DMEM with 10% fetal calf serum (FCS) (Sigma), 50 U/mL penicillin and 50 µg/mL streptomycin (Sigma) (D10 buffer) until they reached ~80% confluency and harvested by trypsinization for 5-15 min at 37°C, 5% CO_2. After trypsin inactivation by addition of D10 buffer, cells were centrifuged at 1,500 rpm for 3 min, and resuspended at 2.5 x 10^6 cells/mL in DMEM with 1% FCS, 50 U/mL penicillin and 50 µg/mL streptomycin (D1 buffer). 100 µL of cells/condition was used.

To compare the effect of cholesterol on cell recovery, samples were incubated with or without 250 µg/mL cholesterol-water soluble (Sigma) for 30-60 min at 25°C, before incubation with the suitable binding agent. For testing the effect of antibody affinity on immunomagnetic cell isolation, two biotinylated anti-HER2 Fab variants, Fab 0.11 and Fab 0.35 (named after their nanomolar K_d) (Gerstner et al., 2002) were added to cells at 1 µg/mL and incubated at 25°C for 10 min. Cells were spun to remove unbound Fab, resuspended in 500 µL D1 buffer and then added to 25 µL Dynabeads Biotin Binder beads at 4 × 10^8 beads/mL (2.8 µm diameter superparamagnetic polystyrene beads coupled to recombinant streptavidin, Life Technologies) previously washed twice with 500 µL PBS and once with an equal volume of D1 buffer. Samples were incubated with end-over-end rotation (Stuart Equipment) for 1 h at 25°C and after incubation 100 µL of the cells-beads mixture were pipetted out for counting the total number of cells in the cell-bead mixture. The

remaining cells were placed onto a magnet and unbound cells pipetted out for counting of flow through cells. Cells bound to magnetic beads were washed with 500 µL of D1 buffer and finally resuspended in 100 µL of D1 buffer. Cells in the bead-cell mixture, in the flow through and recovered cells were counted on a Coulter Counter (CasyR Model TT, Innovatis) using a 150 µm measuring capillary, 400 µL sample volume and evaluation cursor of 7.5-50 µm. Recovery of cells was calculated as 100 x (number of recovered cells/ number of cells in the cell-bead-mixture prior to magnetic isolation).

2.10.2 Comparison of different antibody linkages to the beads for immunomagnetic isolation of cells

For analyzing the dependence of antibody-bead linkage, cells were incubated with either biotinylated or non biotinylated anti HER2 Fab 0.11 at 0.1 µg/mL, or with biotinylated or non biotinylated mouse anti EpCAM antibodies (eBioscience, clone 1B7) at 1 µg/mL. Cells were incubated with antibodies at 25°C, for 10 min, in 100 µL D1 buffer. Cells treated with biotinylated antibodies were isolated by direct linkage to 25 µL of Dynabeads Biotin Binder beads at 4×10^8 beads/mL, whereas cells incubated with non biotinylated antibodies were captured by saturating streptavidin-beads for 30 min at 25°C with a biotinylated goat anti-mouse (Sigma) or goat anti-human κ light chain immunoglobulins (Thermo Scientific). The volume of the cell-bead mixture was adjusted to 500 µL with D1 buffer and samples were incubated with end-over-end rotation for 1 h at 25°C. Cell isolation and counting was performed as described in section 2.10.1.

2.10.3 Beading of cells with polymeric and monomeric beads

To compare the efficiency in immunomagnetic isolation of polymeric and monomeric beads, cells were incubated with or without 250 µg/mL cholesterol for 1 h at 25°C, before incubation with 12.5 µL of polymeric or monomeric beads at 2×10^9 beads/mL, prepared as described in section 2.5.4. The volume of the cell-bead mixture was adjusted to 500 µL and samples were mixed for 20 min at 25°C with end-over-end rotation. Cell isolation and counting was performed as described in section 2.10.1.

2.10.4 Spiking and recovery of cancer cells from human blood

Cells were harvested by trypsinization, washed once with D10 buffer, spun at 1,500 rpm for 3 min, and resuspended in PBS containing 1% FCS (PBS-1), before resuspending at 10^6 cells/ml in PBS-1. Carboxyfluorescein succinimidyl ester (CFSE, Life Technologies) was added to 1 x 10^6 cells/mL and incubated at 37°C in the dark for 15 min. Cells were spun at 1,300 rpm for 3 min, and following supernatant removal, were resuspended in D10 buffer. After incubation at 37°C in the dark for 30 min, cells were spun at 1,300 rpm for 3 min and resuspended in D1. 250,000 CFSE-labelled cells were spiked into 1 ml of human blood (obtained upon approval by the University of Oxford Central University Research Ethics Committee, CUREC). Whole-blood samples containing CFSE-labelled cells were transferred into red blood cell lysis buffer (154 mM NH_4Cl, 10 mM $KHCO_3$, 0.1 mM EDTA pH 7.2) at a ratio of 25 mL lysis buffer per 1 mL blood, and incubated at 25°C for 7 min. Cells were spun at 1,500 rpm for 3 min, and washed once with 1 mL D1 before resuspension in 100 µL D1 buffer. Cells were incubated for 1 h at 25ºC in 100 µL D1 with or without 250 µg/mL cholesterol-water soluble.

For comparison between enhanced (biotinylated Fab 0.11, direct antibody-magnetic bead linkage and cholesterol loading) and standard conditions (Fab 0.35, secondary antibody linkage to beads, no cholesterol loading), cells were incubated with 10 µg/mL biotinylated Fab 0.11 or 10 µg/mL non biotinylated Fab 0.35 for 10 min at 25°C. Cells were spun at 1,300 rpm to remove Fab excess, and then samples treated with biotinylated Fab 0.11 were isolated by direct linkage to 25 µL of Dynabeads Biotin Binder beads at 4×10^8 beads/mL, whereas cells incubated with non biotinylated Fab 0.35 were captured using the same amount of Dynabeads Biotin Binder beads previously saturated for 30 min at 25°C with a biotinylated goat anti-mouse antibody. The volume of the cell-bead mixture was adjusted to 500 µL with D1 buffer and samples were incubated with end-over-end rotation for 1 h at 25°C. After incubation 100 µL of the cell-bead mixture was pipetted out for counting the total number of cells in the cell-bead mixture. The remaining cells were placed onto a magnet and unbound cells discarded. Cells bound to magnetic beads were washed with 500 µL of D1 buffer and finally resuspended in 100 µL of D1 buffer.

For cell isolation from human blood with monomeric or polymeric beads, an anti-HER2 affibody with reduced IgG binding (KTag-AffiHER2-SpyTag_2) was used. Cells were CFSE-labelled, and spiked into human blood as described above. Isolation of spiked cells with monomeric or polymeric beads was performed as indicated in section 2.10.3.

After isolation, cells were washed once with 400 µL of PBS and then fixed by incubating samples in 100 µL of 3% paraformaldehyde (PAF) (Sigma) for 10 min at 25°C. Excess PAF was removed and cells were washed once with 400 µL of PBS and labelled with 100 µL/sample of a 1:20 goat anti-CD45 phycoerythrin (PE)-conjugated antibody solution (Life Technology) for 10 min at 25°C. Antibody excess

was removed by placing samples on a magnet. Cells bound to magnetic beads were washed twice with 100 µL PBS and then resuspended in 30 µL PBS. Cells in the bead-cell mixture and recovered cells were counted on a hemocytometer under the DeltaVision wild-field fluorescence microscope (Applied Precision) and checked for CFSE and CD45 labeling in the FITC and TRITC channels respectively. As a positive control for CD45 staining, a human whole-blood sample was incubated with lysis buffer and washed as above, but was fixed and stained without any magnetic isolation.

Isolated cells and bead-cell mixture from samples incubated with monomeric or polymeric beads were counted on a Coulter Counter as previously described. Cells recovery was calculated as 100 x (number of recovered cells/ number of cells in the cell-bead-mixture prior to magnetic isolation).

2.11 Microscopy

Cells were imaged using a 4x lens and signals from brightfield, FITC channel (for CFSE) and TRITC channel (for CD45-PE) were recorded. Collected images were analyzed using the softWoRx 3.6.2 software (Applied Precision), and background was corrected with the same software. Typical exposure times were 0.25-2 s. Different samples from the same experiment were prepared, imaged and analyzed using identical conditions.

2.12 Analysis of protein polymers killing potential

2.12.1 Combinatorial screening of protein polymers

MDA-MB-231 cells were seeded into a 96-well plate at 40,000/well in 50 µL DMEM serum free containing 1% penicillin and streptomycin (v/v) (DMEM-SF) and incubated at 37°C, 5% CO_2, for 16 h.

Protein polymers assembled as described in section 2.7.7 were added at the final concentration of 200 ng/mL in a total volume of 50 µL/well of DMEM-SF containing 2% BSA (D-BSA). The plate was incubated at 37°C, 5% CO_2, for 40 h and after incubation cell viability was evaluated to determine the ability of chains for killing cancer cells. Cell viability was assessed by adding 20 µL/well of 0.15 mg/mL resazurin sodium salt (Sigma) in PBS pH 7.4 and incubating the plate at 37°C, 5% CO_2, for 4 h. After incubation, the fluorescence of reduced resazurin (λ_{em} 590nm, λ_{ex} 544 nm) was determined using the SpectraMax3 plate reader (Molecular devices).
The percentage of viable cells was calculated as [100x(signal of treated cells – signal without cells)/(signal untreated cells– signal without cells)]. The signal without cells was taken as the resazurin fluorescence in the absence of cells, whereas the signal of untreated cells was derived from the fluorescence of reduced resazurin by cells that were incubated only with D-BSA. All tests were performed in triplicate.

2.12.2 Dose response curve of a nanobody chain

MDA-MB-231 cells were seeded at a density of 40,000 cells/well into a 96-well microplate in DMEM-SF and incubated for 16 h at 37°C, 5% CO_2. Cells were treated with varying concentrations of NNNNE (a chain formed by four SnoopTag-Nano4E6-SpyTag monomers and one anti-EFGR Affibody unit positioned at the end of the chain, see Chapter 5 Figure 5.14) by performing a two-fold serial dilution starting from the concentration of 800 ng/mL to 6.25 ng/mL. As negative control 200 ng/mL HHHHH (a protein polymer entirely composed of five conjugated SnoopTag-SpyTag-AffiHER2x3 units, see Chapter 5 Figure 5.14) was used, whereas as a positive control cells were treated with 200 ng/mL killer TRAIL (recombinant human TRAIL with a linker peptide to promote stable trimerization, Enzo Life Science). After

addition of samples to the cells, the plate was incubated at 37°C, 5% CO_2, for 40 h before analysis. Cell viability was determined as in section 2.12.1, with all measurements performed in triplicate.

2.12.3 Assessment of caspase activation

40,000 MDA-MB-231 cells/well were seeded in a 96-well plate and incubated for 16 h at 37°C, 5% CO_2 in DMEM-SF. Cells were then cultured for 1 h in the presence or absence of 20 µM benzyloxycarbonyl-Val-Ala-Asp-fluoromethylketone (Z-VAD-FMK, a pan-caspase inhibitor, Sigma), before addition of protein polymers. NNNNE, HHHHH, and killer TRAIL were added to cells at 200 ng/mL and the 96-well plate was incubated at 37°C, 5% CO_2 for 5 h. The activity of caspases-3/7 was detected with the Apo-One® Homogeneous Caspase-3/7 kit (Promega) by adding 100 µL/well of the caspase-3/7 reagent diluted 4 times in PBS. The plate was gently mixed at 500 rpm on a ThermoMixer comfort (Eppendorf) and incubated in the dark at 25°C for 1 h. Fluorescence was measured using the SpectraMax3 plate reader (Molecular Devices) with 485 nm excitation and 530 nm emission. All measurements were performed in triplicate.

Chapter 3 : Enhanced immunomagnetic isolation of cancer cells

Investigating the molecular requirements for efficient magnetic isolation of tumour cells

The recent advances in genomics and proteomics have facilitated the qualitative and quantitative analysis of the molecular components expressed in a given biological system. However, most of these approaches are limited by sample heterogeneity and require, for the detection of specific parameters, the isolation of specific cell types and subsets from complex mixtures.

Isolation of cells through affinity-based method has the advantage of being robust, highly specific and easily customizable thanks to the large number of antibodies and ligands commercially available (Dainiak et al., 2007).

Immunomagnetic cell separation relies on the binding of magnetic beads to cells through antibodies directed against extracellular targets (Clarke and Davies, 2001). The antibody-target interaction allows labelling of cells with magnetic particles and subsequently to enrich or deplete magnetically-labeled cells simply by applying a magnetic field. Because of its ease to use, high throughput and low cost, immunomagnetic isolation of cells is a powerful approach for research and clinical applications, most recently for isolating circulating tumour cells (CTCs) (Chen et al., 2015; Lu et al., 2015a, 2015b).

Despite the widespread use of magnetic cells isolation, several questions have not been fully answered. For instance, what is the minimum number of copies of a target antigen on a cell, to ensure cell capture? How does the buffer composition and temperature affect cell recovery?

In addition to shear stress, buffer viscosity, temperature and magnetic moment, the connection between the antibody and beads as well as the antibody affinity for its cognate target are of particular importance. Such interactions, in fact, must withstand the physical forces pulling a captured cell in the magnetic field, ensuring an efficient

cell recovery, necessary to analyze CTCs with microscopic, proteomic or genetic methods (Leary et al., 2010; Yu et al., 2011b).

Although application of CTC analysis is a promising clinical tool, the dependence of cell recovery on high antigen expression levels has been the major impediment for CTCs use in the clinic (Dharmasiri et al., 2010).

With the goal of improving the efficiency of cancer cells isolation, here we analyze the molecular details of some of the unanswered questions concerning immunomagnetic cell isolation. In particular we focused on the importance of the antibody affinity for its cognate target, on the role played by the plasma membrane fluidity and on the nature of the linkage between the antibody and magnetic beads.

3.1 Dependence of antibody affinity on tumour cells capture performance

In order to analyze the dependence of cell capture on antibody affinity, we used two point mutants of the humanized Fab hu4D5 which bind with high affinity the same epitope on the extracellular domain of the human epidermal growth factor receptor-2 (HER2) (Cho et al., 2003b). The availability of such a system, where single point mutants result in the modulation of the Fabs' binding affinity without altering the binding specificity, greatly simplify the analysis of the relationship between antibodies affinity and performance in isolating cancer cells.

The two Fab variants used, Fab 0.11 and Fab 0.35 (named after their nM K_d) (Gerstner et al., 2002), had at the C-terminus of their light and heavy chains of a peptide tag (AviTag, GLNDIFEAQKIEWHE) (cloned by Dr. Jayati Jain) to enable site-specific biotinylation using biotin ligase (BirA) from *E. coli* (Beckett et al., 1999). Site-specific biotinylation allowed the Fabs to bind to streptavidin-coated magnetic beads, so that cells expressing HER2 on the surface could be labelled with magnetic beads and isolated by applying a magnetic field (Figure 3.1).

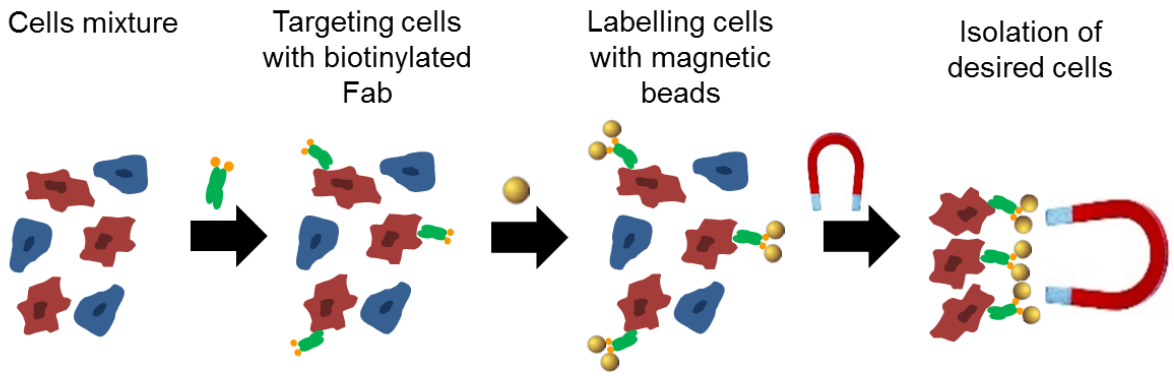

Figure 3.1. Cartoon of the beading procedure. Biotinylated Fab is added to the cells mixture to specifically label cells expressing HER2. Streptavidin-coated magnetic particles are added to the cell mixture, so that magnetic beads-bound cells can be separated from unbound cells simply by applying a magnetic field. Magnetic field removal allows the release of the isolated cells.

The cells isolation efficiency of Fab 0.35 and Fab 0.11 was compared by targeting HER2 expressed on the surface of a human cell line panel, whose expression levels were determined by FACS (Figure 3.2A).

BT474 cells are characterized by elevated expression levels of HER2 and for this reason were used as positive control. MDA-MB-453 cells, a breast cancer cell line, expresses medium levels of HER2, whereas MCF-7 and A431 are low HER2 expressers. As negative control, the MBA-MB-468 HER2-null cell line was used. To compare Fab 0.11 and Fab 0.35, both the antibodies were added to cells at 1 µg/mL and, following incubation at 25°C for 30 minutes, unbound Fab was removed by centrifugation. Streptavidin-coated magnetic beads were applied to cells and incubated with end-over-end rotation at 25°C for 1 hour before megnetic isolation. Captured cells were counted using a Coulter counter (Figure 3.2 B).

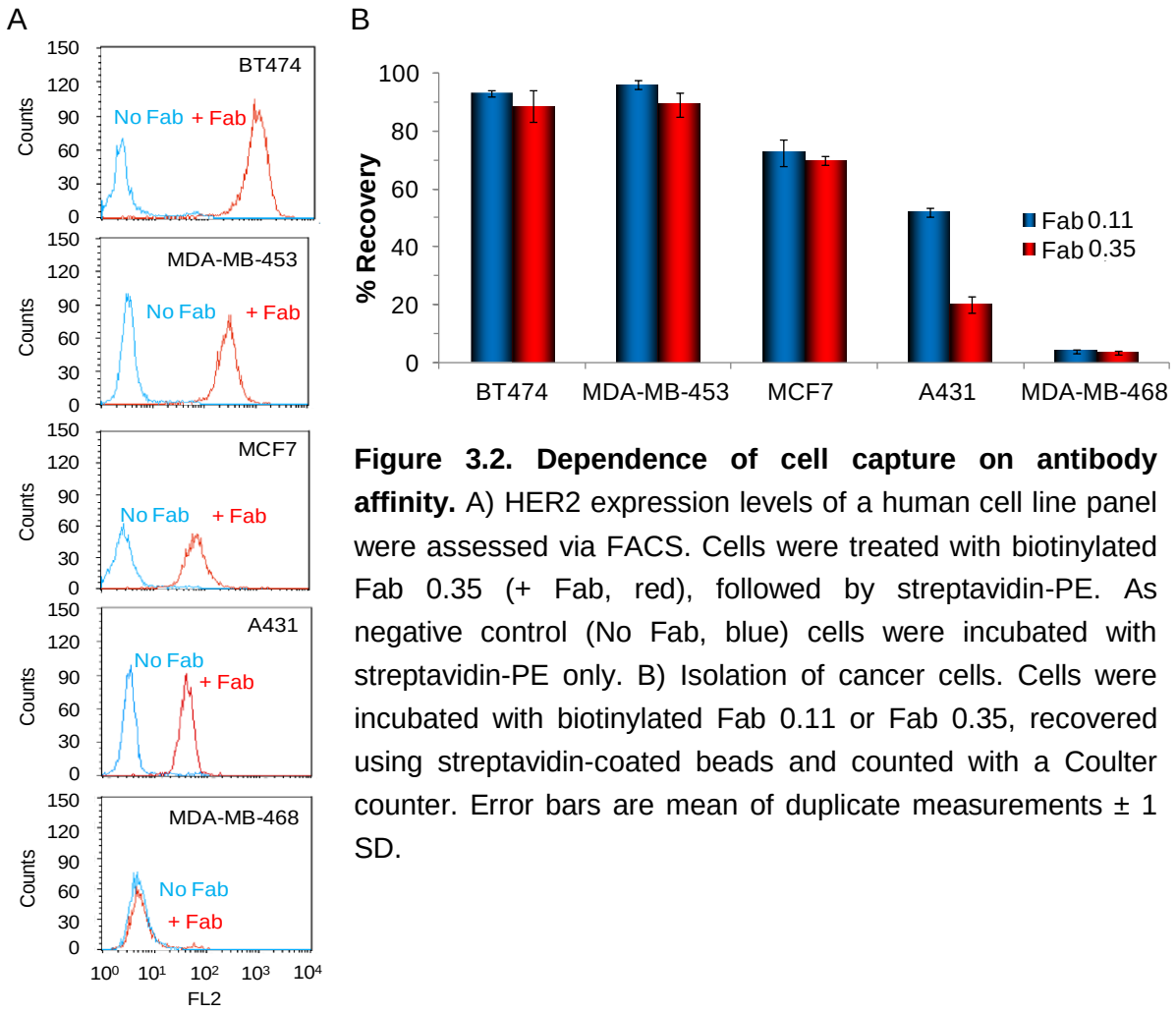

Figure 3.2. Dependence of cell capture on antibody affinity. A) HER2 expression levels of a human cell line panel were assessed via FACS. Cells were treated with biotinylated Fab 0.35 (+ Fab, red), followed by streptavidin-PE. As negative control (No Fab, blue) cells were incubated with streptavidin-PE only. B) Isolation of cancer cells. Cells were incubated with biotinylated Fab 0.11 or Fab 0.35, recovered using streptavidin-coated beads and counted with a Coulter counter. Error bars are mean of duplicate measurements ± 1 SD.

Figure 3.2B clearly shows that the high affinity of biotnylated Fab 0.35 and Fab 0.11 enabled an effective recovery of cancer cells. However, using the Fab with the highest affinity (Fab 0.11) gave improved isolation of A431 cells by 30% ($P < 0.01$, $n = 2$, unpaired *t*-test), indicating that the greater is the affinity of the antibody used in the isolation the better is the capture of cells expressing low levels of the targeted receptor.

3.2 Correlation between the antibody-bead connection and cell capture performance

To efficiently isolate cancer cells (i) a tight binding of the antibody to its target receptor on the cell surface and (ii) a stable interaction between the antibody and the magnetic beads are desirable. In fact, the interactions established by the antibody bridging between the targeted cell and the magnetic particles need to withstand the physical forces applied to the targeted cells, to form a stable cell-bead synapse, ensuring cell isolation.

To analyze the importance of the antibody-magnetic particle interaction, the stability of a direct linkage between a biotinylated Fab and streptavidin-coated beads was compared with that of a secondary linkage mediated by the use of a biotinylated secondary antibody (secondary linkage) (Figure 3.3A).

Fab 0.11, the strongest binder, was used in both the conditions, so that variations in cells capture efficiency could be ascribed only to the effect of different Fab-bead connections. Direct linkage was tested by labelling a cell line panel expressing a wide range of HER2 expression levels with biotinylated Fab 0.11, followed by samples incubation with streptavidin-coated beads. For secondary linkage, cells were labelled with non-biotinylated Fab 0.11 and then isolated by adding streptavidin-coated magnetic particles previously saturated with a biotinylated secondary antibody.

Direct linkage allowed isolation of cells more efficiently than the secondary linkage (Figure 3.3B). In particular, the recovery of low HER2-expressing cell lines was strongly affected by the nature of the linkage, with recovery of MCF7 cells increased by 37% ($P < 0.05$, $n = 2$, unpaired *t*-test), and isolation of A431 cells improved by 67% ($P < 0.01$, $n = 2$, unpaired *t*-test). Further analysis of the antibody-bead linkage (performed by Dr Jayati Jain, Howarth laboratory) evaluated the cell

capture performance of a secondary linkage to the magnetic particles mediated by protein L, an immunoglobulin binding protein with high affinity for κ-chain of human immunoglobulins (Tashiro and Montelione, 1995), validating that intermediary links

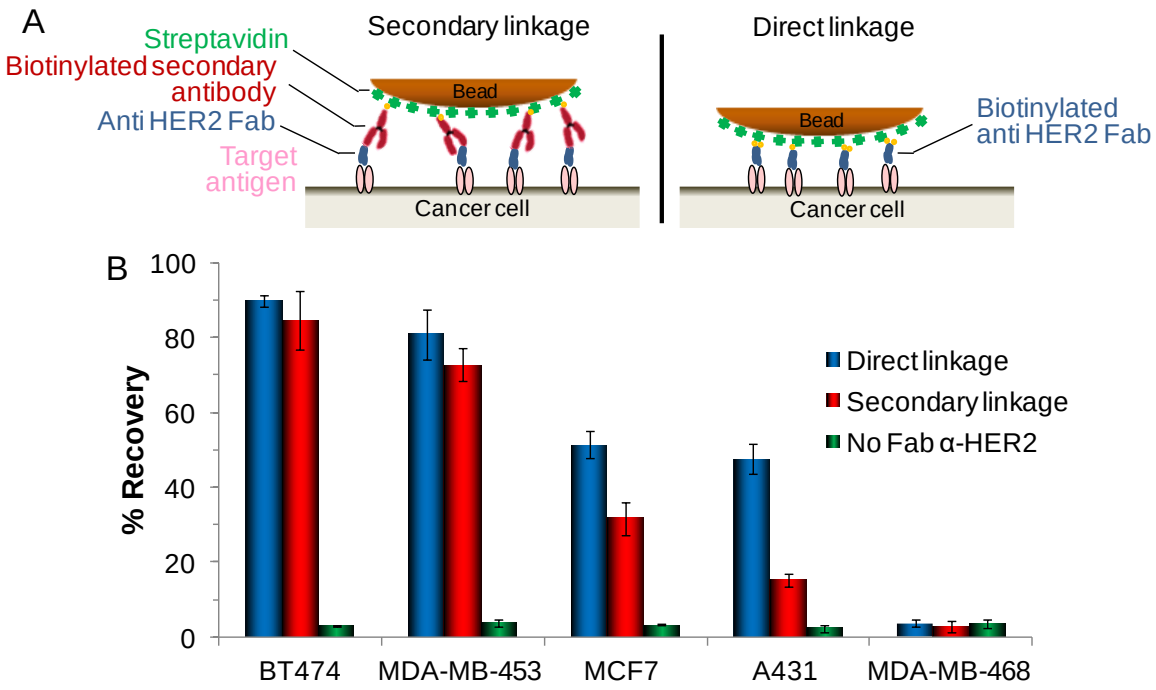

are detrimental for efficient cell capture (Jain et al., 2013).

Figure 3.3. Dependence of cell isolation on the antibody-bead interaction. A) Schematic representation of the two linkages tested. In secondary linkage, non-biotinylated Fab 0.11, used to target HER2 on the cells, interacts with the magnetic particles through a biotinylated secondary antibody. Direct linkage indicates a direct connection between cells labelled with biotinylated Fab 0.11 and streptavidin-coated beads through the biotin/streptavidin system. B) Immunomagnetic cell isolation using different linkages. Cells were labelled with 0.1 µg/mL of Fab 0.11 and recovered using different linkages to the magnetic particles (mean of duplicate ± 1 SD). As control for unspecific binding of cells to the beads Fab 0.11 was omitted (No Fab α-HER2).

To further validate the importance of the bead-antibody interaction, we analyzed such interaction by targeting the epithelial cell adhesion molecule (EpCAM) the most used marker to isolate CTCs (Man et al., 2011b).

A cell line panel varying in EpCAM expression was assembled: A431 cells, characterized by high EpCAM expression levels, were used as positive control for

cell capture experiments, MDA-MB-231 cells express low EpCAM levels, whereas 721.221 EpCAM-null cells were used as negative control (Figure 3.4A),

As previously described for HER2, the isolation efficiency of direct and secondary linkages was compared by using the same biotinylated or non-biotinylated anti EpCAM antibody (Figure 3B). For direct linkage a biotinylated anti-EpCAM antibody was used, whereas for secondary linkage the non-biotinylated anti-EpCAM antibody was bridged to the magnetic beads through a biotinylated secondary antibody.

As observed for HER2, the direct interaction between the antibody used to target cells and the magnetic beads is important to efficiently isolate cells expressing low levels of the target (Figure 3.4B). In fact, recovery of the low EpCAM-expressing cell line MDA-MB-231 increased by 43% ($P < 0.01$, $n = 2$, unpaired t-test).

Therefore, the nature of the connection between the antibody used to target cells and magnetic particles plays a vital role in cell isolation, especially for cells expressing low levels of target antigen.

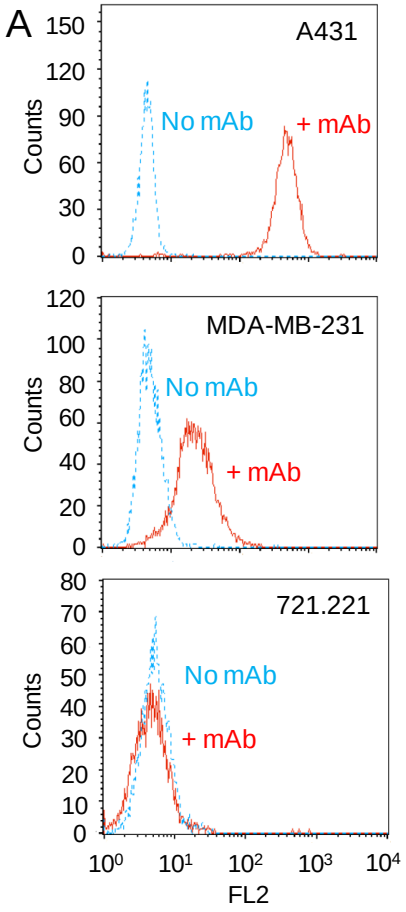

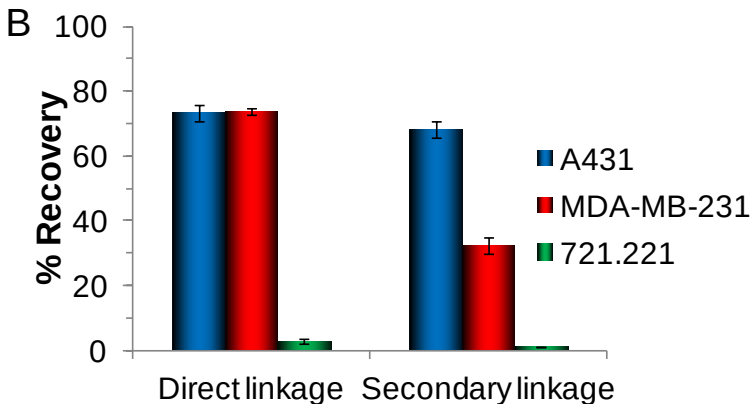

Figure 3.4. Efficiency of EpCAM-based cell isolation using different linkages. A) EpCAM expression levels were determined by flow cytometry. Cells were labelled with anti-EpCAM antibody (+ mAb, red) or without primary antibody (No mAb, blue) prior to staining with a PE-conjugated secondary antibody. A431 cells express high EpCAM levels, MDA-MB-231 cells low EpCAM levels and 721.221 cells are EpCAM-negative. B) Magnetic isolation of a cell line panel varying in EpCAM expression levels using different linkages to the magnetic beads. Error bars are mean of duplicate ± 1 SD.

3.3 Modulation of the cell membrane fluidity to improve magnetic isolation of cells

So far we observed how a tight antibody-target antigen bond and the nanotechnology of the linkage to the magnetic beads enhance cancer cell recovery. The binding of antibodies to cell membrane receptors is dependent on the inherent binding affinity of the antibody, on antibody flexibility (Saphire et al., 2002) and movement (Preiner et al., 2014) as well as on the diffusion and spatial arrangement of the target receptor across the cell membrane (Stanton et al., 1984).

On the basis of these considerations, we analyzed the effect of the modulation of the membrane fluidity on the immunomagnetic isolation of BT474 cells, (Figure 3.5).

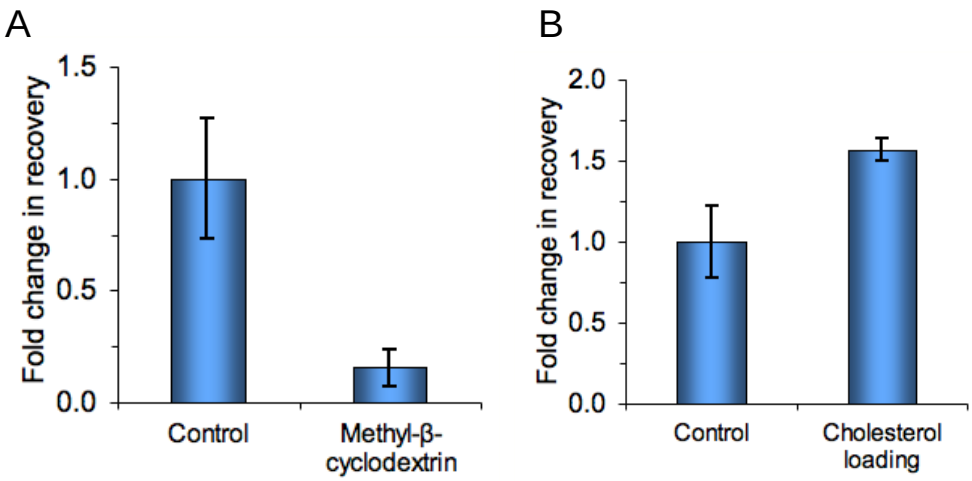

Figure 3.5. Effect of membrane fluidity modulation on cell recovery. BT474 cells were incubated for 1 hour with A) 10 mM methyl-β-cyclodextrin or B) 250 µg/mL water-soluble cholesterol before magnetic isolation. To achieve partial recovery so that even minimal change in capture efficiency would be detectable, BT474 cells were labelled with biotinylated Fab 0.11 at 0.01 µg/mL. prior to cell isolation with streptavidin-coated beads (mean of triplicate ± 1 SD) (data from Dr. Jayati Jain).

Figure 3.5 shows that methyl-β-cyclodextrin, a cyclic oligosaccharide with high affinity for sterols able to deplete cholesterol from the plasma membrane (Zidovetzki and Levitan, 2007) significantly reduced BT474 cell capture (Figure 3.5A, $P < 0.01$, $n = 3$, unpaired *t*-test). Conversely, loading cells with cholesterol before cell isolation improved cell capture by 50% (Figure 3.5B, $P < 0.05$, $n = 3$, unpaired *t*-test), indicating that modulation of the membrane fluidity could affect cell recovery.

Since cholesterol loading of cells resulted in increased BT474 cell isolation, such effect was further investigated on a cell line panel expressing different levels of HER2 (Figure 3.6A) or EpCAM (Figure 3.6B).

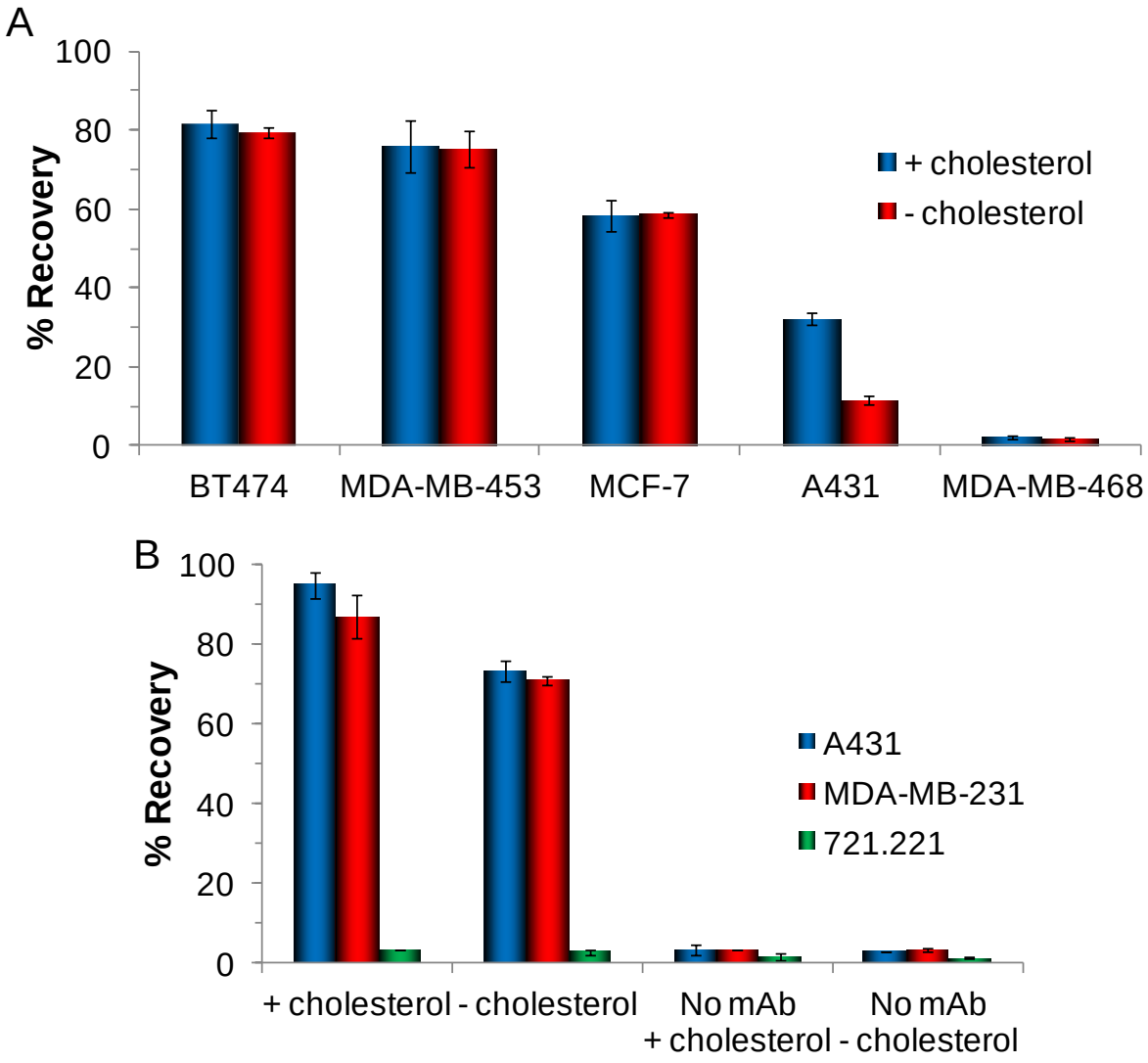

Figure 3.6. Cholesterol effect on the recovery of cells. A) HER2-expressing cells were incubated with or without 250 µg/mL water-soluble cholesterol for 1 hour before labelling with 1 µg/mL biotinylated anti-HER2 Fab 0.11 and magnetic separation with streptavidin-coated magnetic beads. B) Cells varying in EpCAM surface concentration were incubated for 1 hour with or without 250 µg/mL water-soluble cholesterol. Cells were treated with 1 µg/mL biotinylated anti-EpCAM antibody and recovered using magnetic particles coated with streptavidin. As a control for unspecific capture, the primary anti-EpCAM antibody was omitted (no mAb). Error bars are mean of duplicate measurements ± 1 SD.

Loading cells with cholesterol only enhanced capture of cells expressing low levels of the target antigens. Recovery of HER2-low expressing A431 cells improved significantly (Figure 3.6A, $P < 0.005$, $n = 2$, unpaired *t*-test). Capture of MDA-MB-231 cells via EpCAM was enhanced by 1.2-fold, but such improvement was not

statistically significant (Figure 3.6B, *P* = 0.05, n = 2, unpaired *t*-test). Figure 3.6B shows only minimal isolation for EpCAM-null 721.221 or for A431 and MDA-MB-231 in the absence of primary antibody, indicating that the enhancement in cell capture mediated by cholesterol was not dependent on an increased unspecific binding of the magnetic beads to the cells.

To evaluate whether those treatments improved magnetic cell recovery as a consequence of changes in the expression levels of the target receptor, the amount of Fab 0.11 bound to cells in presence of cholesterol or methyl-β-cyclodextrin was determined by flow cytometry (data from Dr. Jayati Jain, Howarth laboratory) (Figure 3.7).

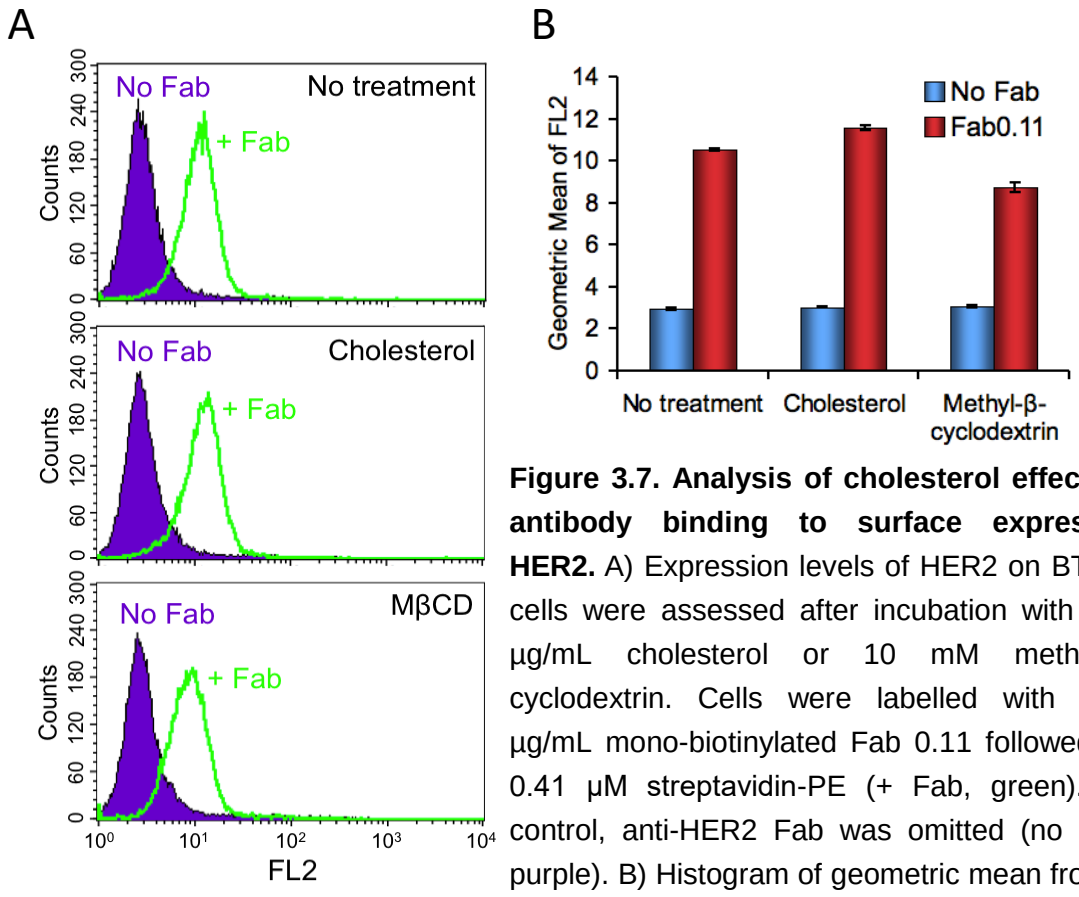

Figure 3.7. Analysis of cholesterol effect on antibody binding to surface expressed HER2. A) Expression levels of HER2 on BT474 cells were assessed after incubation with 250 µg/mL cholesterol or 10 mM methyl-β-cyclodextrin. Cells were labelled with 0.01 µg/mL mono-biotinylated Fab 0.11 followed by 0.41 µM streptavidin-PE (+ Fab, green). As control, anti-HER2 Fab was omitted (no Fab, purple). B) Histogram of geometric mean from A (mean of triplicate ± 1 SD). Presented data are from Dr. Jayati Jain (Howarth laboratory).

Depletion of cholesterol with methyl-β-cyclodextrin decreased by 17% binding of Fab 0.11 to cells ($P < 0.001$, $n = 3$, unpaired *t*-test), whereas cell loading with cholesterol increased cells staining by 9% ($P < 0.001$, $n = 3$, unpaired *t*-test).

Increasing of antibody binding to cell surface receptors upon cholesterol loading has been previously described (Beck et al., 2010; Polyak et al., 2003) and it is likely to be dependent on an alteration of the plasma membrane microenvironment resulting in influence of HER2 conformation and/or accessibility of its epitope.

The reasons for such an improved immunomagnetic isolation of cancer cells after treatment with cholesterol are yet not fully understood. Modulation of the plasma membrane fluidity, in fact, could influence not only the binding of the antibody to its cognate target, but also the receptor diffusion across the plane of the membrane as well as the magnetic bead-cell synapse by promoting cell membrane to wrap around the magnetic particles (Maltez-da Costa et al., 2012). It has already been demonstrated that members of the human epidermal growth factor receptor family are associated with lipid rafts, cholesterol-rich microdomains involved in the membrane trafficking and signalling (Simons and Gerl, 2010). Increasing the content of membrane cholesterol correlated with diffusion of HER2 and EGFR, whereas cholesterol depletion confined mobility of the receptors (Orr et al., 2005). Therefore, the observed enhanced cell recovery after cell loading with cholesterol (Figure 3.6) could be a consequence of increased HER2/EpCAM diffusion across the plane of the membrane, potentially resulting in the formation of receptor clusters at specific membrane microdomains that could enable a better antibody binding.

3.4 Enhanced conditions improve cell recovery with low affinity antibody

Optimizing bead linkage and cholesterol loading allowed efficient isolation of cancer cells expressing low levels of EpCAM and HER2.

To test whether these optimizations were restricted only to antibodies with high affinity, their effect was evaluated using a point mutant of the humanized Fab hu4D5 with moderate affinity (Fab 1.4, K_d= 1.4 nmol/L) (Figure 3.8).

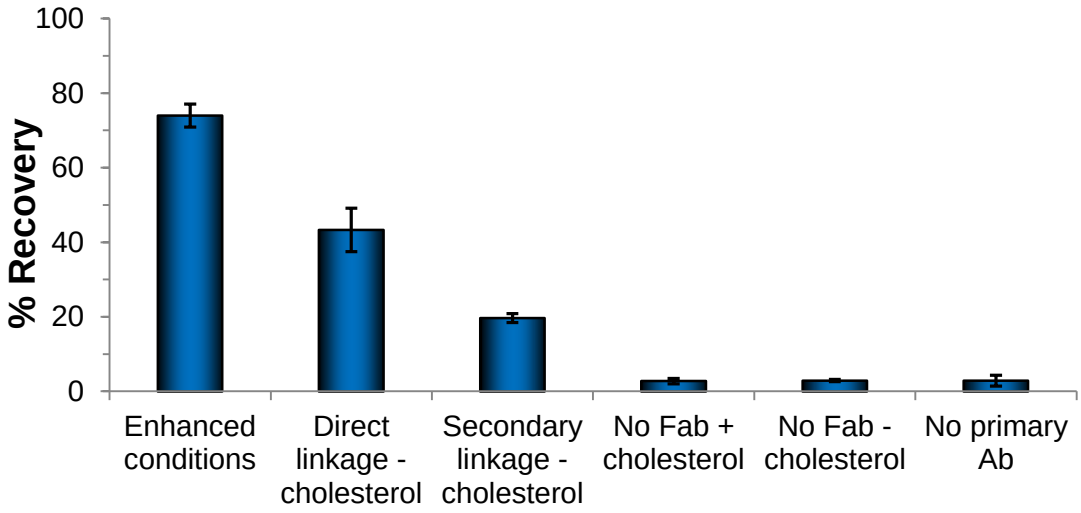

Figure 3.8. Effect of cholesterol loading and direct bead linkage also apply to antibody with moderate affinity. BT474 cells were incubated with 0.1 µg/mL Fab 1.4 and isolation was performed (i) with secondary linkage without cholesterol loading, (ii) with direct linkage without cholesterol treatment or (iii) with cholesterol loading and direct connection to streptavidin-coated beads (enhanced conditions). As a control each of the conditions was tested in the absence of primary antibody (mean of duplicate ± 1SD).

Direct linkage of Fab 1.4 improved BT474 cell recovery by 54% (direct linkage, $P < 0.05$, $n = 2$, unpaired *t*-test), with a further increase in cell isolation by 41% upon cholesterol loading (enhanced conditions, $P < 0.05$, $n = 2$, unpaired *t*-test). These results demonstrated that enhanced conditions (direct connection to magnetic particles and cholesterol loading) are useful even when using moderate binders for capturing cells.

3.5 Effect of enhanced conditions in isolating cancer cells from human blood

So far, we observed how high antibody affinity, cholesterol loading and ultra-stable linkage to the magnetic beads improved the isolation sensitivity of cancer cells.

However the low frequency of CTCs in the peripheral blood of patients (estimated to be one cell per million of white blood cells), rendered isolation of CTCs highly dependent on the presence of high expression levels of tumour antigens, strongly limiting CTCs use in the clinic (Dharmasiri et al., 2010).

To test whether the enhanced conditions previously described would be useful to isolate CTCs from clinical samples, as a model, cancer cell lines were spiked into human blood.

MCF7, A431 and MDA-MB-468 cells were labelled with carboxyfluorescein diacetate succinimidyl ester (CFSE) and spiked into whole human blood prior to hypotonic red blood lysis (Figure 3.9). The resulting cells mixture, containing CFSE-labelled cancer cells and white blood cells, underwent to immunomagnetic isolation under either enhanced conditions (high affinity anti-HER2 Fab 0.11, direct antibody-magnetic beads linkage and cholesterol loading) or standard conditions (anti-HER2 Fab 0.35, secondary antibody linkage to beads, no cholesterol loading). Isolated cells, identified as CFSE-positive and CD45-negative (a marker of leucocytes), were counted via fluorescence microscopy (Figure 3.9).

Isolation of spiked cells with standard conditions poorly enriched spiked cells (Figure 3.9 B). Conversely, enhanced conditions (Fab 0.11, direct antibody-magnetic beads linkage and cholesterol loading) significantly increased the recovery of MCF7 ($P < 0.01$, $n = 2$, unpaired *t*-test) and A431 cells ($P < 0.01$, $n = 2$, unpaired *t*-test) (Figure 3.9B). Capture of cells spiked in human blood was specific as indicated by the lack of isolation of MDA-MB-468 cells (HER2 negative) (Figure 3.9B) and by the absence of CD45-positive cells (Figure 3.9C)

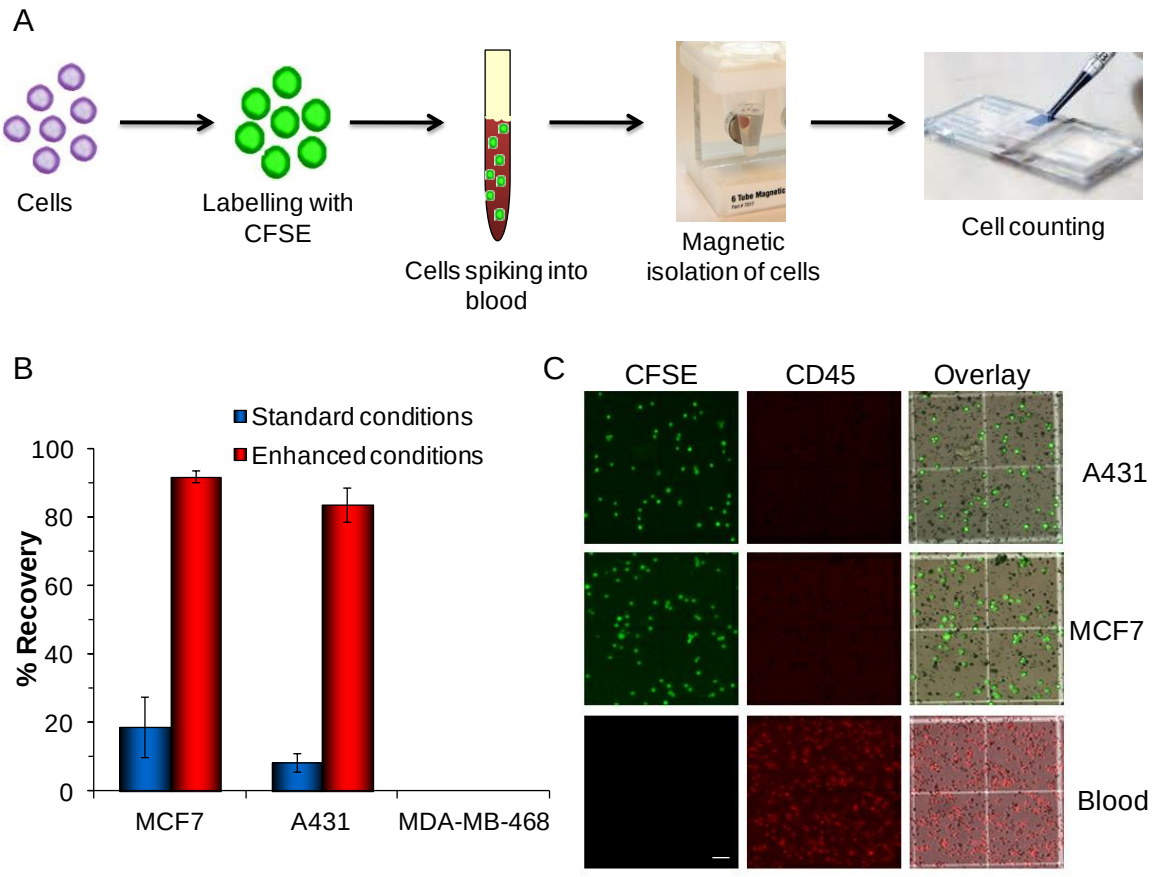

Figure 3.9 Isolation of cells from human blood. A) Cartoon of the procedure to capture cells from human blood. 250,000 CFSE-labelled cells were spiked into 1 mL of human blood to mimic CTC isolation from patient samples. Whole blood underwent hypotonic lysis, cellular debris removed by centrifugation and remaining cells were subjected to magnetic isolation according to standard or enhanced conditions. Recovered cells were counted and identified by fluorescence microscopy. B) CFSE-labelled MDA-MB-468 (HER2 null), MCF7 and A431 cells (both low HER2) were doped into human blood. Following hypotonic lysis of red blood cells, cancer cells were immunomagnetic isolated with standard conditions (10 µg/mL non-biotinylated Fab 0.35, followed by secondary linkage) or enhanced conditions (10 µg/mL biotinylated Fab 0.11, cholesterol loading followed by streptavidin-mediated direct linkage to the magnetic beads). Cells were analyzed by immunofluorescence and only CFSE-positive, CD45-negative cells were counted (mean of duplicate ± 1 SD). C) Fluorescence microscopy of cells isolated with enhanced conditions from human blood. Left column shows CFSE-labelled A431 (top row) and MCF7 cells (middle row). Anti-CD45-PE staining (leucocyte marker) is shown in the middle column and overlay (CFSE: green, anti-CD45-PE: red and brightfield: greyscale) is displayed in the right column. As a positive control for CD45-staining, whole blood was stained following to hypotonic lysis of red blood cells. Scale bar 50 µm.

3.6 Discussion

In this chapter some of the biochemical features important for an efficient immunomagnetic isolation of tumour cells were investigated. In particular we have demonstrated how the antibody affinity, the nanotechnology of the linkage to magnetic particles and cholesterol levels all contribute to enhance magnetic isolation of tumour cells.

By comparing two anti-HER2 Fabs having high affinity for the target receptor (Fab 0.11: K_d = 0.11 nmol/L and Fab 0.35: K_d = 0.35 nmol/L), we demonstrated that the antibody affinity plays a key role for cancer cell capture, with only a limited isolation of cells expressing low levels of HER2 even using a Fab with a high (K_d = 0.35 nmol/L), but not the highest, affinity for HER2. Designing antibodies with exceptional affinity is an attractive route for cancer imaging and therapy (Clark et al., 2006), but antibody affinity below 10 nM could have a negative effect on tumour uptake, by confining antibodies at the tumour margins (Schmidt and Wittrup, 2009). For immunomagnetic isolation of cancer cells, instead, extraordinary antibody affinity is required as the antigen-antibody interaction has to endure the magneric field and the flow-induced shear forces (Dharmasiri et al., 2010).

The importance of the nature of the antibody-magnetic particle linkage was investigated by comparing the direct connection of a biotinylated antibody to streptavidin-coated magnetic particles with a secondary interaction mediated by a secondary biotinylated antibody. Exploiting the ultra-stable interaction of the biotin/streptavidin system to mediate a direct contact between the antibody used to target the cells and the magnetic beads resulted in a substantial enhancement in cell recovery, especially for low HER2 and low EpCAM-expressing cell lines. Comparative studies of direct and indirect (secondary) cells-magnetic bead linkage

have previously quantified cells isolation in terms of magnetophoretic mobility (McCloskey et al., 2001, 2003b). However such reports did not investigate in details the relationship between the bead linkage and the targeted receptors concentration on the cell surface.

Cholesterol plays important roles in the physical properties of the cell membranes, such as fluidity, elasticity and integrity, as well as a stabilization of membrane proteins (Cooper, 1978). The effect of the modulation of the membrane fluidity was investigated by depleting or increasing the cholesterol content of the plasma membrane. We found that cholesterol depletion with methyl-β-cyclodextrin drastically reduced cells isolation, whereas increasing the levels of cholesterol by applying a water-soluble form of the sterol to cells prior to immunomagnetic isolation substantially enhanced cell recovery. Cholesterol loading is easy and quick, so this approach could be applicable to clinical samples.

The reasons for such increased isolation ability upon loading cells with cholesterol are not fully understood. Cholesterol, in fact, can influence the mobility of receptors across the plane of the plasma membrane (Orr et al., 2005), facilitating the formation of large receptor clusters that could be more efficiently bound by antibodies (Nagy et al., 2002). However, alterations of the membrane fluidity could also lead to changes of receptors conformation and/or accessibility, ensuring a better antibody docking. Exploiting Tween-20 to unmask EpCAM epitopes has already proved to be beneficial for isolation of circulating epithelial tumour cells (CETC), but was associated with damaging effects on aging CETC (Hekimian et al., 2012).

All together these results suggest that to enhance recovery of cancer cells bearing low levels of tumour antigen one should (i) load cells with cholesterol, (ii) avoid any intermediary weak link by using a direct and stable connection between the

antibody and the beads and (iii) use the highest affinity biotinylated antibody available.

By testing a panel of human cell lines spanning a wide expression range of HER2 and EpCAM, our enhanced conditions allowed specific and quantitative isolation of cell lines expressing low levels of both the markers.

The work presented in this chapter should guide future approaches for the affinity-based selection of cells and could also extend to other methods. Positive selection of cancer cells by directly targeting tumour antigens has the advantage of being easy, fast and highly customizable, but it requires knowledge about the target, as well as a stable and elevated expression of the targeting antigen (Alix-Panabières and Pantel, 2014). Isolation of CTCs by depletion of leucocytes from blood samples is an interesting alternative to positive selection, but complete removal of white blood cells is hard to achieve, resulting in low samples purity (Liu et al., 2011). Microfluidic-based approaches often combine affinity-dependent and independent selection methods, but sample purity and throughput are still a major issue (Ozkumur et al., 2013). However, both the negative selection and microfluidic isolation strategies could benefit from using antibodies with extraordinary affinity, ultra-stable antibody-bead connections and cholesterol loading to improve cells isolation efficiency. Furthermore, the advancements described in this chapter are not restricted only to the isolation of cancer cells but could apply also to stem cells selection (Gaipa et al., 2003; Perseghin et al., 2005) and sorting of immune cells for adoptive transfer (Di Ianni et al., 2009).

The work presented in this chapter improved the recovery sensitivity of cancer cells, rendering their isolation less constrained by the antigen expression levels.

In this way, it may be possible to enlarge the range of cellular targets and move toward a clinical application of CTC detection for (early) cancer diagnosis.

Chapter 4 : Generation of affibody chains for cancer cell capture

Self-assembly of protein polymers to isolate cancer cells

In Chapter 3 we observed that isolation of cells expressing low levels of tumour markers depends on ultra-stable interactions between the binding protein and the magnetic bead as well as on the affinity of the antibody used.

The large majority of commonly used antibodies has affinity in the 10-100 nanomolar range (Davies and Cohen, 1996) and, according to the presented data, such binding strength could be not sufficient for sensitive cell capture (Chapter 3, Figure 3.2B).

A way to overcome this limit is represented by multivalency, a powerful principle used in several biological processes as well as in the synthesis of supramolecular complexes to achieve strong and specific molecular recognition events (Kiessling et al., 2000, 2006; Krishnamurthy et al., 2006).

Several approaches have been recently developed to enhance capture of CTCs through the use of multi-dentate ligands. Dendrimers, thanks to their highly-branched structure and large number of functional ending groups, represent a versatile scaffold for the development of multivalent and multifunctional nanoconjugates (Kaltenbach et al., 2011; Silpe et al., 2013). Multivalent antibody-decorated dendrimers have proved effective in isolating cancer cells (Myung et al., 2011, 2014). However antibody immobilization on the dendrimer surface is usually non site-specific (Fischer-Durand et al., 2010; Wängler et al., 2008) and could require the use of chemicals that may affect the antibody's paratope.

Microfluidic surfaces and nanoparticles coated with multivalent DNA aptamers also showed promise for rare cells isolation (Sheng et al., 2013; Zhao et al., 2012).

However, the strong charge of DNA aptamers can limit their structural diversity (Ahmad et al., 2011) and may increase non-specific binding to cationic surfaces or pattern-recognition receptors (Mogensen, 2009).

With the aim of improving the efficiency of cancer cells isolation, in this chapter will be presented a peptide-peptide covalent ligation system and its application to generate affibody chains for sensitive isolation of tumour cells.

4.1 Generation of SpyLigase and its features

Peptide tags are useful tools to extend the properties of a protein. Modifying a protein of interest with small peptide tags is a generic route to achieve efficient purification, detection, immobilization and derivatization, with minimal disturbance of the protein folding or activity (Huh et al., 2003; Rashidian et al., 2013). However, peptide tags generally form weak and reversible interactions with protein partners (London et al., 2010), and therefore, the development of peptide-protein or peptide-peptide pairs forming irreversible covalent bonds would be of great value for biotechnology.

To create a peptide-peptide covalent ligation system, Dr. Jacob Fierer (a Howarth laboratory member) engineered the second immunoglobulin-like collagen adhesion domain (CnaB2) of the fibronectin-binding protein FbaB from *Streptococcus pyogenes*. By dissecting the CnaB2 domain as has been done previously for SpyTag/SpyCatcher (Figure 4.1A) (Zakeri et al., 2012), a new peptide tag (KTag) containing the isopeptide bond-reactive Lysine was obtained (Figure 4.1B).

SpyTag was left unmodified, whereas the remaining CnaB2 domain scaffold, bearing the reactive Glutamate residue was circularly permuted (Yu and Lutz, 2011) to obtain SpyLigase (Figure 4.1B) (Fierer et al., 2014). To test whether SpyLigase could irreversibly lock the two peptide tags, SpyTag was fused at the N-terminus of maltose binding protein (SpyTag-MBP) and KTag at the C-terminus of the small ubiquitin-like modifier (SUMO, SUMO-KTag). 10 μM SpyTag-MBP and 10 μM SUMO-KTag were mixed with 40 μM SpyLigase and incubated for 24 h at 4°C prior

to SDS-PAGE (Figure 4.1C). Figure 4.1C shows that incubating SpyLigase with the two peptide tags enabled the formation of a covalent adduct capable of resisting boiling in SDS (lane 6). Conversely, using in the reaction mixture a variant of SpyLigase where the reactive Glutamate was mutated to Glutamine (SpyLigase EQ, lane 7), SpyTag containing an Alanine mutation of the reactive Aspartate (SpyTag DA, lane 8) or mixing SpyLigase with only one peptide tag at a time (lanes 9-10) did not result in the generation of the complex. Therefore, when the three partners are mixed together SpyLigase could dock SpyTag and KTag, reconstituting the isopeptide-reactive triad ensuring the amide bond formation, so locking covalently the two peptides.

To verify whether SpyLigase covalently locks together the two peptide tags, SUMO-SpyTag and SUMO-KTag were mixed with SpyLigase and analyzed by electrospray-ionization mass spectrometry. The mass of the formed complex (26,660 Da) was consistent with the individual masses of the proteins minus the mass of water released upon formation of the isopeptide bond (26,659 Da), confirming the covalent nature of the interaction (Figure 4.1D).

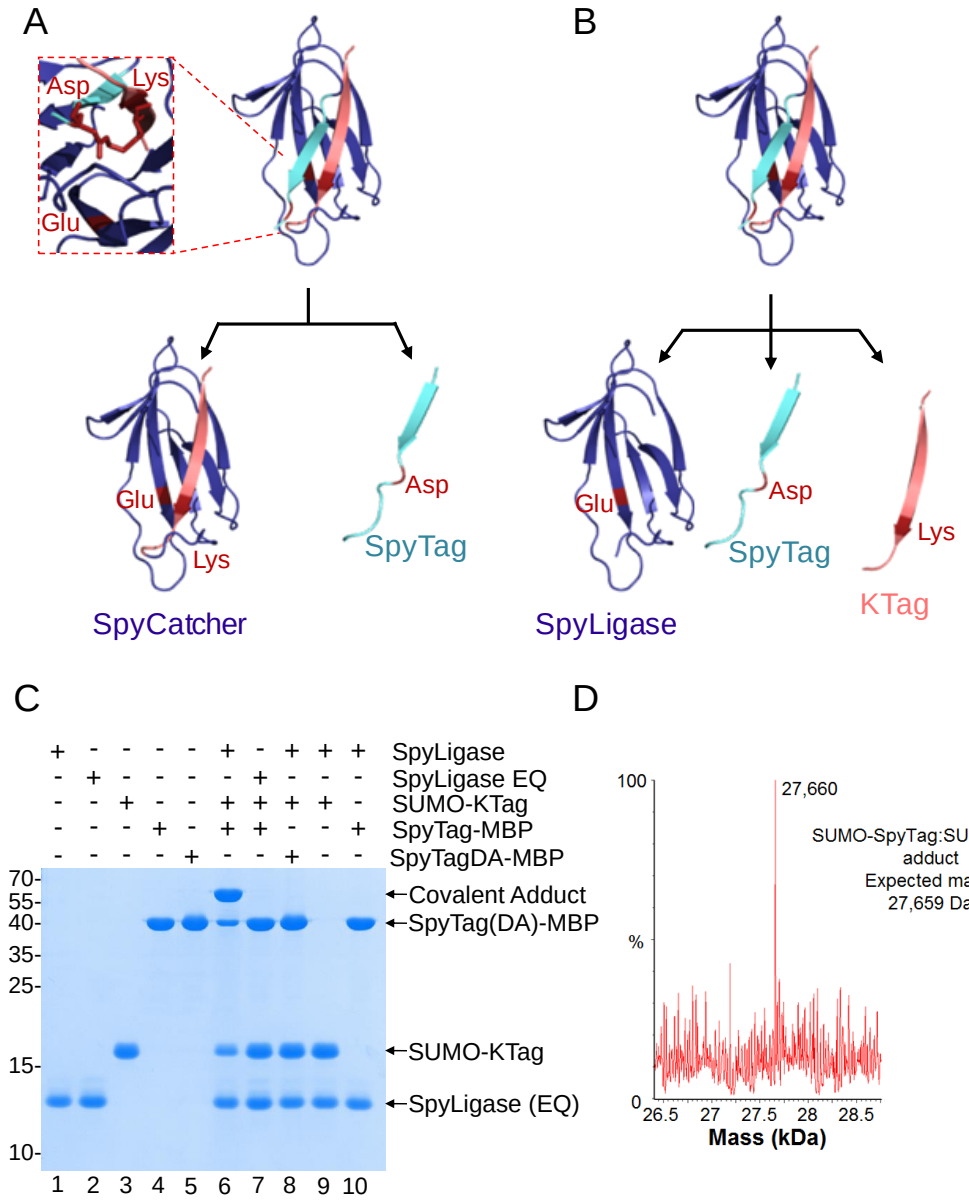

Figure 4.1. Engineering the CnaB2 domain. A) Cartoon of splitting the CnaB2 domain into a protein/peptide pair (based on PDB 2X5P). The cyan-coloured β-strand containing the reactive Aspartate identifies SpyTag, whereas SpyCatcher (purple) bears the reactive Glutamate and Lysine (in the pink-coloured β-strand). Key residues for the isopeptide bond formation are in red. Inset shows the isopeptide bond's structure. B) Cartoon of the splitting strategy to make two peptide tags: SpyTag (cyan) with the reactive Glutamic acid and KTag (pink) bearing the reactive Lysine. The remaining protein domain (SpyLigase, purple) contains the reactive Glutamic acid residue. Isopeptide bond-reactive residues are shown in red. C) SpyTag-MBP and SUMO-KTag formed a covalent complex when mixed with SpyLigase for 24 h (lane 6). Mutation of the reactive residues in SpyLigase (SpyLigase EQ) and SpyTag (SpyTag DA) as well as mixing SpyLigase with only one peptide tag at a time did not result in formation of the complex, consistent with the SpyLigase-mediated peptide-peptide covalent ligation. D) Mass spectrometry of the complex between SUMO-SpyTag and SUMO-KTag. Data in panels C and D are from Dr. Jacob Fierer (Howarth laboratory).

4.1.1 Stability of SpyLigase and its effect on ligation efficiency

Splitting and engineering the CnaB2 domain enabled the generation of a new peptide-peptide covalent ligation system. To better understand the SpyLigase reaction, the effect of the temperature was analyzed. 10 µM SUMO-KTag and 10 µM SpyTag-MBP were incubated with 40 µM SpyLigase and let to react for 24 h at 4, 12, 25 and 37°C prior to SDS-PAGE analysis (Figure 4.2A).

SpyLigase enabled maximum ligation of the two peptide tags at 4°C with gradual decrease of ligation performance as the temperature increased to 37°C (Figure 4.2.A).

To assess whether the temperature-dependent reduction of the SpyLigase-mediated ligation efficiency was due to a loss of structural stability of SpyLigase, circular dichroism (CD) studies were performed (Figure 4.2B and C).

The temperature-dependent profile of SpyLigase showed a change in secondary structure for SpyLigase as temperature was increased from 4ºC to 37ºC, consistent with a temperature-dependent loss of structural order (Figure 4.2B). Moreover to identify the temperature causing a transition in SpyLigase's structure, thermal denaturation measurements were performed (Figure 4.2C).

SpyLigase showed a gradual transition typical of molten globules (Vamvaca et al., 2004), indicating that the protein domain is characterized by a dynamic structure (Figure 4.2C).

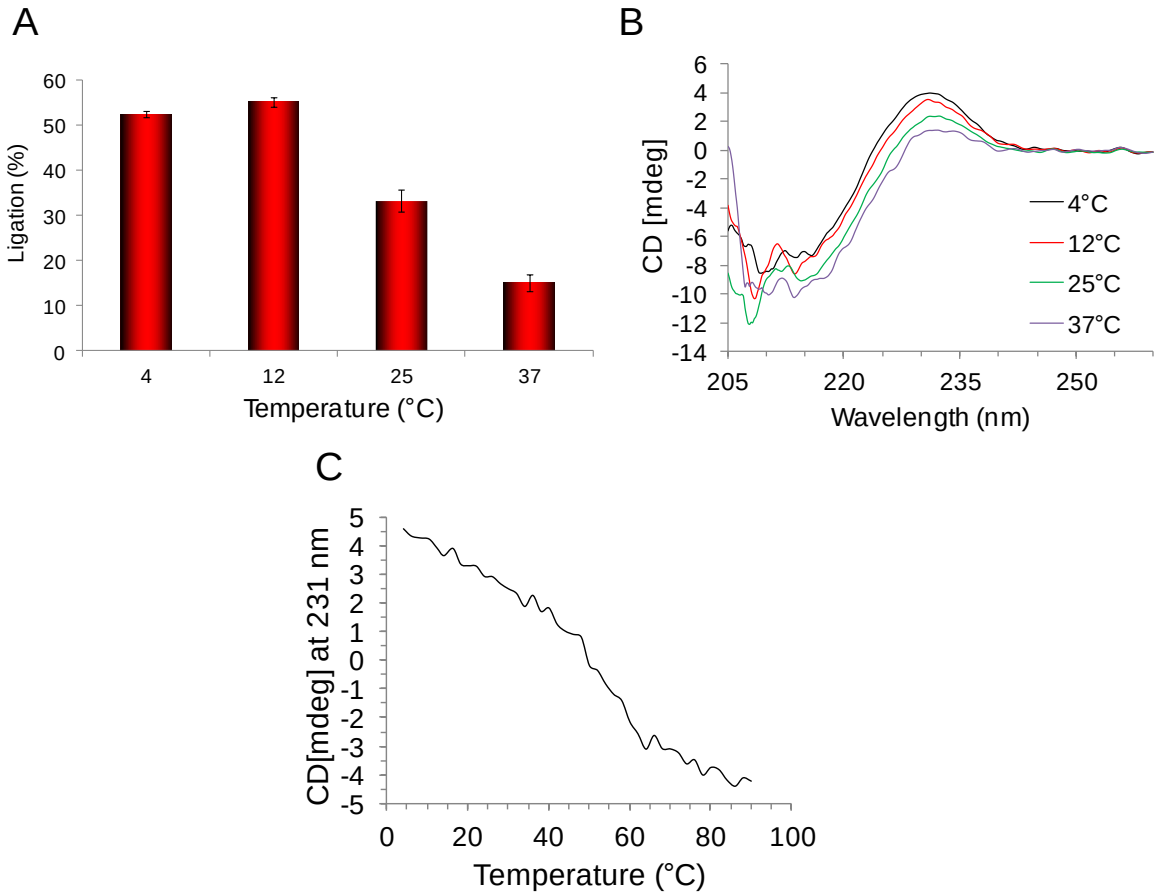

Figure 4.2. Temperature dependence of SpyLigase reaction. A) SpyLigase was incubated with SUMO-KTag and SpyTag-MBP for 24 h at the indicated temperature before SDS-PAGE. Ligation efficiency was quantified by densitometry. Data (from Dr. Jacob Fierer) are mean of triplicate ±1 SD. B) Far UV-spectra of SpyLigase were recorded in the wavelength range 205-260 nm at 4, 12, 25 and 37°C, collecting data at 0.2 nm intervals. C) Thermal unfolding profile of SpyLigase. SpyLigase was heated from 4 to 90°C at 2°C/min and spectra recorded between 215 and 250 nm. Circular dichroism intensity at 231 nm (corresponding to the peak observed in B) was plotted. Spectra were recorded in triplicate, averaged and smoothed with a Savitzky-Golay filter (Savitzky and Golay, 1964).

4.1.2 Effect of SpyTag and KTag topology on covalent bioconjugation

Protein engineering enabled the development of several techniques for bioconjugation, including native chemical ligation (Thapa et al., 2014), split inteins (Shah and Muir, 2011), sortase (Ritzefeld, 2014) and subtiligase (Wildes and Wells, 2010). However, application of these methods is restricted to the use of protein termini, thus enabling to form only linear conjugates.

So far we observed that SpyLigase enables the formation of a covalent bond between SpyTag and KTag simply by mixing together the three molecular partners. To explore whether our covalent peptide-peptide ligation system could enable the formation of non-linear architectures, the effect of topology of the peptide tags on SpyLigase reaction was investigated. SpyTag and KTag were fused at the N-terminus, C-terminus or in the middle of a protein and their ability in forming an amide bond upon mixing with SpyLigase was determined by SDS-PAGE (Figure 4.3). KTag was fused at the N-terminus of MBP (KTag-MBP), at the C-terminus of SUMO (SUMO-KTag) or inserted in the middle of a protein (MBP-KTag-Zif-DA, characterized by the presence of KTag between MBP and the Zif268 zinc finger and a C-terminal unreactive SpyTag) and allowed reacting with SpyTag-MBP in presence of SpyLigase overnight at 4°C before SDS-PAGE. KTag was able to form a complex with SpyTag-MBP when placed at the N-terminus (Figure 4.3A, lane 7), C-terminus (Figure 4.3A, lane 8) or inserted in the middle of a protein (Figure 4.3A, lane 9). Similarly to KTag, the topology-dependence of SpyTag was assessed by incubating SpyTag-MBP (N-terminal SpyTag), SUMO-SpyTag (C-terminal SpyTag) and MBP-SpyTag-Zif-DA (internal SpyTag) with SUMO-KTag and SpyLigase. Reactions proceeded overnight at 4°C and ligation was assessed by SDS-PAGE with Coomassie staining (Figure 4.3B).

Figure 4.3B shows that SpyLigase reaction is unaffected by SpyTag position (lanes 7-9). Moreover, SpyLigase-mediated ligation of SpyTag and KTag occurred even when both the peptide tags were position in the middle of a protein, enabling the generation of protein conjugates with non-linear structures (Figure 4.3B, lane 10).

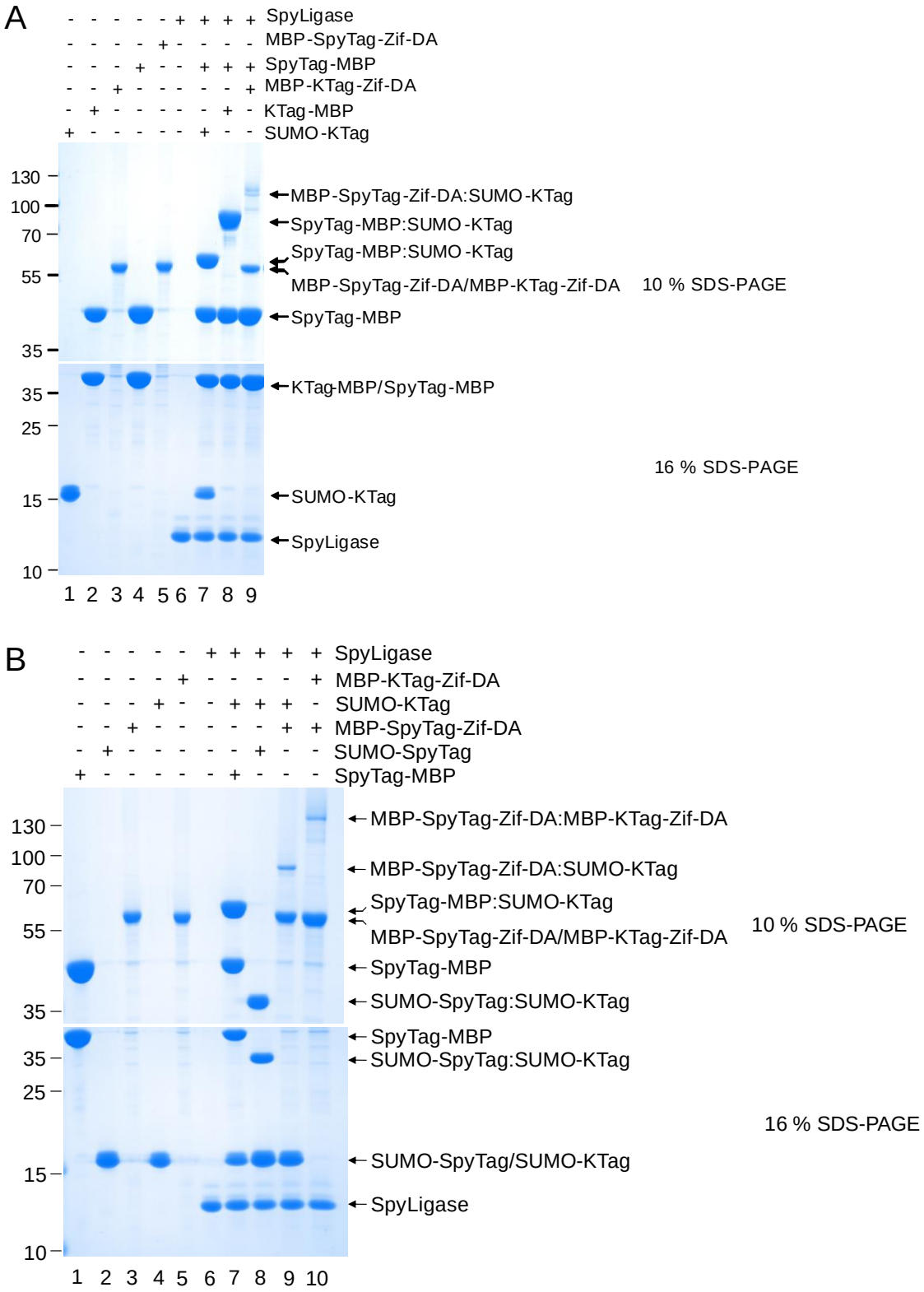

Figure 4.3. SpyTag/KTag topology effect on SpyLigase reaction. A) KTag was placed at the C-terminus, N-terminus or internal to a protein and analyzed, after reaction overnight at 4°C with SpyLigase, by SDS-PAGE and Coomassie staining. B) SpyTag placed at the termini or in the middle of interest proteins reacted overnight at 4°C with proteins bearing KTag upon mixing with SpyLigase.

4.2 Generation and characterization of protein polymers

In chapter 3 we observed that efficient immunomagnetic capture of cancer cells is strongly dependent on (i) high expression levels of tumour markers, (ii) high affinity of the antibody for its cognate target, and (iii) ultra-stable links at the antibody-bead interface.

To reduce the biomarkers expression level required for cell recovery, we hypothesized that forming self-assembled chains of antibodies would have the advantage of establishing multivalent interactions with the target cell, helping the magnetic beads to encounter more copies of the tumor antigen. Therefore, antibody chains could form more stable immune-synapses, overcoming the need for binders with exceptional affinity. Moreover, since weak links are detrimental for cell isolation, it is vital that multivalent antibody chains are linked together and to the magnetic beads through irreversible covalent bonds.

Self-assembled antibody polymers have been previously made by exploiting complementary oligonucleotides (Kazane et al., 2013), protein-small molecules interactions (Li et al., 2010b) and self-associating peptides (Wang et al., 2013b; Zhu et al., 2010). Although all these methods successfully built antibody multimers, antibody monomers were linked together through non-covalent reversible interactions, potentially resulting in multimer dissociation and rearrangement. Therefore, with the aim to generate self-assembled covalent antibody polymers for sensitive cell capture, we decided to exploit the SpyLigase system.

4.2.1 Generation of affibody and antibody chains

To develop multivalent binding molecules for improved isolation of cancer cells, SpyLigase was incubated with affibodies (a non-immunoglobulin scaffold binding protein) (Löfblom et al., 2010) tailored with SpyTag and KTag (Figure 4.4A).

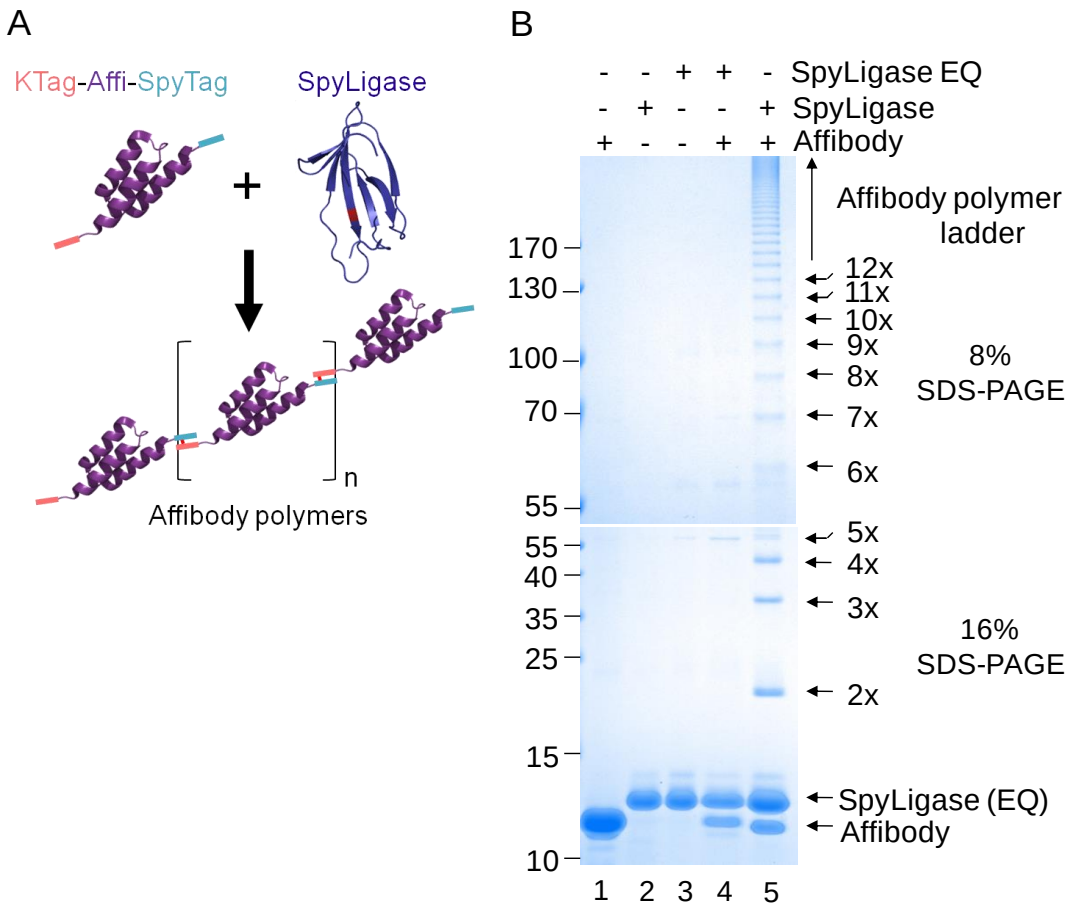

Figure 4.4. Generation of affibody polymers. A) Cartoon of the SpyLigase-mediated polymerization of affibody bearing KTag at the N-terminus and SpyTag at the C-terminus. B) Polymerization of an anti-EGFR affibody (cloned by Dr. Jacob Fierer). Affibody was incubated at 4°C for 24 h with SpyLigase before SDS-PAGE. As control, affibodies were mixed with SpyLigase EQ, an unreactive mutant of SpyLigase. Lower panel (16% gel) shows low molecular weight (Mw) species, whereas the upper panel (8% gel) displays high Mw polymers.

Figure 4.4B shows that incubating affibodies tailored with both the peptide tags in presence of SpyLigase ensured the efficient formation of polymers resistant to

boiling in SDS (lane 5). No affibody polymers formed with the non-reactive SpyLigase EQ (lane 4), consistent with the isopeptide bond formation-based polymerization.

To further elucidate the SpyLigase-based polymerization, the formation of affibody polymers over time was investigated. 5 µM KTag-Affi-SpyTag was incubated with 20 µM SpyLigase at 4°C for 0.5, 1, 2, 4, 6, 8, 12, 24 and 48 hours. Polymerization was stopped by addition to the reaction mixtures of Laemmli buffer (Laemmli, 1970) and sample boiling. Samples were analyzed by SDS-PAGE and polymerization extent was determined by densitometry (Figure 4.5).

SpyLigase covalently locked affibody monomers quickly, with affibody tetramers formed after 0.5 h of incubation (Figure 4.5A, lane 3). Longer incubation time resulted in increased polymerization extent, with affibody polymers extending more than 16 units after 24 and 48 hours of incubation (Figure 4.5A, lanes 10-11). Interenstingly, it is possible to note the presence of a band with molecular weight similar to that of affibody dimer (2x) and trimer (3x) (Figure 4.5A, lanes 8-11) but characterized by a higher electrophoretic mobility. These species are likely to be the result of the affibody dimer and trimer cyclization (Figure 4.5B) and could compete with the forming linear chains, preventing to reach polymerization completion.

Notably, the decrease over time of small polymeric species (Figure 4.5A, lane 10, dimer and trimer), suggests that short polymers might act as seeds for the generation of larger polymers.

To quantify the polymerization extent affibody was mixed with SpyLigase as previously described. Polymerization was stopped at the indicated time by addition to the reaction mixtures of Laemmli buffer followed by samples boiling. The amount of formed polymers was analyzed by SDS-PAGE with Coomassie staining.

Polymerization extent was determined by densitometry and expressed as in function of the amount of reacted affibody over time (Figure 4.5C).

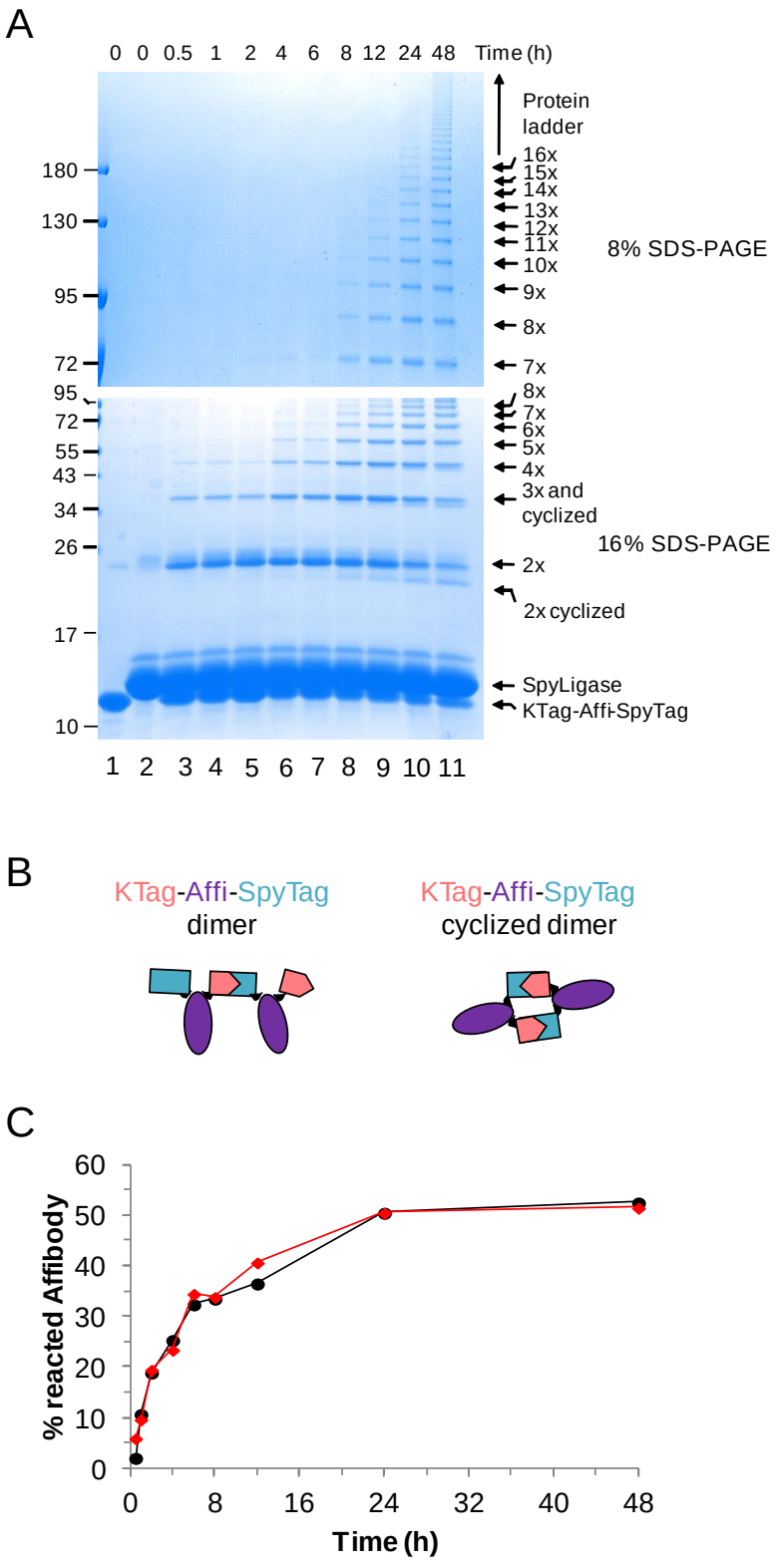

Figure 4.5. Analysis of affibody polymerization over time. A) SpyLigase-mediated polymerization was followed over time by stopping the reaction with Laemmli buffer and samples boiling. Lower panel (16% SDS-PAGE) shows low molecular weight species, whereas larger polymers are displayed in the upper panel (8% SDS-PAGE). B) Cartoon of affibody dimer and cyclized affibody dimer. C) Quantification of the polymerization extent. 5 µM KTag-Affi-SpyTag was mixed with 20 µM SpyLigase and incubated at 4°C for the indicated time. Samples were analyzed by SDS-PAGE with Coomassie staining. The amount of formed polymers was determined by quantifying through densitometry the band corresponding to KTag-Affi-SpyTag.

Affibody chains self-assembled quickly, with 50% of the maximum polymerization reached in ~4 hours (Figure 4.5C).

To validate the generality of the SpyLigase-dependent polymerization, an anti-HER2 Fab antibody fragment was used to build antibody multimers. To perform self-assembly of the Fab fragment, the N-terminus of the heavy chain was tailored with SpyTag, whereas KTag was fused at the C-terminus of the light chain. The antibody was mixed with SpyLigase and incubated at 4°C for 24 hours prior to SDS-PAGE (Figure 4.6).

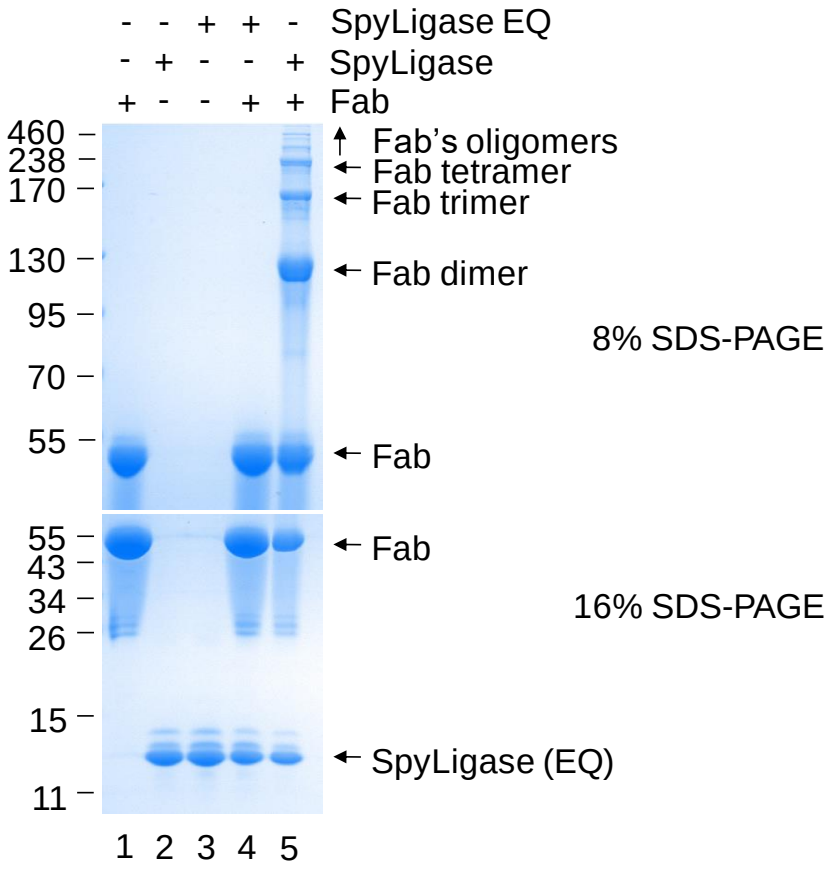

Figure 4.6. Self-assembly of antibody polymers. 150 µM SpyLigase was incubated with 50 µM SpyTag-Fab-KTag (Fab) at 4°C for 24 h, and polymerization was verified by SDS-PAGE with Coomassie staining. As control, Fab was incubated with the non reactive SpyLigase EQ.

As previously observed for affibody polymerization, SpyLigase enabled the efficient formation of antibody multimers (Figure 4.6, lane 5). Incubation of the Fab fragment with the non reactive SpyLigase EQ completely abolished the formation of antibody polymers, consistent with the SpyLigase-dependent ligation.

According to the data presented, SpyLigase provides a valuable tool for the irreversible self-assembly of SpyTag/KTag-tailored proteins. In fact, in addition to efficiently and quickly promoting the formation of protein polymers, the small size of SpyTag (13 residues) and KTag (10 residues), enabled the tags conjugation in a topology-independent way, opening new routes for the development of protein assemblies with non-linear and complex architectures.

4.3 Affibody polymers for magnetic isolation of tumour cells

Immunomagnetic isolation of cancer cells relies on the binding of antibodies labelled with magnetic particles to cell surface targets, with cells isolation performed by applying a magnetic field. Therefore, the interactions established between the antibody and the target need to be strong enough to withstand the forces pulling a captured cell in the magnetic field (Chen et al., 2015; Clarke and Davies, 2001).

Antibody polymers, by establishing simultaneous multiple interactions resulting in enhanced binding affinity, kinetics and specificity (Boruah et al., 2013; Kazane et al., 2013; Kim et al., 2012), provide an attractive candidate to form ultra-stable bonds.

Thus, we decided to take advantage of SpyLigase-mediated covalent protein polymerization to build affibody polymers, so enabling the formation of multivalent interactions (polymeric beads, Figure 4.7A). The cancer cells capture efficiency of affibody polymers was compared with that of magnetic beads coated with an affibody monolayer (monomeric beads, Figure 4.7A).

Since any weak links at the antibody-bead interface impairs cells recovery (Chapter 3, Figure 3.3B), affibody directed against the epidermal growth factor receptor 1 (EGFR) was covalently anchored to the magnetic particles using the SpyTag/SpyCatcher system. To enable precise anchoring of SpyLigase-polymerized affibodies, Cys-SpyCatcher (a variant of SpyCatcher having a Cysteine at the N-

terminus) was immobilized on magnetic beads via a disulfide bond, so affibody polymers attached to the beads could be released simply by boiling the particles with dithiothreitol (DTT) (Figure 4.7B).

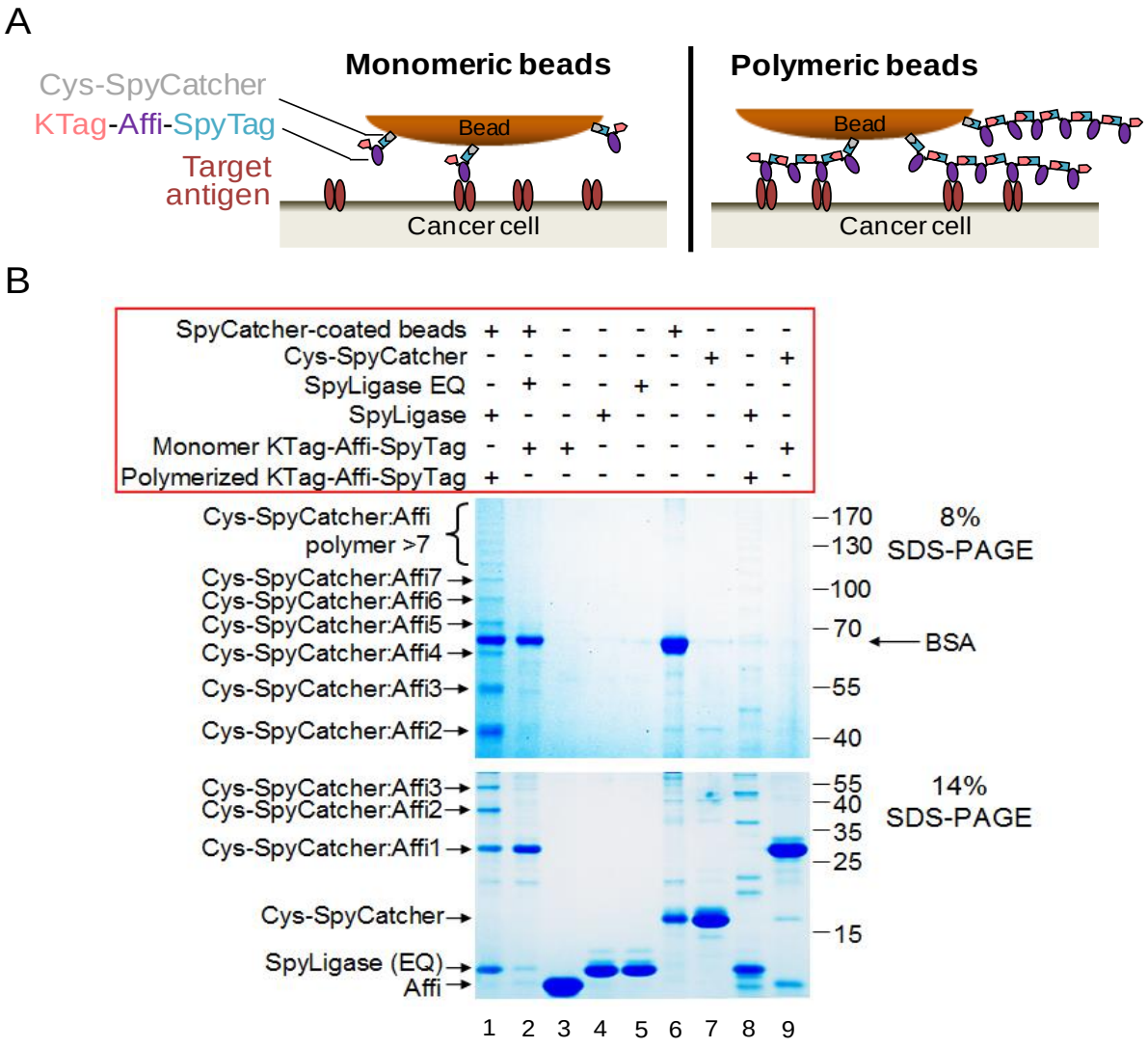

Figure 4.7. Coating magnetic beads with affibody polymers for enhanced cell capture. A) Cartoon of the bead-cell interface of affibody monomers and affibody chains. B) Analysis of affibody polymers on beads. KTag-AffiEGFR-SpyTag (Affi) was incubated at 4°C for 72 hours with SpyLigase and SpyCatcher-coated magnetic beads to promote affibody self-assembly (lane 1). Monomeric beads (monomer KTag-Affi-SpyTag, lane 2) were obtained by incubating affibody at 4°C for 72 hours with SpyCatcher-coated magnetic beads, but in the presence of SpyLigase EQ. Samples were boiled in presence of DTT and analyzed by SDS-PAGE with Coomassie staining. Lanes 8-9 show affibody polymers and the affibody-SpyCatcher complex obtained in isolation. The band at 66 kDa corresponds to BSA present in the bead storing solution. Samples eluted from the beads are indicated as Cys-SpyCatcher irreversibly linked to different affibody units (e.g. Cys-SpyCatcher:Affi1, lane 1).

In order to analyze whether polymeric beads enhance the isolation of cancer cells, a human cell line panel with varying expression levels of EGFR was assembled (Figure 4.8A).

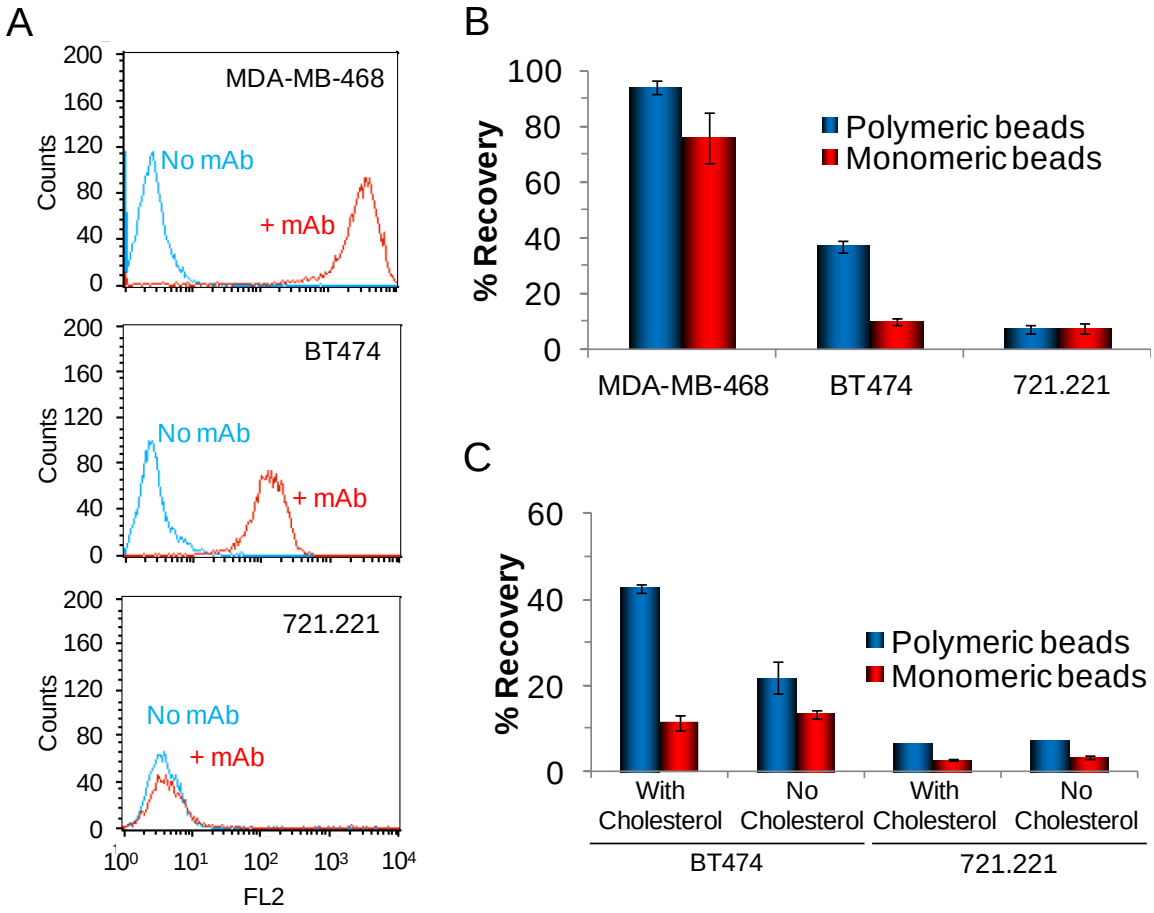

Figure 4.8. Enhaced cells capture with affibody polymers. A) EGFR expression levels were determined by flow cytometry using an anti-EGFR mAb (+ mAb, red), followed by a secondary PE-conjugated antibody. As control, cells were incubated only with the secondary antibody (No mAb, blue). B) Immunomagnetic isolation of a cancer cell line panel using SpyLigase-polymerized affibody (polymeric beads) or magnetic particles coated with an affibody monolayer (monomeric beads). As control the EGFR non-expressing 721.221 cells were used. C) Effect of cholesterol on cells recovery. BT474 and 721.221 cells were loaded with or without 250 µg/mL water-soluble cholesterol for 1 h at 25°C before magnetic isolation with anti-EGFR affibody polymers (polymeric beads) or affibody monomers (monomeric beads). Error bars are mean of triplicate ± 1 SD.

MDA-MB-468 cells are characterized by high EGFR levels, BT474 express low levels, whereas 721.221 do not express detectable levels of the receptor (Figure 4.8A).

To compare the capture efficiency of polymeric and monomeric beads, cells were loaded with cholesterol and incubated for 20 minutes with magnetic particles. Cell recovery was determined by counting isolated cells using a Coulter counter (Figure 4.8B).

Figure 4.8B shows that monomeric beads enabled efficient recovery only of the highest EGFR-expressing cells (MDA-MB-468), but were unable to isolate BT474 cells (expressing low levels of EGFR). Conversely, polymeric beads, not only improved significantly the isolation of MDA-MB-468 cells ($P = 0.03$, $n = 3$, unpaired *t*-test), but also greatly enhanced the recovery of BT474 ($P < 0.0001$, $n = 3$, unpaired *t*-test). Affibody polymers did not impair bead specificity, since recovery of EGFR-null 721.221 cells was equivalent to monomeric beads ($P = 0.97$, not significant, $n = 3$, unpaired *t*-test).

The effect of cholesterol on cell recovery has already been evaluated for HER2 and EpCAM targerting. To test the generality of the cholesterol loading approach, cells were incubated with or without cholesterol before performing isolation (Figure 4.8C).

As shown in Figure 4.8C, cholesterol loading improved recovery of BT474 using polymeric beads ($P = 0.01$, $n = 3$, unpaired *t*-test), but did not have an effect on isolation with monomeric beads. Cholesterol did not have a major effect on the binding specificity of the beads, with almost negligible amount of captured 721.221 cells. These data validate the importance of cell membrane modulation for improving cancer cell capture.

Therefore, generation of multivalent affibody chains via SpyLigase-dependent polymerization could provide a simple and fast method for the efficient isolation of cancer cells.

4.4 Isolation of cancer cells from human blood using affibody polymers

To further test whether affibody chains would enable efficient isolation of cancer cells from clinical samples, anti-HER2 affibody polymers, generated using SpyLigase, were used to capture cells doped into human blood.

A cell line panel varying in HER2 expression was assembled, cells were CFSE-labelled and spiked into whole human blood. Red blood cells were removed by hypotonic lysis followed by centrifugation and CFSE-labelled cancer cells were isolated by using magnetic beads coated with anti-HER2 affibody polymers (polymeric beads) or beads decorated with an affibody monolayer (monomeric beads) (Figure 4.9A).

Figure 4.9A shows that monomeric beads enabled a poor isolation of spiked cells, even of cells characterized by elevated expression of HER2 (BT474). Conversely, using beads coated with affibody polymers significantly enhanced the capture of BT474 (P = 0.0005, n = 3, unpaired t-test) and low-HER2 expressing MCF-7 cells (P = 0.0001, n = 3, unpaired t-test).

Recovery of HER2-null 721.221 cells was equivalent for polymeric and monomeric beads (P = 0.87, not significant, n = 3, unpaired t-test), indicating that polymeric beads are specific.

The specificity of affibody chains in capturing cancer cells spiked into human blood was also evaluated via fluorescence microscopy, by identifying isolated cells as CFSE-positive and CD45-negative (a marker of leucocytes) (Figure 4.9B).

Figure 4.9B shows that polymeric beads did not impair the capture specificity of cancer cells, with comparable isolation of leucocytes to that of monomeric beads (Figure 4.9B), indicating that leucocyte binding is due to the intrinsic nature of the magnetic beads.

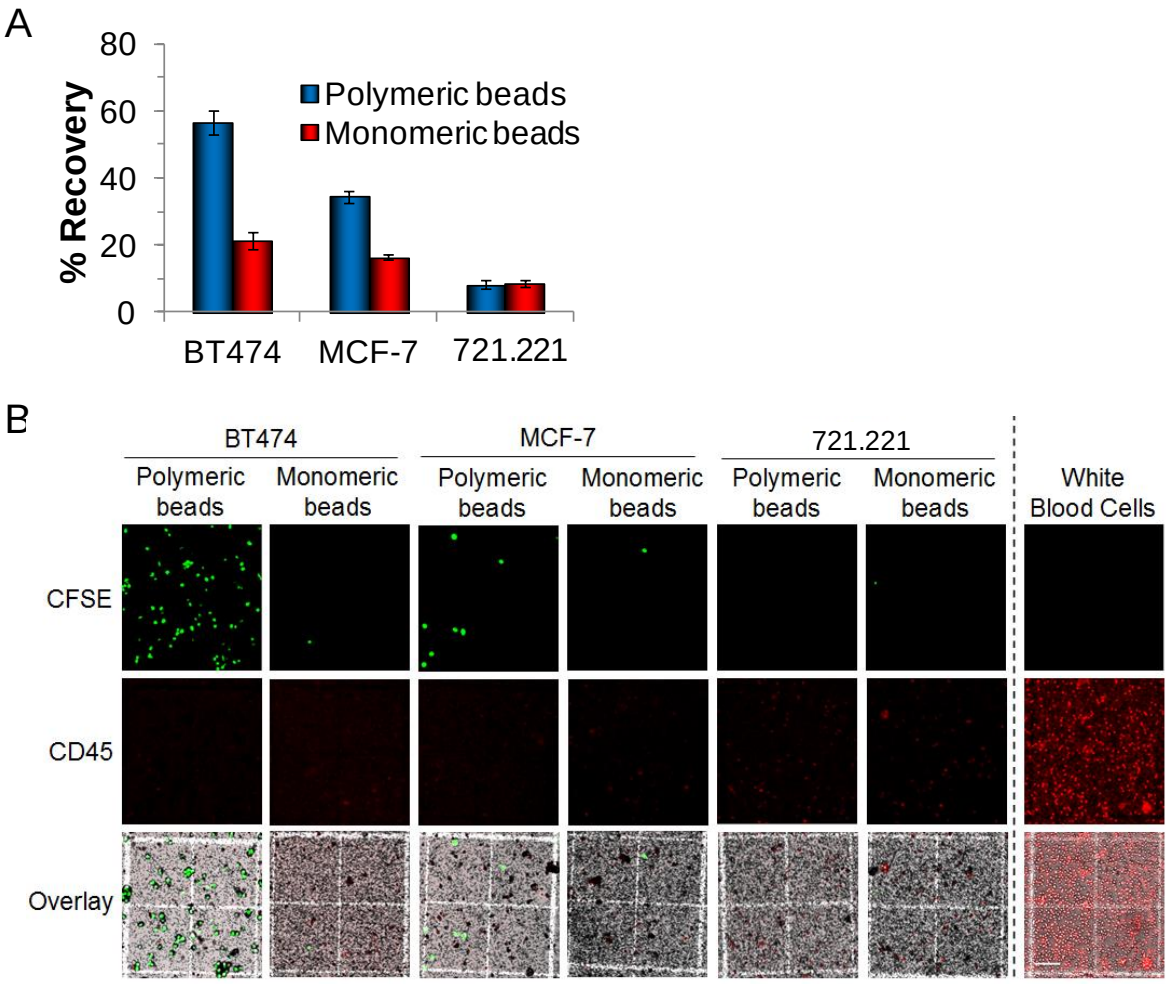

Figure 4.9. Isolation of cancer cells from human blood. A) Isolation of spiked cancer cells into human blood. 250,000 cells with high (BT474), low (MCF-7) or no HER2 expression (721.221) were labelled with CFSE and doped into human blood. Following hypotonic lysis of red blood cells, spiked cancer cells were isolated using magnetic beads coated with anti-HER2 affibody monomers (monomeric beads) or polymers (polymeric beads) and counted using a Coulter counter. Error bars are mean of triplicate ± 1SD. B) Cancer cells were isolated with polymeric or monomeric beads and recovery specificity was assessed by fluorescence microscopy. Top row shows CFSE-labelled cells, middle row shows staining for CD45 (a common marker of leucocytes) and overlay (CFSE: green, CD45: red and brightfield: greyscale) is displayed in the bottom row. White blood cells, obtained by hypotonic lysis of red blood cells from the whole blood, were used as positive control for CD45 staining (right column). Scale bar 50 µm.

4.5 Discussion

Peptide tags are commonly used to analyze or control proteins function, representing an ideal tool for biotechnology (Huh et al., 2003).

In the literature, there is a vast *corpus* on genetically-encoded peptides used to conjugate or modify proteins. A method of particular interest is represented by split proteins. Splitting proteins in two molecular partners enabled to develop genetically-encoded reporters (Ozawa, 2006), but this system requires to fuse the protein of interest with large and potentially folding-disruptive protein domains. There are fewer precedents for splitting a protein into three: tripartite inteins ensured covalent peptides ligation (Sun et al., 2004), but inteins application is limited by the need of placing inteins at specific location in the protein.

To develop a new peptide-peptide covalent ligation system the CnaB2 domain of *Streptococcus pyogenes* has been split into three parts, generating two peptide tag, SpyTag and KTag, and a protein domain named SpyLigase.

When mixed together, SpyLigase can dock SpyTag and KTag, reconstituting the CnaB2 domain ensuring the spontaneous formation of an amide bond, so locking covalently the two peptide fragments.

Because of the small size of SpyTag (13 residues) and KTag (10 residues), SpyLigase is able to conjugate the tags in a topology-independent way. Peptide-peptide conjugation, in fact, occurred when SpyTag and KTag were placed indifferently at the N-terminus or C-terminus of proteins and even when they were both inserted in the middle of a protein, opening the route for the generation of non-linear architectures. However, this technology is not yet optimal: SpyLigase ligation is slow and low yielding (reaction rate ~50% in 24 hours) and requires a specific buffer containing the chemical chaperone trimethylamine N-oxide (TMAO). Moreover, due

to SpyLigase structural fragility, the reaction is highly thermo-sensitive, with conjugation proceeding efficiently at 4 and 12°C, but poorly at 37°C, potentially limiting the application of this technology *in vivo*. Furthermore, although SpyLigase enabled the efficient generation of affibody and antibody polymers, the presence of side products (cyclized dimer and trimer) could compete with the formation of linear chains, lowering even further the reaction yields.

Nevertheless, the unique properties the SpyLigase technology make this system a promising starting point for linking protein building-blocks with minimal modifications.

SpyLigase enabled the efficient formation of self-assembled affibody and antibody polymers, promising to be a valuable tool for the generation of polymeric biomaterials.

Antibody multimers have been widely explored to modulate tissue penetration, pharmacokinetics and improving affinity (Cuesta et al., 2010), most recently for the isolation of circulating tumour cells (CTCs) (Myung et al., 2011, 2014). However, the current technologies available to generate antibody polymers need to design the multimerization strategy case-by-case, limiting their broad application. To overcome this limit we took advantage of SpyLigase flexibility to generate affibody polymers for the sensitive isolation of cancer cells. Affibody polymers, generated by exploiting SpyLigase, were covalently anchored with precise orientation to the surface of magnetic beads and used to immunomagnetic isolate tumour cells. Multivalent SpyLigase-assembled affibody polymers significantly improved the recovery sensitivity of cancer cell-lines without loss of specificity. The enhanced isolation sensitivity of affibody chains, even of cells expressing low levels of tumour markers,

could potentially extend the range of cellular antigens and biomarkers that can be targeted for isolation of CTCs (Shahneh, 2013).

The work presented in this chapter enabled the development of a powerful peptide-peptide covalent ligation system. Although there is much to improve in SpyLigase, this technology represents a good starting point for the development of complex protein conjugates and biomaterials.

Chapter 5 : Development of an approach to produce controlled protein polymers

Precise synthesis of polyproteins for killing cancer cells

The assembly of proteins into well defined and controlled multimodular systems to perform complex biochemical functions is an attractive but still unmet challenge. The main limit in the development of highly defined protein assemblies is the lack of simple and efficient synthetic strategies that allow a great control over the assembly of protein units. This is mainly due to the intrinsic delicate nature of proteins, to their large number of reactive groups and to the limited amount of available orthogonal chemical reactions (Sletten and Bertozzi, 2009).

Joining protein monomers into polyproteins has been achieved through several methods including genetically encoding the desired polymer in one long open reading frame (Zaher and Green, 2009), driving monomer assembly through metal–ligand interactions (Zhang et al., 2012b), DNA strands (Kazane et al., 2013), antigen-antibody recognition (Nuraje et al., 2004) or protein-protein (King et al., 2012) and protein-ligand binding (Carlson et al., 2006). However the large majority of the exploited strategies are poorly modular, so that the generation of polyproteins needs be deeply investigated case-by-case.

The use of modular and mutually-unreactive chemical reactions to incorporate step-by-step amino acids forming the desired peptide chain, enabled the development of solid-phase peptide synthesis, introducing a long-lasting scientific revolution (Merrifield, 1963). However, because of the proteins' limited stability to harsh chemical conditions, the application of the same approach is unpractical. Since proteins are structurally and biochemically delicate the ideal methods for their solid-phase assembly requires specific features: (i) proteins should be assembled under mild conditions to preserve their folding and function, (ii) the assembly should be quantitative to avoid the formation of side products which removal would require complex chromatographic steps, (iii) protein units should be linked together with high

modular connectors to simplify the reaction and (iv) elution of the desired polyprotein chains should occur easily without the use of components that need to be removed by chromatography.

With the aim of developing a new modular method for the precise and controlled assembly of polyproteins, in this chapter will be described the generation of a new protein-peptide pair able to form a spontaneous isopeptide bond. To irreversibly link together protein monomers, this peptide-protein pair will be used in combination with SpyTag and SpyCatcher to assemble protein chains with good control.

5.1 Splitting the RrgA domain

To develop a new molecular tool for the precise synthesis of covalently linked polyproteins, a protein domain containing a spontaneously occurring isopeptide bond was engineered.

The pilus-associated adhesin RrgA from *Streptococcus pneumoniae* (Nelson et al., 2007), was selected as the ideal candidate because of (i) the presence of an isopeptide domain in the D4 immunoglobulin-like domain between residues Lys742 and Asn854, (ii) the absence of Cysteine residues, (iii) its small size and (iv) the lack of structurally relevant metal-binding sites.

Using the principles established for SpyTag/SpyCatcher (Zakeri et al., 2012), the RrgA D4 domain was split by Raphaël Gayet (a lab member) into two molecular partners, obtaining the protein domain RrgACatcher (residues 749-860) and the peptide tag RrgATag (residues 734-748) (Figure 5.1A).

To improve the reactivity of the RrgACatcher/RrgATag pair, RrgATag was shortened by removing its last 3 C-terminal amino acids (generating SnoopTag), whereas the G842T point mutation was introduced into RrgACatcher to stabilize a β-strand. To further enhance the reactivity of RrgACatcher a second point mutation,

D848G, was added to stabilize a hairpin turn in proximity to the reactive site of RrgACatcher G842T (Figure 5.1B). The efficiency of the protein domain in forming the isopeptide bond upon mixing with SnoopTag was assessed by SDS-PAGE and quantified by densitometry (Figure 5.1C). We named the optimized version of the peptide tag SnoopTag, whereas the improved protein domain (containing both the G842T and D848G mutations) was called SnoopCatcher.

Figure 5.1C shows that mutations introduced in RrgACatcher to generate SnoopCatcher (G842T, D848G) dramatically increased the ability of the protein pair to form an isopeptide bond with SnoopTag.

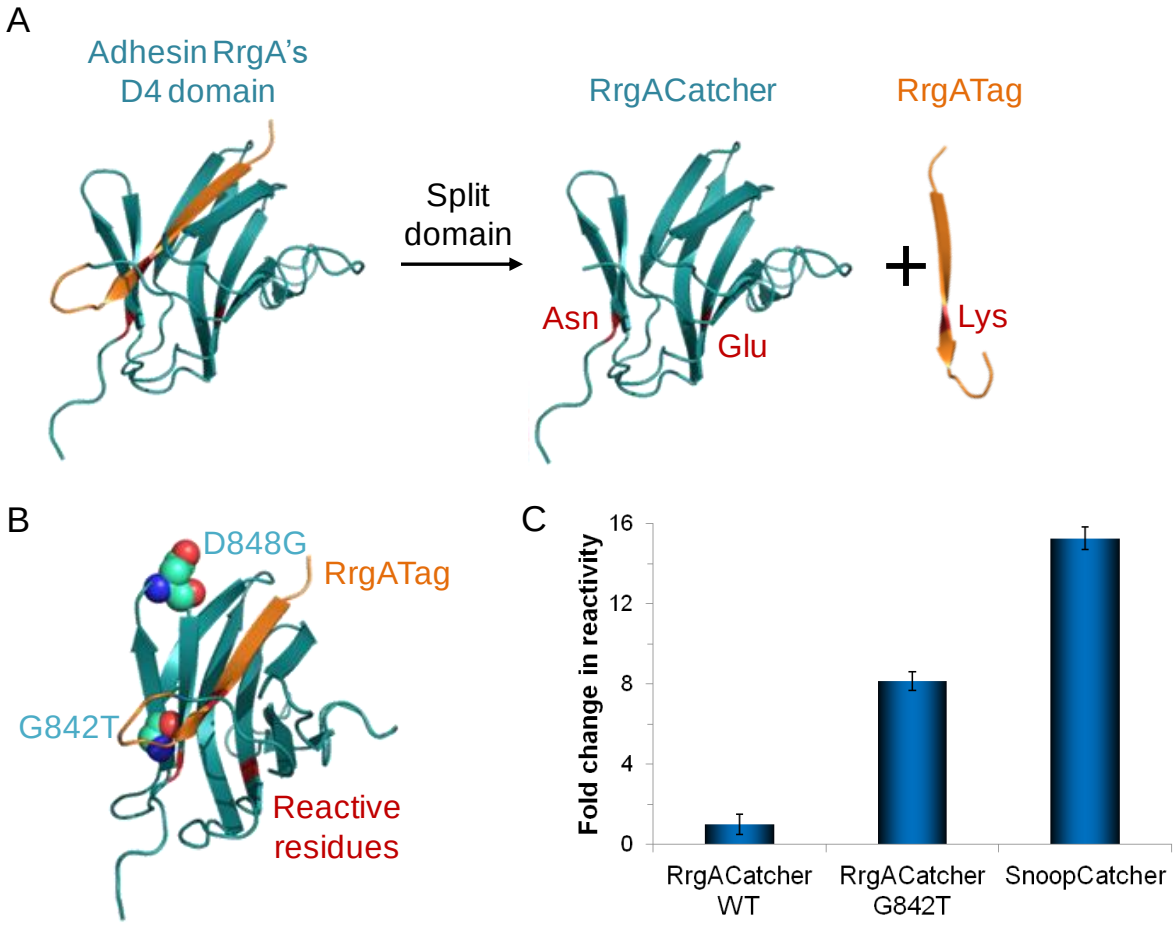

Figure 5.1. Splitting the D4 domain from RrgA. A) Cartoon of splitting RrgA D4 domain to obtain RrgACatcher and RrgATag (based on PDB 2WW8). Reactive residues are in red. B) Mutations introduced in RrgACatcher to make SnoopCatcher. Reactive residues are in red, whereas mutated residues are displayed as cyan spheres. Mutagenesis was performed by Tomohiko Nakamura (Howarth laboratory). C) 10 µM SnoopTag was mixed with either 10 µM RrgACatcher (RrgACatcher WT), RrgACatcher G842T or SnoopCatcher and incubated for 1 h at 25°C. Samples were analyzed by SDS-PAGE and isopeptide bond formation efficiency quantified by densitometry (mean of triplicate ± 1 SD).

5.1.1 Features of SnoopCatcher and SnoopTag reaction

Splitting and engineering the RrgA D4 domain allowed us to generate a new peptide tag-protein domain pair able to form a spontaneous isopeptide bond. To better understand and apply this system, the features of SnoopTag-SnoopCatcher reaction were investigated under several conditions.

SnoopTag was fused to the N-terminus of maltose binding protein (SnoopTag-MBP), mixed at equimolar concentration with SnoopCatcher and incubated at 25°C

for 2 hours prior to SDS-PAGE. As shown in Figure 5.2A SnoopTag-MBP and SnoopCatcher, simply upon mixing, formed a complex able to survive boiling in SDS (lane3). Alanine mutations of the reactive Lysine in SnoopTag (KA) or of SnoopCatcher's reactive Asparagine (NA) completely abolished the formation of the complex validating the isopeptide bond formation between the two partners (lanes 4-7).

The covalent nature of the bond formed between SnoopTag and SnoopCatcher was further validated by mass spectrometry (Figure 5.2B). A main peak having a mass corresponding to the sum of the mass of SnoopCatcher and a synthetic SnoopTag peptide with loss of ammonia was detected alongside with acetylated and gluconylated side-products (common for *E.coli* expression).

The SnoopCatcher/SnoopTag-MBP reaction was assessed over time: SnoopCatcher and SnoopTag-MBP were either mixed at equimolar concentration or using a 2:1 SnoopCatcher:SnoopTag-MBP molar ratio and incubated at 25°C. Reactions were stopped by adding SDS-PAGE loading dye and boiling the samples. Mixing the two partners at equimolar concentration yielded ~80% conjugation, whereas a 2:1 SnoopCatcher:SnoopTag-MBP molar ratio enabled reaction completion in about 30 min (Figure 5.2C).

The influence of the temperature on the spontaneous formation of the amide bond between SnoopCatcher and SnoopTag was also investigated. The two partners were mixed at equimolar concentration and incubated at different temperatures for 1 hour. SnoopTag/SnoopCatcher reaction proceeded efficiently at temperatures in the range 12-37°C, with reduced performance at 4 and 42°C (Figure 5.2D).

SnoopTag and SnoopCatcher formed a covalent complex in presence of commonly used detergents and, due to the lack of Cysteine residues in their sequences, the isopeptide bond formation was insensitive to dithiothreitol (DTT) (Figure 5.2E).

To further analyze the biochemical properties and the limits of the SnoopTag/SnoopCatcher reaction, the effect of pH on the covalent complex formation was assessed (Figure 5.2F). The reaction proceeded efficiently at pH 6-9 with optimal formation of the isopeptide bond at pH 8-9 and decreased conjugation's efficiency at pH 5 (Figure 5.2F).

To further analyze the SnoopTag/SnoopCatcher reaction and determine whether this peptide-protein pair is suitable for the controlled assembly of polyproteins through sequential isopeptide peptide bond formation, orthogonality with SpyTag/SpyCatcher was assessed.

SpyTag is a peptide tag containing a reactive Aspartate that efficiently reacts with its partner SpyCatcher under various conditions (Zakeri et al., 2012). Contrary to SpyTag, SnoopTag is characterized by the presence of a reactive Lysine, fundamental for the amide bond formation with SnoopCatcher. Both the peptide tags were mixed with their cognate partners and incubated overnight at 25°C. To assess whether the two tags are mutually unreactive, SnoopTag and SpyTag were also mixed with SpyCatcher and SnoopCatcher respectively (Figure 5.3).

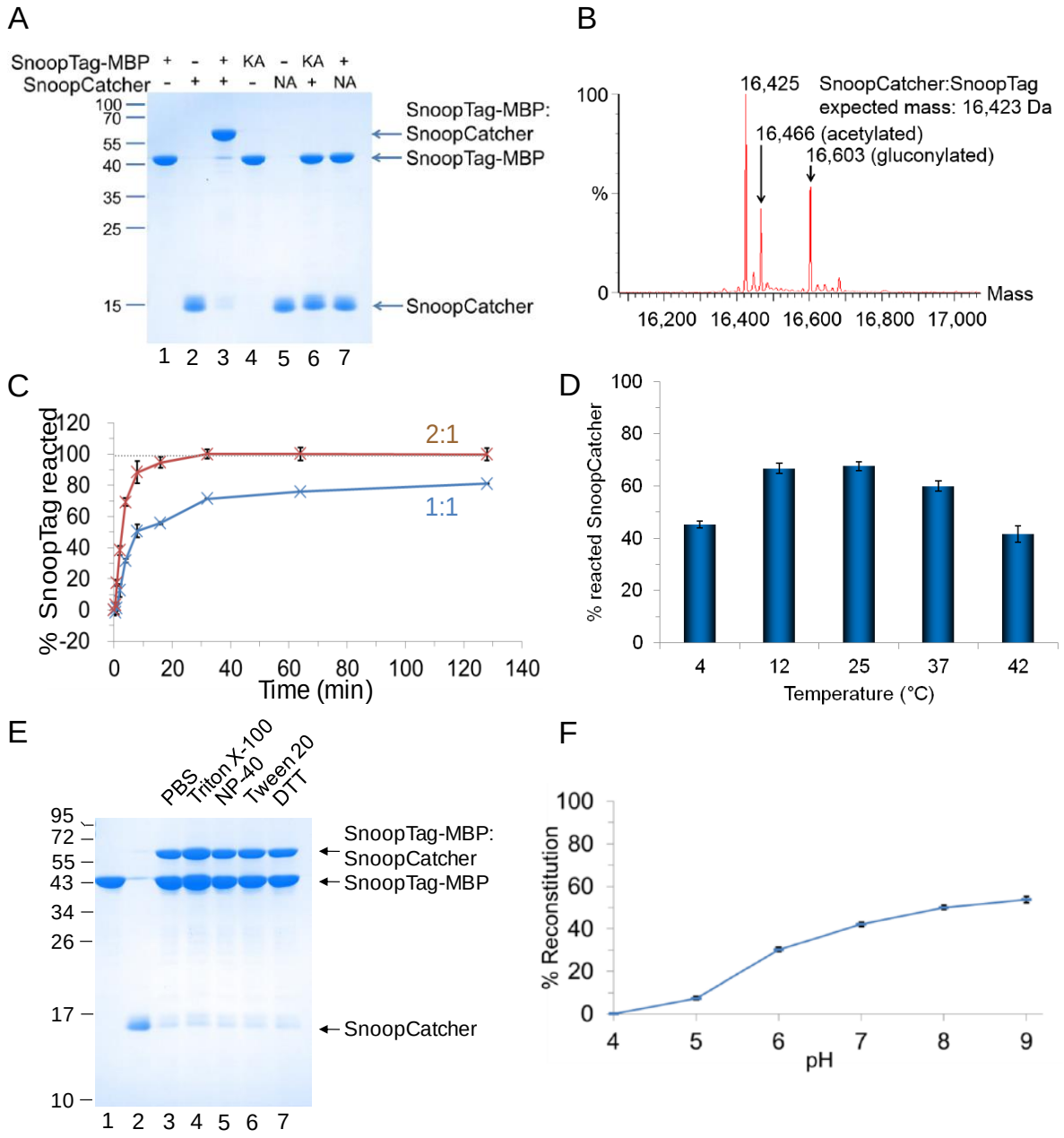

Figure 5.2. Features of the SnoopTag-SnoopCatcher reaction. A) SnoopCatcher and SnoopTag form a covalent complex simply upon mixing. Alanine mutation of the isopeptide-reactive residues of SnoopTag (KA) or SnoopCatcher (NA) completely suppressed the formation of the covalent adduct. B) Mass spectrometry of the complex between SnoopCatcher and a synthetic SnoopTag peptide. C) Time-course analysis of the reaction with 1:1 or 2:1 SnoopCatcher:SnoopTag-MBP molar ratio. D) Temperature-dependence of the reaction: 5 µM SnoopTag-MBP and 5 µM SnoopCatcher were incubated for 20 min at the indicated temperature prior to SDS-PAGE analysis. E) Effect of detergents and DTT on the amide bond formation. F) Influence of pH on the SnoopTag-MBP/SnoopCatcher reaction Data presented in panels A,B,C and F are from Tomohiko Nakamura (Howarth laboratory). All error bars are mean of triplicate ± 1 SD.

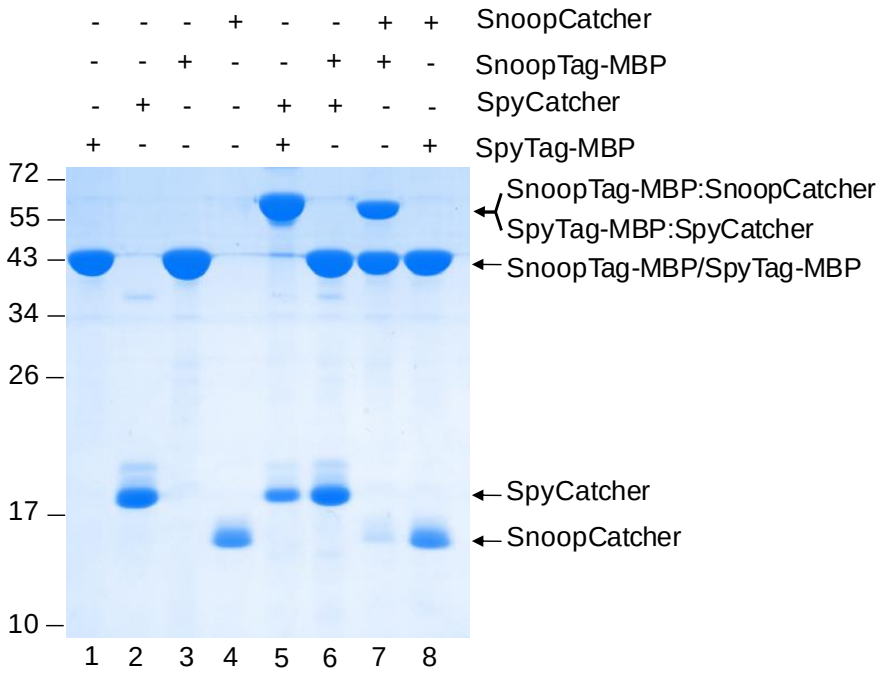

Figure 5.3. Orthogonality of the SnoopTag/SnoopCatcher and SpyTag/SpyCatcher pairs. SnoopTag and SpyTag were incubated with SnoopCatcher or SpyCatcher overnight at 25°C. Proteins were mixed at 10 µM and their reactivity was assessed by SDS-PAGE with Coomassie staining.

Both the peptide tags formed a covalent bond only with their cognate partner (lanes 5 and 7, Figure 5.3), with no detectable cross-reactivity even after overnight incubation (lanes 6 and 8, Figure 5.3). It is thus possible to conclude that SpyTag/SpyCatcher and SnoopTag/SnoopCatcher are orthogonal pairs.

The SnoopTag/SnoopCatcher pair provides, therefore, a robust system able to form an irreversible amide bond rapidly and with quantitative yields under various conditions. Moreover, SnoopTag/SnoopCatcher is mutually unreactive with SpyTag/SpyCatcher, so that these two protein-peptide tag pairs provide good candidates to be used for solid-phase synthesis of polyproteins.

5.2 Solid-phase synthesis of polyproteins via sequential isopeptide bond formation

Protein bioconjugation methods are widely used to join together protein units for sophisticated biochemical functions, like vaccines development (Bachmann and Jennings, 2010) and tissue engineering (Han et al., 2015).

Bioconjugation often exploits the reactivity of amino acid side chains, usually Lysine, Cysteine or carboxylic acids conveniently found on the protein surface. However the reduced regioselectivity of the available chemistries (Chen et al., 2011) hampers the bioconjugation of multiple protein units in a one-pot reaction.

Solid-phase protein bioconjugation, even if laborious, represents a good alternative. Protein monomers, in fact, are introduced one step at a time, followed by removal of the unreacted building blocks from the support matrix simply by filtration, thus allowing the protein chain to grow while immobilized.

With the goal of developing a platform for the solid-phase synthesis of polyproteins, the most important molecular requirements will be analyzed.

5.2.1 Importance of strong interaction between the extending chain and the matrix

The success of the solid-phase peptide synthesis is strongly related to the solid support and its binding properties. The desired solid support, in fact, should be characterized by (i) a good capacity so to maximize yields, (ii) good solvation and accessibility to reagents, (iii) mechanical and physical stability, (iv) elevated affinity for the first building block that will anchor the extending chain to the matrix and (v) being suitable for the repeated use of the same solid-phase.

To satisfy all these conditions we reasoned that a good candidate would be amylose resin, an affinity matrix used for the isolation of recombinant proteins fused to maltose binding protein (MBP). MBP is often used to increase solubility of fusion

proteins (Fox and Waugh, 2003), so the use of amylose resin and therefore of an MBP-fusion protein as initial building block would have the dual effect of increasing the solubility of the extending polyprotein and acting as affinity tag for efficient immobilization on the resin. Moreover, elution from amylose resin occurs simply by adding maltose to the matrix, thus avoiding exposure of the synthesized polyproteins to harsh conditions or protease removal.

To use amylose resin as solid-phase and synthesize polyproteins via sequential isopeptide bond formation, SpyCatcher was fused at the C-terminus of MBP so that MBP-SpyCatcher can reversibly bind the matrix, allowing the irreversible linkage of the next protein through the SpyTag/SpyCatcher system (Figure 5.4A).

To assess whether this approach was suitable for the assembly of polyproteins, affibodies (a non-immunoglobulin scaffold binding protein) (Löfblom et al., 2010) were chosen as model proteins to build a chain. An anti-HER2 affibody bearing at the N-terminus SnoopTag and at the C-terminus SpyTag was added in large excess to the resin-immobilized MBP-SpyCatcher to drive reaction to completion. Protein excess was washed away from the resin and affibody was conjugated via its free SnoopTag handle to BiCatcher, a fusion of SpyCatcher to SnoopCatcher mediated by a helical spacer. By multiple repeats of this process an affibody chain was made and its extension followed by elution with maltose and SDS-PAGE analysis (Figure 5.4A and 5.4B).

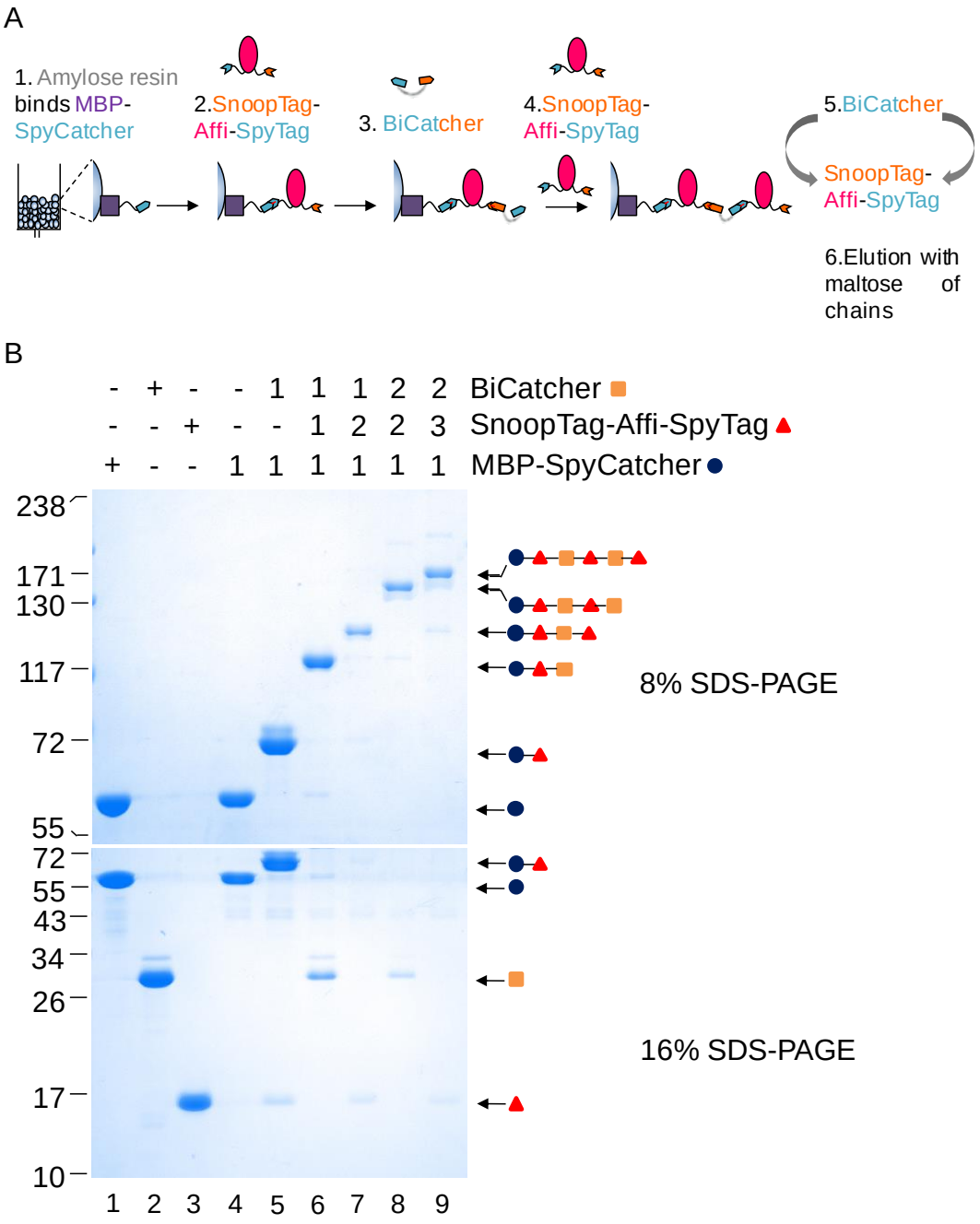

Figure 5.4. Solid-phase synthesis of affibody chains. A) Schematic of the affibody chain synthesis. MBP-SpyCatcher is immobilized on amylose resin. Affibody bearing SnoopTag and SpyTag can form an isopeptide bond with SpyCatcher (red line represents the amide bond). Affibody monomers are bridged with BiCatcher (a fusion of SnoopCatcher and SpyCatcher). Sequential addition of SnoopTag-Affi-SpyTag and Bicatcher allows extension of the desired chain. Assembled polyproteins are eluted from the resin by adding maltose. B) SDS-PAGE analysis of formed affibody chains. Lanes 1-3 show MBP-SpyCatcher, SnoopTag-Affi-SpyTag and BiCatcher in isolation, used as controls. Lanes 4-9 show stepwise elongation of the affibody chains. After each conjugation stage one aliquot of sample was eluted with maltose from the resin and analyzed by SDS-PAGE with Coomassie staining.

From Figure 5.4B it is evident that the approach for the assembly of affibody chains is effective. The assembly of the desired polyproteins was quantitative with complete conjugation of each building block at each step.

The developed method ensured the controlled synthesis of affibody chains with little side-products detectable, so that further extensive purification steps are not required. However the presence of unconjugated BiCatcher after each addition step is appreciable.

Affibody chains were able to survive boiling in SDS, indicating that all the protein units were covalently held together by the sequential formation of isopeptide bonds.

Despite the success of the presented method, from Figure 5.4 it is possible to note an incremental loss of the synthesized polyproteins after each addition step and specifically after the conjugation of the third building block (lanes 6-9).

MBP is characterized by a dissociation constant for maltose of 1.2 μM (Telmer and Shilton, 2003). Such affinity is suitable for protein purification but could be insufficient to withstand the extensive washing steps performed during the assembly procedure. To increase the affinity of MBP-SpyCatcher for amylose, an improved version of the fusion, called MBPx-SpyCatcher, was generated by Tomohiko Nakamura (Howarth laboratory). MBPx-SpyCatcher was made by introducing the A312V and I317V mutations in MBP (Walker et al., 2010) and deleting residues 172, 173, 175 and 176 from MBP (Telmer and Shilton, 2003).

MBPx-SpyCatcher was then applied to amylose resin and assembly of affibody polymers was performed by sequential addition of SnoopTag-Affi-SpyTag and BiCatcher units (Figure 5.5).

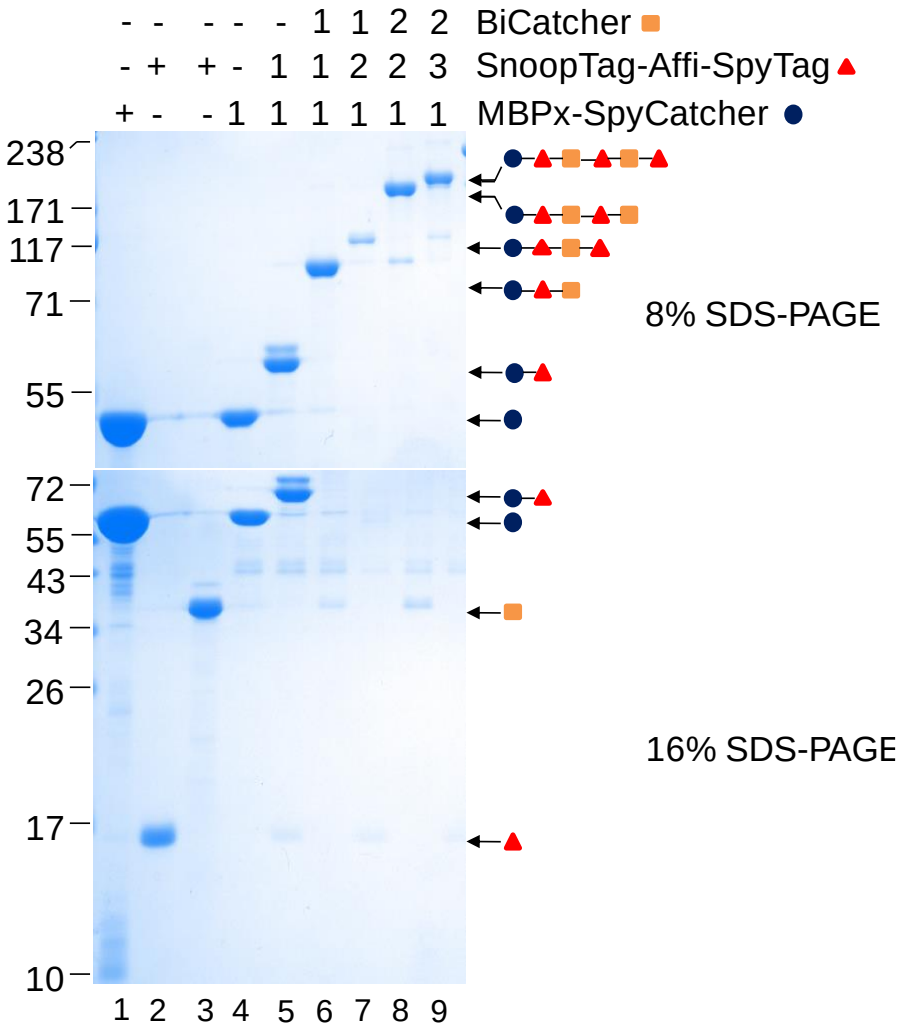

Figure 5.5. Solid-phase synthesis of affibody polyproteins using MBPx-SpyCatcher. MBPx-SpyCatcher bearing mutations and deletions to improve the affinity of MBP for maltose was immobilized on amylose resin. Stepwise assembly of polyproteins was performed by repeated additions of SnoopTag-Affi-SpyTag and BiCatcher units followed by extensive washing steps to remove unreacted components (lanes 4-9) As controls MBPx-SpyCatcher, SnoopTag-Affi-SpyTag and BiCatcher were loaded in isolation (lanes 1-3).

The mutations and deletion introduced in MBP to generate MBPx-SpyCatcher improved the binding of the fusion protein to the solid-phase, ensuring better anchoring of extending chain to the matrix. In fact, the amount of recovered polyproteins decreased with the increasing of the washing steps (lanes 7-9) but to a lesser extent than MBP-SpyCatcher (Figure 5.4B).

To decrease even further the dissociation of the anchoring building block from amylose resin, SpyCatcher was fused at the C-terminus of tandemly linked MBPx (2xMBPx-SpyCatcher, cloned by Tomohiko Nakamura).

Sequential addition of SnoopTag-Affi-SpyTag and BiCatcher enabled efficient chain growth (Figure 5.6), extending to a product 6 units long (Figure 5.6, lane 9). The multivalent interaction of 2xMBPx-SpyCatcher, mediated by the presence of two linked MBPx units, enabled extensive washing of the resin during the chain synthesis with less polymer loss.

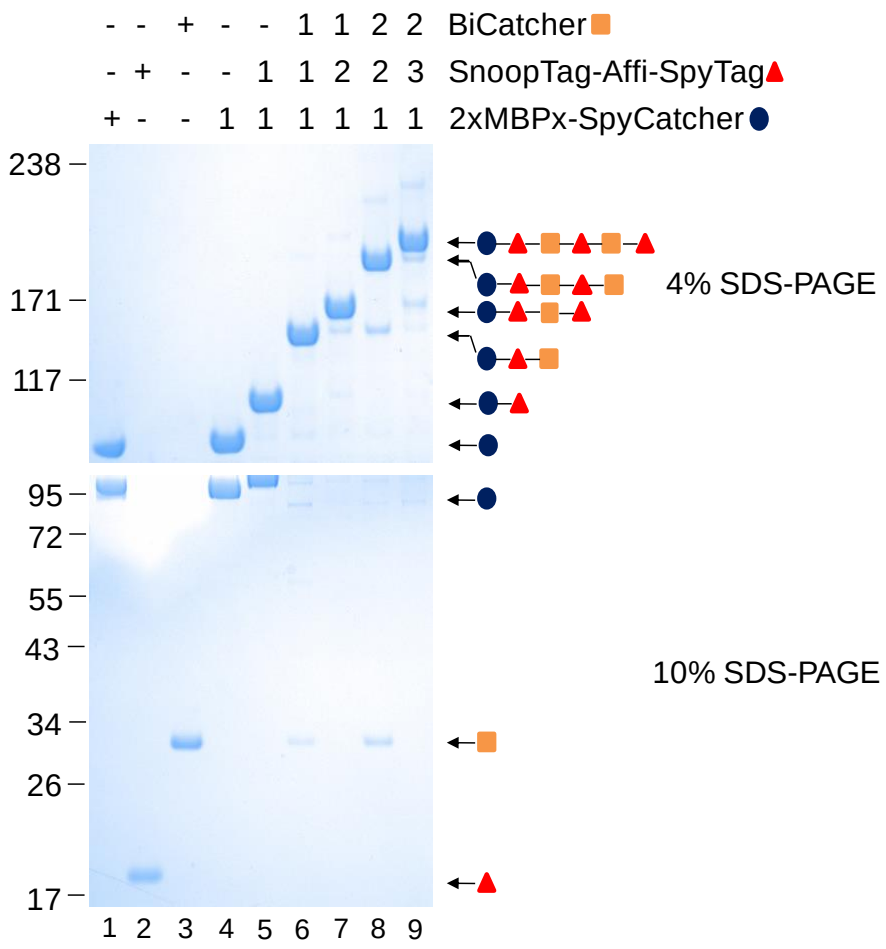

Figure 5.6. Assembly of affibody chains using 2xMBPx-SpyCatcher. To decrease dissociation from amylose resin upon extensive washing steps, two tandem repeats of MBPx were linked together and fused to SpyCatcher (2xMBPx-SpyCatcher). Chain extension proceeded through sequential addition of SnoopTag-Affi-SpyTag and BiCatcher. Assembly was monitored step-by-step by eluting an aliquot of sample with maltose. Samples were analyzed by SDS-PAGE using Tris-acetate gels with Coomassie staining. As controls, 2xMBPx-SpyCatcher, SnoopTag-Affi-SpyTag and BiCatcher were loaded in isolation (lanes 1-3).

To verify the versatility of the solid-phase synthesis of polyproteins, another solid-phase attachment was investigated. A version of SpyCatcher containing an acceptor peptide for site-specific enzymatic biotinylation (Beckett et al., 1999) was used. Biotinylated-SpyCatcher was linked to a matrix coated with monomeric avidin and affibody chains were synthesized by addition of SnoopTag-Affi-SpyTag monomers bridged by BiCatcher. Assembled polyproteins were eluted with an excess of free biotin (Figure 5.7).

The use of a different solid-phase attachment to synthesize affibody chains did not affect the efficiency of the polymerization reaction, with chains extending up to 10 components (lane 13, Figure 5.7A). As observed for MBP-based attachment, the synthesis of the desired polyproteins was quantitative. Moreover, the ultra-stable interaction of the avidin-biotin ensured recovery of polyproteins without minimal loss due to the multiple rounds of washing. However, the elevated stability of the biotin-avidin binding hampered the complete recovery of affibody chains, with only a partial recovery of the synthesized chains even after 4 hours of incubation in presence of an excess of free biotin. In fact, by adding to each sample a supplementary excess of free biotin, followed by overnight incubation of the samples at 25°C, it was still possible to elute affibody chains (Figure 5.7B).

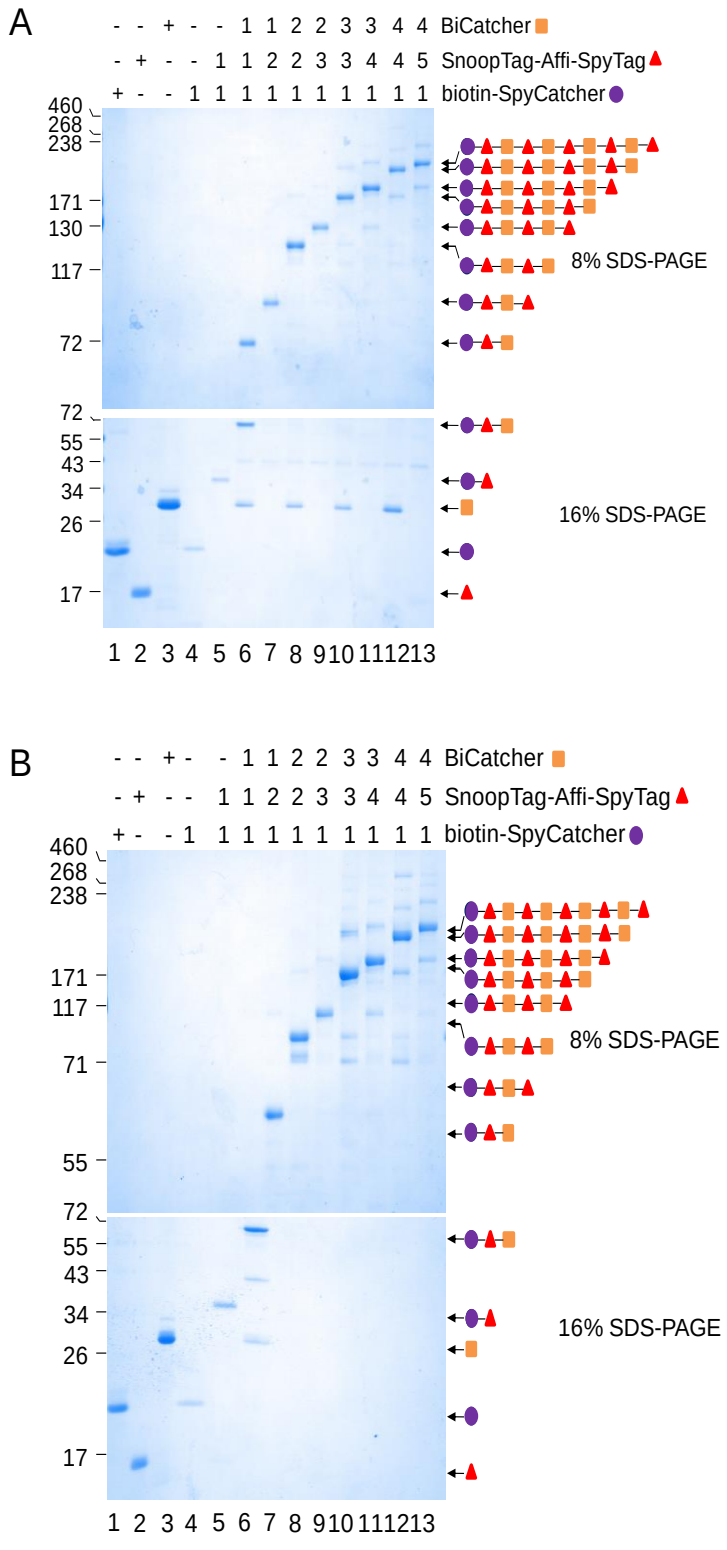

Figure 5.7. Solid-phase polyprotein synthesis using biotin-mediated anchoring. A) Affibody chains were anchored on solid-phase through the ultra-stable avidin-biotin interaction (lanes 4-10). Lanes 1-3 show biotin-SpyCatcher, SnoopTag-Affi-SpyTag and BiCatcher in isolation. Biotin-SpyCatcher was immobilized to monomeric avidin-coated beads and chain extension was performed by stepwise addition of SnoopTag-Affi-SpyTag and BiCatcher up to a decamer (lane 13). Formation of the desired polyproteins was assessed by eluting one aliquot of sample with 1 mM D-biotin at 25 °C for 4 h. B) After elution with 1 mM D-biotin at 25 °C for 4 h, biotin was newly added to each sample. Chains were collected after overnight incubation with biotin at 25 °C before SDS-PAGE analysis.

5.2.2 Optimization of BiCatcher for optimal conjugation

So far we observed how a tight binding between the building block anchoring the growing chain to the solid-phase is vital for the efficiency of the synthesis. In the solid-phase synthesis of peptides, the use of hetero bifunctional linkers to connect the functional monomers allowed the great simplification of the synthetic process, enabling to reduction of the number of orthogonal reactions required to synthesize the desired product (Moss, 2001). Therefore, we reasoned that using a modular connector to bridge the functional units forming the desired chain would be helpful. However, in order to withstand the extensive washing steps required to remove unreacted building blocks, the interactions established by such a connector should be covalent.

On the basis of these considerations, we developed a fusion of SnoopCatcher to SpyCatcher (named BiCatcher) and exploited the selective specificity of the SnoopCatcher-SnoopTag and SpyCatcher-SpyTag interactions to precisely control the synthetic process. In addition to its selectivity, BiCatcher has the advantage of modifying protein monomers only with the two peptide tags, ensuring minimal disruption to the units' folding and function (Modica et al., 2012).

Figures 5.4 to 5.7 demonstrated that BiCatcher enables the covalent linkage of building blocks tailored with SnoopTag and SpyTag driving chain extension.

BiCatcher was generated by Tomohiko Nakamura (Howarth laboratory) fusing SpyCatcher through a Gly/Ser spacer at the N-terminus of SnoopCatcher. In order to find the best conditions for optimal incorporation of BiCatcher in the growing chain, the effect of different buffers was tested (Figure 5.8).

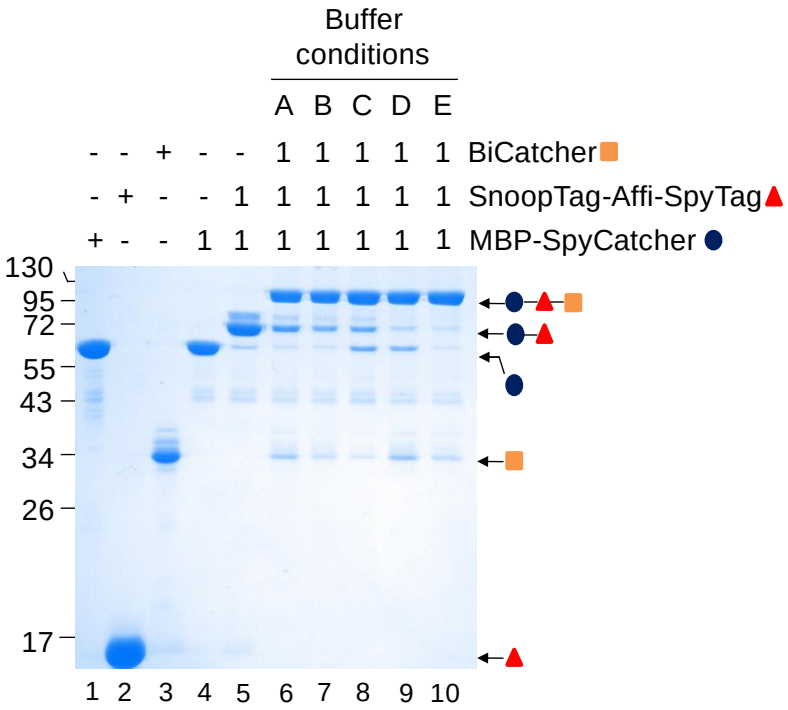

Figure 5.8. Screening of optimal conditions for BiCatcher conjugation. Lanes 1-3 show MBP-SpyCatcher, SnoopTag-Affi-SpyTag and BiCatcher in isolation. MBP-SpyCatcher was bound to resin (lane 4) and chains were extended by addition of SnoopTag-Affi-SpyTag (lane 5), followed by BiCatcher (lanes 6-10). BiCatcher was added to the extending chain in (A) 50 mM Tris 50 mM NaCl (TBS) pH 7.5, (B) TBS pH 8.0, (C) TBS + 0.1 M $NaHCO_3$ pH 9.0, (D) TBS + 0.1 M $NaHCO_3$ pH 10.0 or (E) TBS pH 8.0 containing 1.5 M TMAO.

From Figure 5.8 it is possible to appreciate the effect of the buffer composition on BiCatcher's conjugation, with TBS pH 8.0 containing the chemical chaperone trimethylamine N-oxide (TMAO) (Yancey, 2004) enabling nearly complete conjugation of the protein.

To further optimize the efficiency of BiCatcher's incorporation, variants of this fusion protein were generated (cloned by Tomohiko Nakamura). A more flexible version of BiCatcher was made by increasing the length of the Gly/Ser spacer between SpyCatcher and SnoopCatcher (BiCatcher long linker). Conversely, a variant with increased rigidity was generated by replacing the Gly/Ser linker with an α-helical spacer (Kuhlman et al., 1997) and deleting 35 residues from SpyCatcher's N-terminus (Li et al., 2014) (BiCatcher helical linker) (see Appendix for sequence alignments).

The incorporation efficiency of such variants (BiCatcher long linker and BiCatcher helical linker) was tested alongside with regular BiCatcher (BiCatcher wt) to generate a trimer (Figure 5.9).

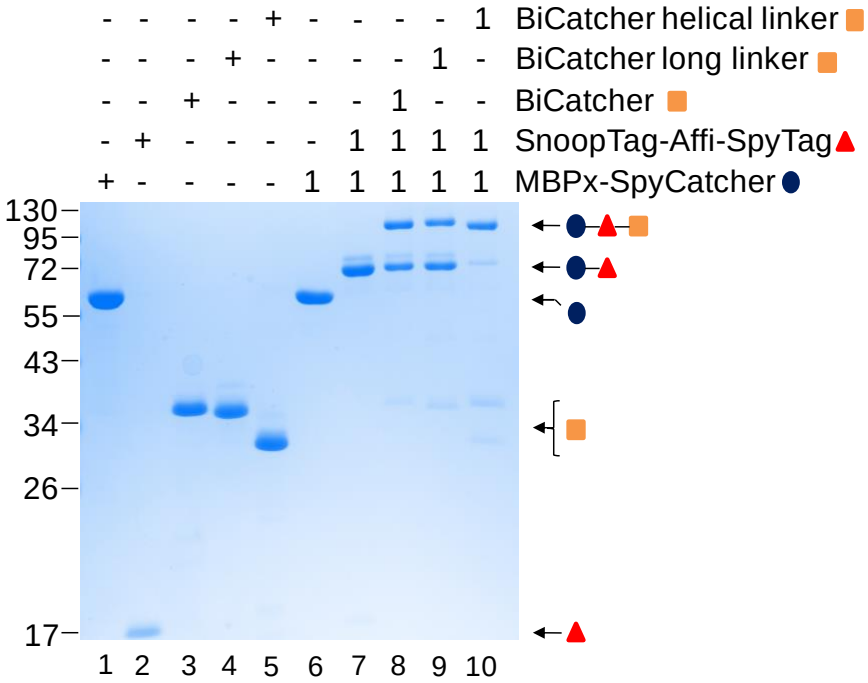

Figure 5.9. Screening of BiCatcher variants. To further improve the conjugation of BiCatcher, different variants of the protein were tested. MBPx-SpyCatcher, SnoopTag-Affi-SpyTag and BiCatcher mutants were loaded onto the gel in isolation as control (lanes 1-5). Following MBPx-SpyCatcher immobilization on the resin (lane 6) and addition of SnoopTag-Affi-SpyTag (lane 7), different BiCatcher variants were added to each sample (lanes 8-10). To better appreciate differences in the conjugation efficiency, BiCatcher variants were added in TBS pH 8.0 without TMAO, to reduce their incorporation efficiency. Conjugation efficiency was assessed by eluting samples with maltose prior to SDS-PAGE analysis with Coomassie staining.

BiCatcher wt and BiCatcher long linker allowed only a partial conjugation to the MBP-SpyCatcher:SnoopTag-Affi-SpyTag complex. Conversely, BiCatcher helical linker (N-terminal short SpyCatcher fused through α-helical spacer to SnoopCatcher) enabled reaction completion (Figure 5.9). Since helical BiCatcher proved to be the best reacting connector this fusion protein will be hereafter used in all the presented results. Moreover, for simplicity I will hereafter refer to it as BiCatcher.

5.2.3 Assembly of affibody decamer

To investigate the biochemical properties of the synthesized polyproteins, we decided to assemble, as a model, a chain containing 10 units (Figure 5.10).

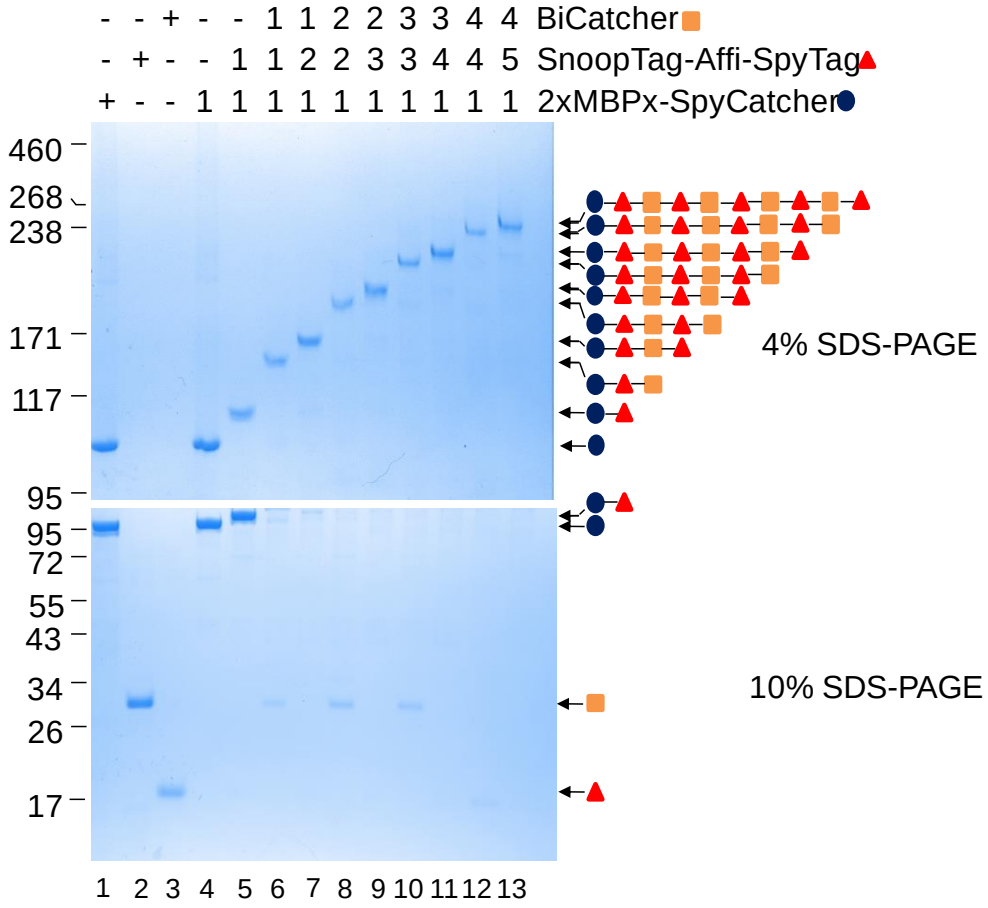

Figure 5.10. Synthesis of a decamer. To assemble a decamer, 2xMBPx-SpyCatcher was immobilized on amylose for optimal anchoring. Sequential addition of anti-HER2 affibody monomers tailored with SnoopTag and SpyTag (SnoopTag-Affi-SpyTag) and BiCatcher (SpyCatcher- α-helical spacer-SnoopCatcher) enabled assembly formation. Decamer formation was monitored via SDS-PAGE by eluting samples with maltose after each conjugation step and loading samples, without further purification, onto Tris-acetate gels (lanes 4-13). As controls 2xMBPx-SpyCatcher, SnoopTag-Affi-SpyTag and BiCatcher were loaded in isolation (lanes 1-3).

Stepwise assembly of the desired polyprotein chains was effective, with quantitative conjugation of each building block, forming a product 10 units long (a decamer, Figure 5.10, lane 13).

To validate the identity of the assembled decamer, electrospray ionization mass spectrometry (ESI-MS) was performed (Figure 5.11A). Mass spectrometry was consistent with the formation of the desired polyprotein chain, showing a good correspondence between the observed decamer mass (285 ± 3 kDa) and the decamer expected mass (282.5 kDa, containing nine isopeptide bonds).

To assess whether the assembled polyprotein chain forms aggregates in solution, decamer was analyzed by size-exclusion chromatography (SEC) (Figure 5.11B). Decamer eluted from the gel-filtration column as major peak with negligible self association (Figure 5.11B). According to the calibration curve of the column, the observed molecular mass of decamer (287 kDa) was in agreement with the expected decamer mass (282.5), thus confirming the identity of the assembly.

To further characterize the decamer properties, its thermostability and stability over time were investigated (Figure 5.12). Decamer was heated at different temperatures ranging from 25 to 70°C, which revealed a good stability with only marginal loss of solubility at 70°C (Figure 5.12A). Analysis of decamer stability showed a good integrity to storage of the assembly, with only limited degradation and minimal loss of solubility (Figure 5.12B).

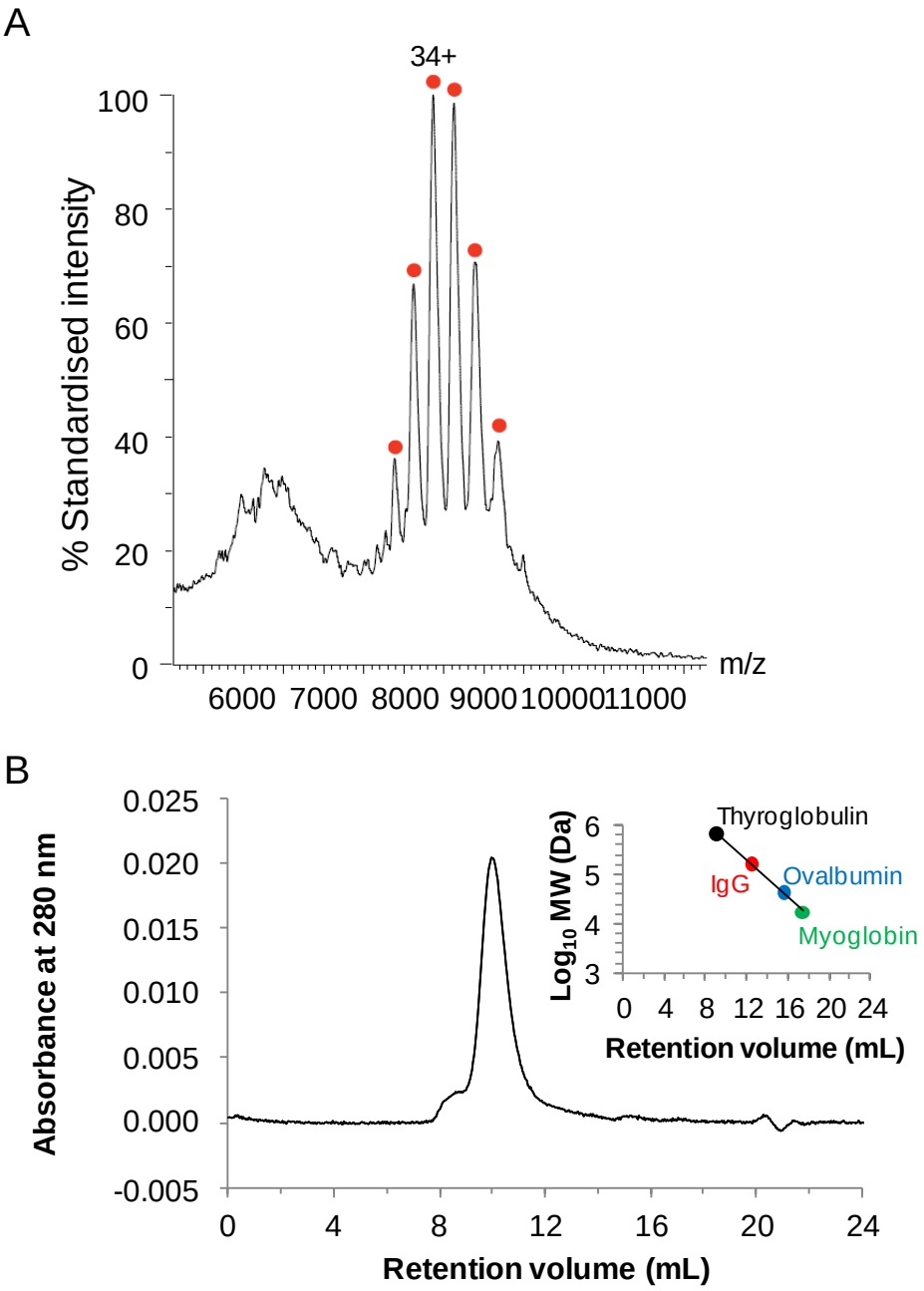

Figure 5.11. Characterization of the assembled decamer. A) Mass spectrometry of decamer, 2xMBPx-SpyCatcher:(SnoopTag-Affi-SpyTag:BiCatcher)$_4$:SnoopTag-Affi-SpyTag. Peaks corresponding to decamer are marked with red circles, along with the charged state of the highest peak. Decamer expected mass (282.5 kDa) was calculated as the sum of the mass of each component (assuming cleaved fMet) considering loss of water (-18 Da) from each SpyTag/SpyCatcher reaction and loss of ammonia (-17.03 Da) deriving from the formation of each SnoopTag-SnoopCatcher amide bond B) Size-exclusion chromatography profile of decamer, 2xMBPx-SpyCatcher:(SnoopTag-Affi-SpyTag:BiCatcher)$_4$:SnoopTag-Affi-SpyTag. Inset shows the column's calibration curve.

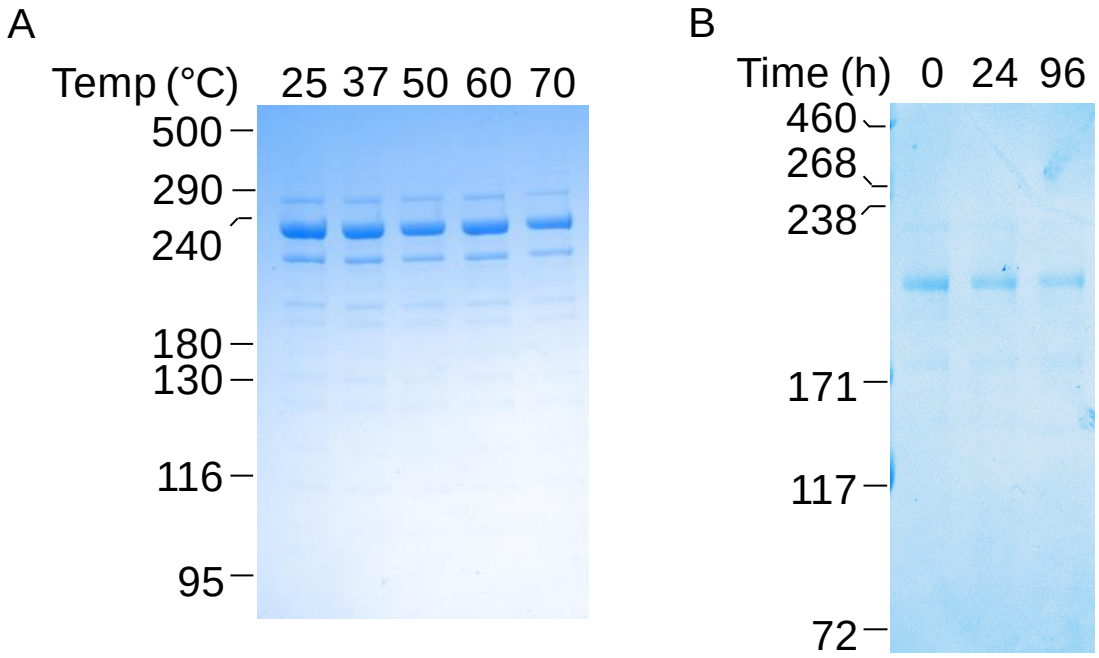

Figure 5.12. Stability of decamer. A) Decamer, 2xMBPx-SpyCatcher:(SnoopTag-Affi-SpyTag:BiCatcher)$_4$:SnoopTag-Affi-SpyTag was heated at the indicated temperature for 3 min and centrifuged to remove aggregates before analysis of its integrity by SDS-PAGE B) Decamer, biotin-SpyCatcher:(SnoopTag-Affi-SpyTag:BiCatcher)$_4$:SnoopTag-Affi-SpyTag was incubated at 25°C for 1-4 days and analyzed by SDS-PAGE with Coomassie staining to check for degradation.

5.3 Combinatorial assembly of protein polymers

Despite the growing interest in the development and production of highly controlled multicomponent assemblies, a general and a versatile platform for the production of polyproteins is still missing. According to the data so far presented, the solid-phase synthesis of polyproteins via sequential isopeptide bond formation could represent a general method for the successful production of protein assemblies.

To test whether our approach would be a reliable platform, protein polymers, composed of different units targeting cancer-relevant death receptors and growth factor receptors, were assembled in a combinatorial fashion.

5.3.1 Killing cancer cells using combinatorially assembled nanobody-based polyproteins

As a model for the combinatorial assembly of polyproteins, an agonist nanobody (a single domain antibody) directed against the death receptor 5 (DR5) was conjugated with affibodies to cancer-relevant growth factor receptors.

Since targeting DR5 receptor enables triggering of cancer cells death through the activation of the extrinsic apoptosis pathway, anti-DR5 agonist antibodies are emerging as cancer therapeutics (Bajaj and Heath, 2011) (Figure 5.13).

For efficient signal transduction and apoptosis initiation, DR5 clustering is essential (Ashkenazi, 2002). However, some agonist anti-DR5 antibodies are unable to induce apoptosis through receptor clustering and require further cross-linking to exhibit anti-tumour activity (Wilson et al., 2011). Therefore, since our assembly method would provide an ideal platform to synthesize chains of agonist anti-DR5 nanobodies, we decided to build chains enabling the simultaneous targeting of DR5 and growth factor receptors to combine their signaling for enhanced anti-cancer activity.

Our solid-phase assembly approach was exploited to precisely build polyproteins containing repeats of an anti-DR5 nanobody and affibodies to either epidermal growth factor receptor 1 (EGFR), insulin growth factor 1 receptor (IGF1R) or epidermal growth factor receptor 2 (HER2). To identify the best nanobody and affibody combination, a combinatorial assembly scheme was designed to synthesize chains containing four nanobody repeats and one affibody unit whose position was varied across the chain (Figure 5.14).

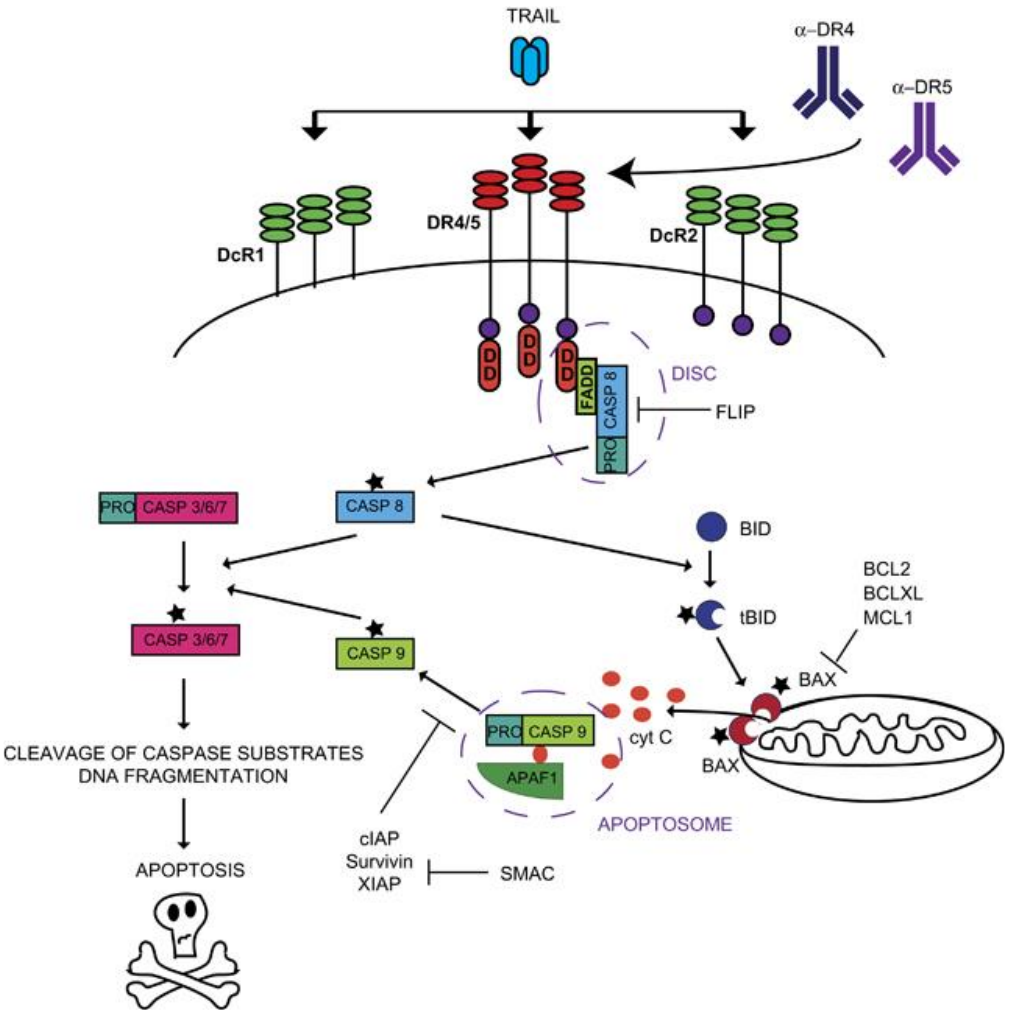

Figure 5.13. The TRAIL apoptotic pathway. Schematic overview of the TRAIL signalling cascade from Dimberg et al., 2013 (permission obtained). Interaction of TRAIL or agonist antibodies with DR4, DR5, DcR1 (decoy receptor-1) or DcR2 induces oligomerization of the receptors. Upon clustering DR4/DR5 recruit, through the death domain (DD) in their cytoplasmatic tail, the Fas-associated protein with death domain (FADD) and pro-caspase 8 (proCASP8), enabling the formation of the death-inducing signalling complex (DISC). DISC activates proCASP8 which initiate apoptosis by directly activating the effector caspases -3, -6 and -7 (extrinsic pathway) or by triggering the intrinsic apoptosis pathway through cleavage of BID and caspase-9 activity. Activation of the effector caspases results in DNA fragmentation and cell death.

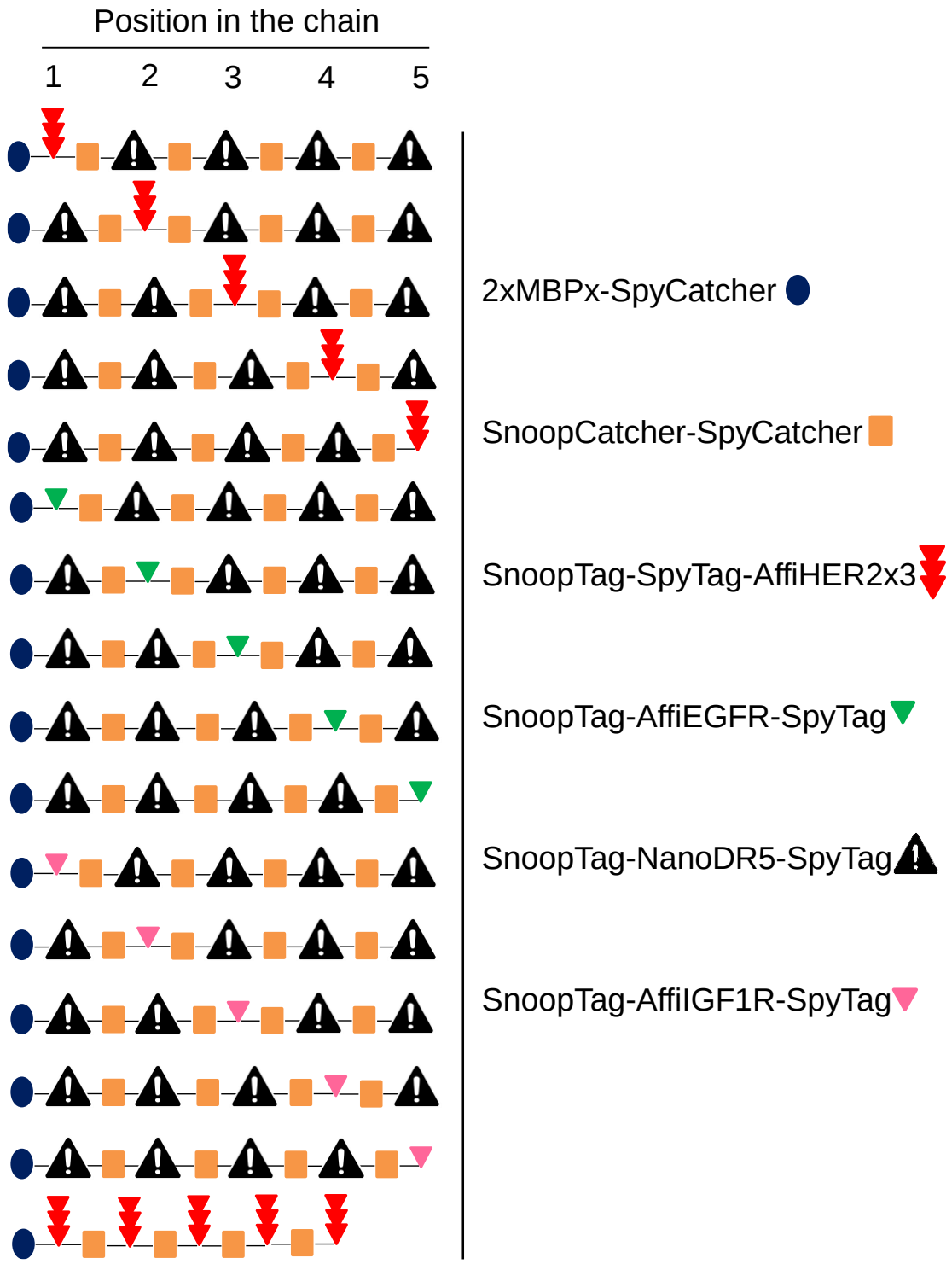

Figure 5.14. Combinatorial assembly of nanobody-based polyproteins. Schematic representation of the combinatorial synthesis scheme. Desired polyproteins contain four nanobody repeats and one affibody unit whose position is varied across the chain.

Nanobody-based polyproteins were combinatorially assembled with good purity (Figure 5.15A) and screened for their ability in killing the breast cancer cell line MDA-MB-231 (Figure 5.15B).

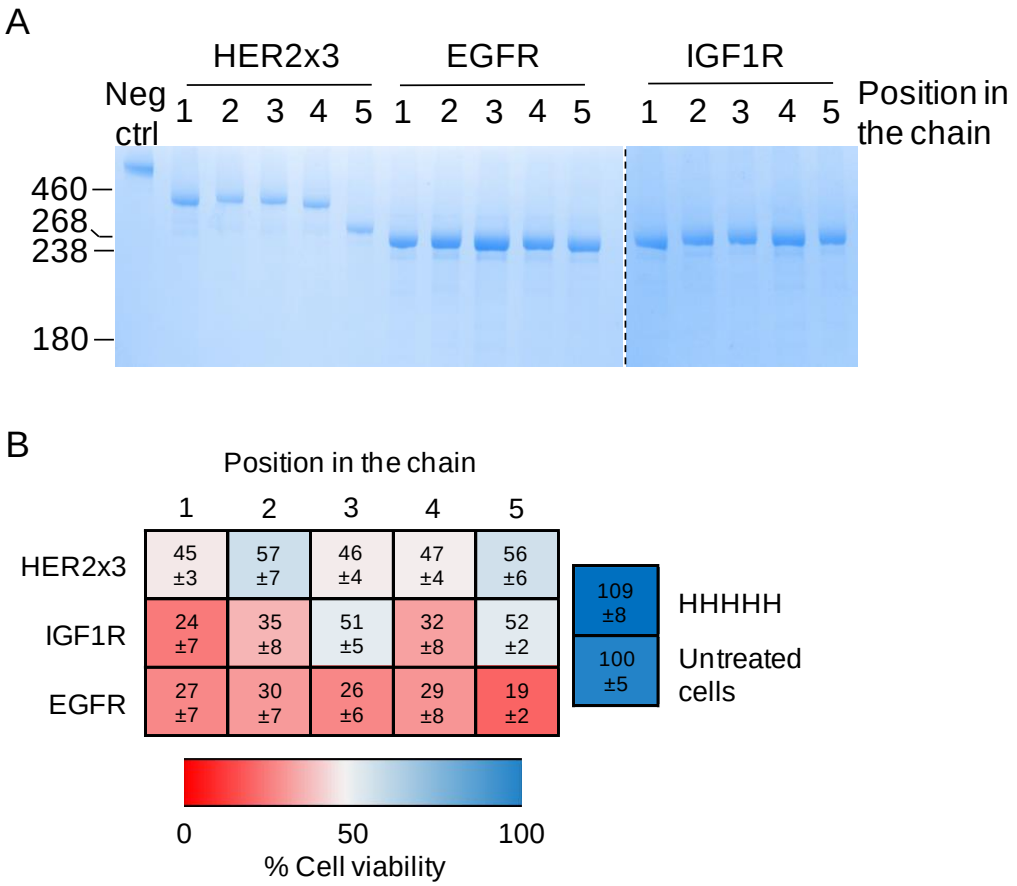

Figure 5.15. Combinatorial synthesis of polyproteins. A) Nanobody-based chains were assembled according to the presented combinatorial scheme and analyzed by SDS-PAGE with Coomassie staining. B) Assembled polyproteins were incubated for 40 h with a breast cancer cell line and screened for their ability in killing cells. A chain formed by five anti-HER2 affibodies (HHHHH) was used as negative control. All error bars are mean of triplicate ± 1 SD.

The modularity of our approach enabled the efficient synthesis of the desired chains (Figure 5.15A). Controlling the position of affibodies in the chain enabled us to identify the optimal nanobody-affibody combination to kill MDA-MB-231 cells, with optimal killing by targeting simultaneously the DR5 and EGFR receptors (Figure 5.15B). Only moderate killing was obtained by an assembly formed of anti-DR5 and anti-HER2 modules, whereas combinations of anti-DR5 nanobody and anti-IGF1R

affibodies had a major effect on the viability of the tested cell line, with anti-IGF1R affibody position affecting the cytotoxicity of the polyproteins (IGF1R position 3 and 5, Figure 5.15.B).

Since optimal killing was obtained with a polyprotein formed by four nanobodies followed and one affibody to EGFR (NNNNE, Fig. 5.15B), such a nanobody-based chain was selected for further analysis.

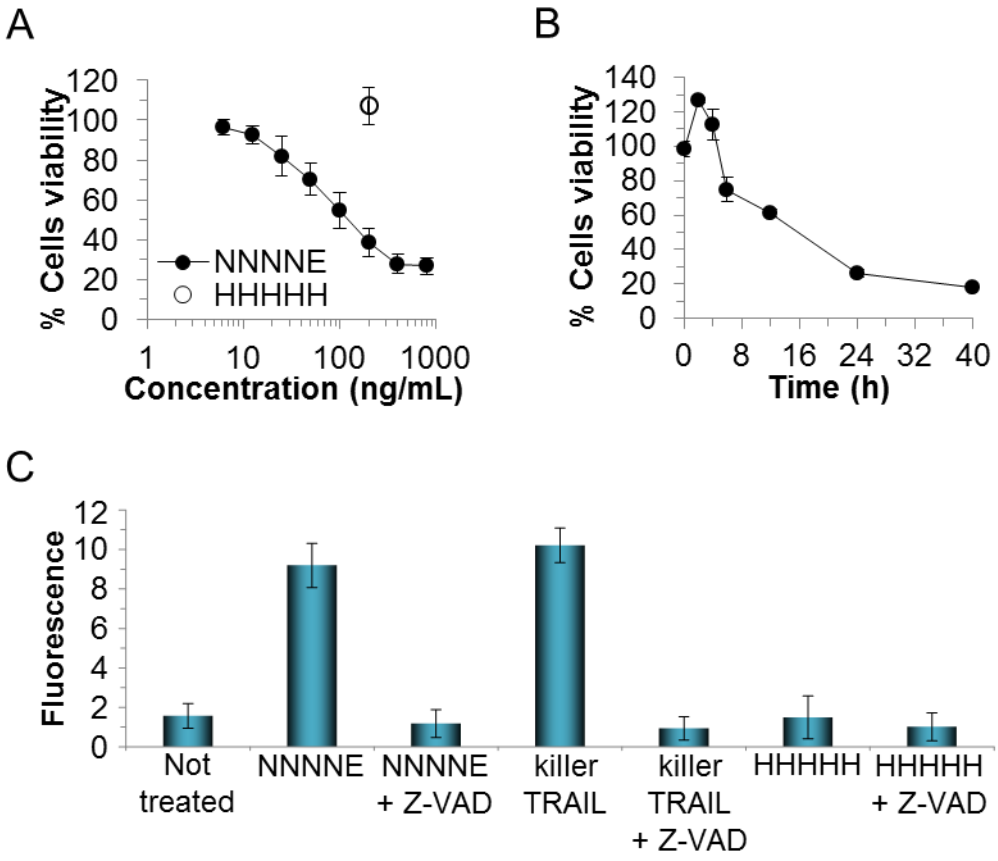

Figure 5.16. Characterization of NNNNE. A) Dose-response curve of NNNNE cytotoxicity. Cells were treated with varying concentrations of NNNNE before viability was assessed by resazurin assay after incubation for 40 h. As negative control 200 ng/mL HHHHH was used. B) The selected nanobody-based chain was added to cells at 200 ng/mL and incubated at 37°C 2, 4, 6, 12, 24 and 40 hours before analysis of cells viability. C) Assessment of caspase activation. Cells were incubated in presence or absence of the pan-caspase inhibitor Z-VAD-FMK before addition of NNNNE, HHHHH (negative control) or the positive control killer TRAIL (recombinant human TRAIL with a linker peptide to promote stable trimerization). All error bars are mean of triplicate ± 1 SD.

NNNNE killed MDA-MB-231 cells in a dose-dependent manner, with a 100 ng/mL apparent EC_{50} (Figure 5.16A). The assembled chain decreased cell viability after as little as 6 hours of incubation, managing to kill 50% of cells in ~15 hours (Figure 5.16B). NNNNE, but not HHHHH, elicited pro-apoptotic signals via caspase activation, with undetectable activation of caspase in presence of the pan-caspase inhibitor Z-VAD-FMK (Figure 5.16C).

Taken together these results clearly demonstrate how the developed method ensures the combinatorial assembly of polyproteins with good control. Assembled chains were functional and allowed us to identify protein combinations for efficient cancer cells killing.

5.4 Discussion

The vast number of available activities makes proteins an exceptional tool for the generation of functional assemblies.

However, the structural and biochemical complexity of proteins has, so far, strongly hampered the development of platforms for the precise synthesis of nano-assemblies. Moreover, the majority of the methods used to construct protein polymers are based on the formation of non-covalent linkages that could result in limited stability and potential rearrangement of the assemblies, so covalent linkage is preferable.

Native chemical ligation (Bayley et al., 2009), split inteins (Chattopadhaya et al., 2009), sortase (Levary et al., 2011) and transglutaminase (Dennler et al., 2014) allow covalent ligation of proteins, but require specific conditions, limiting the repertoire of usable building blocks. SpyTag/SpyCatcher (Zakeri et al., 2012), a covalent ligation system based on the formation of a spontaneous amide bond simply upon mixing of the two partners, has already been proved to have the potential for the generation of

protein polymers (Zhang et al., 2013b). Therefore, this technology is suitable for the generation of protein assemblies. However, the presence of only two molecular partners to drive assembly of polyproteins greatly limits the synthetic freedom. To overcome this limitation, by splitting the RrgA D4 domain from *Streptococcus pneumoniae*, a new peptide-protein pair (SnoopTag and SnoopCatcher) able to spontaneously form an isopeptide bond has been developed. SnoopTag/SnoopCatcher formed an irreversible bond rapidly with quantitative yields under various conditions. SnoopTag/SnoopCatcher and SpyTag/SpyCatcher are orthogonal, so that they could be used for the high-yielding solid-phase synthesis of nano-assemblies under mild conditions.

Solid-phase attachment followed by sequential isopeptide bond formation mediated by the selective specificity of the SnoopCatcher-SnoopTag and SpyCatcher-SpyTag interactions enabled to construct, with molecular precision, a 10 units long protein polymer (decamer).

The assembled decamer was homogeneous with negligible tendency to form aggregates and good stability over time.

The high modularity of the system enabled me to assemble, in a combinatorial fashion, protein polymers directed against DR5 and cancer-relevant growth factor receptors.

Targeting death receptors with antibodies is an attractive therapeutic strategy to promote apoptosis of cancer cells (Graves et al., 2014). In fact, monoclonal antibodies (mAbs) targeting death receptors, and specifically DR5, have been reported to preferentially elicit pro-apoptotic signals in cancer cells, but not in normal cells (Ashkenazi et al., 1999). Despite the therapeutic potential of such approach, clinical outcomes have been, so far, disappointing (Dimberg et al., 2013), due to the

poor ability of the used mAbs in clustering the receptor, a fundamental requirement for DR5-induced apoptosis (Ashkenazi, 2002). Moreover, the occurrence of resistant phenotypes negatively affected the therapeutic impact of anti-DR5 targeting, forcing clinicians to move towards the use of combined immunotherapies (Fuchs et al., 2013; Saltz et al., 2012).

To overcome these limits, multivalent anti-DR5 protein polymers for efficient receptor clustering were assembled. In order to explore the potential synergy of different anti-tumour signals, in addition to anti-DR5 units, the assembled polyproteins contained affibodies to either HER2, IGF1R or EGFR. Solid-phase polyproteins synthesis enabled to build protein polymers with exquisite precision, so position of affibodies in the chains was controlled.

Screening of the synthesized assemblies revealed that combination of anti-EGFR affibody and anti-DR5 nanobody ensures optimal killing of cancer cells and that the position of the affibodies in the chains contribute to tune the anti-cancer efficacy of the nano-assemblies.

The work presented in this chapter enabled the development of a powerful platform for the controlled assembly of polyproteins and to dissect the spatial requirements to optimize the anti-cancer activity of immuno-assemblies.

Chapter 6 : Summary and general discussion

The ability of tailoring protein sequences to alter proteins structure and function led to the protein engineering revolution (Brannigan and Wilkinson, 2002). Rational engineering and *in vitro* evolution (Chen, 2001) enabled scientists to develop important protein-based tools, including biosensors (Ehrick et al., 2005), biocatalysts (Bommarius et al., 2011) and protein therapeutics (Leader et al., 2008).

With the aim of improving the sensitivity of cancer cells isolation and developing new technologies for the synthesis of protein polymers, the work presented in this thesis provided a clear example of how expanding the functional space of proteins through engineering enables to perform complex biochemical tasks.

Isolation and enumeration of circulating tumour cells (CTCs) from the peripheral blood has emerging as a quantifiable method for cancer prognosis and diagnosis (Tang et al., 2013; Wang et al., 2013a).

However, the very low frequency of CTCs in the bloodstream renders their detection and characterization extremely challenging, thereby limiting their application in the clinics. In the past years, different techniques have been used to successfully isolate CTCs (Hong and Zu, 2013), but methods with superior isolation sensitivity are still needed.

Immunomagnetic-based methods have the advantage of being easy, fast and highly customizable, but their performance is limited. In Chapter 3 the molecular requirements for an efficient immunomagnetic isolation of tumour cells were investigated and we observed that the antibody affinity, the connection of the antibody to magnetic beads and the membrane cholesterol levels play a major role on the efficient isolation of tumour cells.

In fact, to enhance the capture of cancer cells expressing low levels of the target antigen it has been demonstrated that one should: (i) use the highest affinity antibody available, (ii) seeking for the strongest available linkage between the antibody and the magnetic beads, and (iii) load the cells with cholesterol prior to isolation. However, since each of these improvements individually had a positive effect on the isolation of cancer cells, they could be singularly translated to other CTCs capture methods (e.g. CellSearch™, herringbone chip) (Balic et al., 2012; Stott et al., 2010), potentially amplifying their detection sensitivity.

Despite the combination of all these enhancements had a significant effect on the recovery from human blood of cancer cells expressing low HER2 levels, such improvements present some challenges.

Since any intermediary connection is detrimental for cancer cells isolation, covalent or ultra-stable linkages between the antibody and the magnetic particle are preferable. In Chapter 3 we observed that the high stability of the streptavidin/biotin system gave a major improvement in the isolation of cells expressing low levels of HER2 and EpCAM. In future, it may be interesting to use antibody-bead connections with even a greater stability than streptavidin (Chivers et al., 2010; Holm et al., 2009) and to develop a universal platform for the site-specific immobilization of antibodies on magnetic particles. A way to achieve this goal could be the use IgG binding domains, such as Protein A (Mazzucchelli et al., 2010) or Protein G (Lee et al., 2011), to enable the oriented site-specific immobilization of antibodies on the magnetic particles. However, Protein A and Protein G bind IgG non-covalently resulting in limited stability of the complex. This limitation could be addressed by

multimerizing these domains, so to increase the affinity of the system by establishing multivalent interactions (Krishnamurthy et al., 2006).

The work presented in this thesis demonstrated how loading cells with cholesterol enhances the recovery of cancer cells expressing low HER2, EGFR and EpCAM levels. Such improvement was cell-type dependent, and could be due to differences in the endogenous cholesterol content of cell membranes (Awad et al., 2003; Yeagle, 1985). The reasons for such cholesterol-mediated effect are not clear: reports have highlighted that cholesterol increases the mobility of the two tyrosine kinase receptors HER2 and EGFR across the membrane plane (Orr et al., 2005), but such evidence is lacking for EpCAM, indicating that cholesterol may have an effect on other membrane receptors and that this should be assessed before performing the immunomagnetic isolation of cancer cells. Therefore, in the future it would be interesting not only trying to elucidate the mechanism underlying the correlation between cholesterol-loading and improved cancer cells isolation, but also to screen other compounds or their combinations (e.g. other sterols, lipids) to identify the best treatment to maximize cell capture. Loading cells with cholesterol is easy and quick, requiring as little as 30 min of incubation, and therefore the identification of other molecules that could enhance cell isolation, simply by doping the samples, represents an attractive approach to improve the detection sensitivity of CTCs from clinical samples.

In Chapter 3 we observed that antibody affinity is crucial for efficient isolation of cancer cells, with even a Fab having a K_d of 0.35 nM not being optimal. Therefore, when designing a cell isolation experiment it is fundamental to consider antibody affinity. For efficient cell recovery, the antibody-antigen interaction must be able to

withstand the shear forces pulling the cell-magnetic bead complex into the magnetic field (Dharmasiri et al., 2010). Antibodies are commonly selected by phage display and ribosome display (Dufner et al., 2006) but are rarely optimized for their ability to form biophysically stable immune-synapses or for the highest affinity. Therefore, with the aim of avoiding cell-bead dissociation, in the future, by exploiting some antibody engineering approaches (Chmura et al., 2001; Holm et al., 2009), it will be valuable to generate ultra-stable antigen-antibody interactions and evaluate their impact on cell isolation.

Another strategy to improve antibody affinity relies in the use of multivalent interactions. Multivalency is a powerful way used by nature to dramatically enhance ligand binding affinity, specificity and kinetics (Ahmad et al., 2012; Albertazzi et al., 2013).

In Chapter 4 it has been shown how affibody polymers, generated using the SpyLigase system, enabled to significantly increase cell recovery, especially of cancer cells expressing low levels of the target antigen. However, the used system requires engineering of the antibodies with specific peptide tags, rendering the method not universally applicable. To overcome this downside, in the future it could be interesting to develop polymers of immunoglobulin binding domains, so that polymerization of commercially available antibodies would be possible without the need for antibody engineering. Moreover, by titrating the antibody concentration on IgG binding domain polymers, it would be possible to obtain antibody polymers with defined valency, so that it could be possible to investigate in details the relationship between multivalent interactions and cell isolation performance.

Although SpyLigase mediated the efficient generation of protein polymers and allowed the conjugation of proteins in a topology-indipendent manner, this technology needs to be improved. In fact, SpyLigase is slow reacting, low yielding and requires specific reaction conditions. Evolving SpyLigase to obtain a protein variant with increased structural stability, faster reaction rate and able to direct isopeptide bond formation and protein assembly under a broader range of biochemical conditions, will be a key step to further improve this peptide-peptide covalent ligation system.

In Chapter 4 we observed how head-to-tail polymerization of proteins via SpyLigase was efficient but uncontrollable, generating polymers ranging from 2 to more than 16 units. Therefore, with the aim of assembling protein monomers into well defined protein polymers via isopeptide bonds formation, a new peptide tag orthogonal to SpyTag was developed.

As shown in Chapter 5, SnoopTag is a 12 amino acids peptide tag that forms a spontaneous isopeptide bond with its protein partner (SnoopCatcher) simply upon mixing. SnoopTag/SnoopCatcher form a spontaneous amide bond rapidly and with quantitative yields under a wide range of conditions, without specific buffer components. Because of its robustness, SnoopTag/SnoopCatcher hold the promise for *in vivo* protein bioconjugation and this feature will be tested in the future. Furthermore, this protein-peptide pair could be used as scaffold for the generation of a new peptide-peptide ligation system by creating SnoopLigase. In fact, by leaving SnoopTag unmodified and excising from SnoopCatcher the β-strand containing the reactive Asparagine, it would be possible to create a peptide-peptide covalent ligation system orthogonal to SpyLigase. In addition, since the β-strand bearing the reactive Asparagine is located at the C-terminal region of SnoopCatcher, it is unlikely that the

removal of this β-strand can highly destabilize the structure of the resulting protein domain as observed for SpyLigase, thereby potentially generating a stable and fast reacting SnoopLigase.

In Chapter 5 we observed that SnoopTag/SnoopCatcher and SpyTag/SpyCatcher are orthogonal protein-peptide pairs, and how they ensured, through isopeptide bond formation, the solid phase assembly of robust and programmable protein polymers. Protein polymers initiation, extension and release steps occurred under mild aqueous conditions, so that this system could be applied to a wide range of proteins. However, to improve the solid-phase synthesis of protein polymers even further, other solid-phase immobilization strategies should be explored. Attaching the nascent chain to the resin through the biotin/avidin interaction enabled to avoid polymers dissociation during washing steps, but resulted in only partial recovery of the synthesized chain. On the other hand, MBP-based immobilization was suitable for complete and easy elution of polymers from the resin, but could incur chains loss during the extensive washing steps.

Nanobody agonist for DR5 and an affibody to either HER2, EGFR, IGF1R were linked into precise programmed nano-assemblies for efficient cancer cells killing, with tuning the affibody position in the chain able to affect cancer cell citotoxicity. This effect could be dependent either on the conformation assumed by chains, resulting in variations of the receptor engagement at the cell surface and therefore influencing the extent of the DR5 receptor clustering, or it could be due to the synergy between the death receptor and the growth factor receptors signalling pathways. To test the first hypothesis, a systematic analysis of the nano-assemblies by atomic force

microscopy (AFM) could give some indications about the spatial organization of the chains interacting with the targeted receptors on the cell surface (Raab et al., 1999).

Instead, to test whether affibody position in the chain can tune cells citotoxicity by modulating the strength of the induced signals, quantitative analysis of the amount of formed DISC complex and the phosphorylation levels of the targeted tyrosine kinase receptor should be performed.

Thanks to its modularity and simplicity, our solid-phase assembly of protein polymers via sequential formation of isopeptide bond could provide an ideal platform to synthesize controlled protein chains.

In the future it will be interesting to use such technology to generate controlled antibody polymers to isolate cancer cells. In this way, in fact, it would be possible not only to synthesize multivalent and/or multispecific antibody assemblies, but also to precisely determine, given a specific binder, the minimal number of multivalent interactions required to enhance cancer cells capture. Moreover, by generating both antibody polymers for cell isolation and antibody chains to promote cells death, it could be possible to develop a platform suitable for the isolation of CTCs from patient samples, and subsequent selection of the best antibody polymer to kill the isolated CTCs, so to identify the best personalized treatment.

An area where the controlled synthesis of polyproteins could be incredibly useful is immunity (Davis et al., 2011). In fact, since the low affinity of T cell receptor (TCR) for peptides-loaded major histocompatibility complex (MHC) (Matsui et al., 1991), multimerization of peptide-MHC complexes provides the only useful approach for improving their binding affinity to the TCR (Davis et al., 2011). Multimeric peptide-MHC complexes allowed the analysis of specific immune responses in infectious

disease (Day et al., 2003) and cancer (Haanen et al., 2000), as well as the purification of antigen-specific T cells for adoptive transfer (Cobbold et al., 2005). Therefore, the possibility of producing peptide-MHC complexes with the desired valency and controlled spatial requirements would provide an excellent target to gain a better insight into the TCR activation and for the development of new therapeutic approaches.

Another possible application for polyproteins could be the generation of nano-assemblies formed by cancer targeting molecules and T cell-engaging antibodies. This approach has already being exploited and allowed the generation of blinatumomab, a bispecific T-cell engager (BiTE) targeting the CD19 antigen present on lymphoblasts and the CD3 receptor on T cells (Bargou et al., 2008). Since varying the concentration of anti-CD3 antibodies influences T cells activation (Borovsky et al., 2002; Matic et al., 2013), the generation of highly tumour-specific protein polymers bearing defined number of cancer specific molecules and anti-CD3 antibodies could allow (i) *in vivo* active targeting of cancer with superior specificity and (ii) the modulation of T-cells activation, generating an immune response with the desired strength to potentially increase the efficacy of such immunomodulatory assembly.

Moreover, since antigenic multimers have the potential to directly stimulate B cells (Bachmann et al., 1993) and/or increase the antigen uptake of antigen-processing cells (APCs) (Jones et al., 2011), developing controlled antigen polymers would be a simple route for the generation of new vaccines.

Bibliography

Aggarwal, C., Meropol, N.J., Punt, C.J., Iannotti, N., Saidman, B.H., Sabbath, K.D., Gabrail, N.Y., Picus, J., Morse, M.A., Mitchell, E., et al. (2013). Relationship among circulating tumor cells, CEA and overall survival in patients with metastatic colorectal cancer. Ann. Oncol. Off. J. Eur. Soc. Med. Oncol. ESMO *24*, 420–428.

Ahmad, K.M., Oh, S.S., Kim, S., McClellen, F.M., Xiao, Y., and Soh, H.T. (2011). Probing the Limits of Aptamer Affinity with a Microfluidic SELEX Platform. PLoS ONE *6*, e27051.

Ahmad, K.M., Xiao, Y., and Soh, H.T. (2012). Selection is more intelligent than design: improving the affinity of a bivalent ligand through directed evolution. Nucleic Acids Res. gks899.

Albertazzi, L., Martinez-Veracoechea, F.J., Leenders, C.M.A., Voets, I.K., Frenkel, D., and Meijer, E.W. (2013). Spatiotemporal control and superselectivity in supramolecular polymers using multivalency. Proc. Natl. Acad. Sci. *110*, 12203–12208.

Alix-Panabières, C. (2012). EPISPOT assay: detection of viable DTCs/CTCs in solid tumor patients. Recent Results Cancer Res. Fortschritte Krebsforsch. Prog. Dans Rech. Sur Cancer *195*, 69–76.

Alix-Panabières, C., and Pantel, K. (2014). Challenges in circulating tumour cell research. Nat. Rev. Cancer *14*, 623–631.

Amelung, S., Nerlich, A., Rohde, M., Spellerberg, B., Cole, J.N., Nizet, V., Chhatwal, G.S., and Talay, S.R. (2011). The FbaB-type fibronectin-binding protein of Streptococcus pyogenes promotes specific invasion into endothelial cells. Cell. Microbiol. *13*, 1200–1211.

Ashkenazi, A. (2002). Targeting death and decoy receptors of the tumour-necrosis factor superfamily. Nat. Rev. Cancer *2*, 420–430.

Ashkenazi, A., Pai, R.C., Fong, S., Leung, S., Lawrence, D.A., Marsters, S.A., Blackie, C., Chang, L., McMurtrey, A.E., Hebert, A., et al. (1999). Safety and antitumor activity of recombinant soluble Apo2 ligand. J. Clin. Invest. *104*, 155–162.

Ashworth T. R. (1869). A case of cancer in which cells similar to those in the tumours were seen in the blood after death. Australian Med. J. *14*, 146.

Awad, A.B., Williams, H., and Fink, C.S. (2003). Effect of phytosterols on cholesterol metabolism and MAP kinase in MDA-MB-231 human breast cancer cells. J. Nutr. Biochem. *14*, 111–119.

Babayan, A., Hannemann, J., Spötter, J., Müller, V., Pantel, K., and Joosse, S.A. (2013). Heterogeneity of estrogen receptor expression in circulating tumor cells from metastatic breast cancer patients. PloS One *8*, e75038.

Bachmann, M.F., and Jennings, G.T. (2010). Vaccine delivery: a matter of size, geometry, kinetics and molecular patterns. Nat. Rev. Immunol. *10*, 787–796.

Bachmann, M.F., Rohrer, U.H., Kundig, T.M., Burki, K., Hengartner, H., and Zinkernagel, R.M. (1993). The influence of antigen organization on B cell responsiveness. Science *262*, 1448–1451.

Bajaj, M., and Heath, E.I. (2011). Conatumumab: a novel monoclonal antibody against death receptor 5 for the treatment of advanced malignancies in adults. Expert Opin. Biol. Ther. *11*, 1519–1524.

Balic, M., Lin, H., Williams, A., Datar, R.H., and Cote, R.J. (2012). Progress in circulating tumor cell capture and analysis: implications for cancer management. Expert Rev. Mol. Diagn. *12*, 303–312.

Bargou, R., Leo, E., Zugmaier, G., Klinger, M., Goebeler, M., Knop, S., Noppeney, R., Viardot, A., Hess, G., Schuler, M., et al. (2008). Tumor regression in cancer patients by very low doses of a T cell-engaging antibody. Science *321*, 974–977.

Barriere, G., Fici, P., Gallerani, G., Fabbri, F., Zoli, W., and Rigaud, M. (2014). Circulating tumor cells and epithelial, mesenchymal and stemness markers: characterization of cell subpopulations. Ann. Transl. Med. *2*.

Bayley, H., Cheley, S., Harrington, L., and Syeda, R. (2009). Wrestling with native chemical ligation. ACS Chem. Biol. *4*, 983–985.

Beck, Z., Balogh, A., Kis, A., Izsépi, E., Cervenak, L., László, G., Bíró, A., Liliom, K., Mocsár, G., Vámosi, G., et al. (2010). New cholesterol-specific antibodies remodel HIV-1 target cells' surface and inhibit their in vitro virus production. J. Lipid Res. *51*, 286–296.

Beckett, D., Kovaleva, E., and Schatz, P.J. (1999). A minimal peptide substrate in biotin holoenzyme synthetase-catalyzed biotinylation. Protein Sci. Publ. Protein Soc. *8*, 921–929.

Berrade, L., and Camarero, J.A. (2009). Expressed protein ligation: a resourceful tool to study protein structure and function. Cell. Mol. Life Sci. *66*, 3909–3922.

Bidard, F.-C., Fehm, T., Ignatiadis, M., Smerage, J.B., Alix-Panabières, C., Janni, W., Messina, C., Paoletti, C., Müller, V., Hayes, D.F., et al. (2013). Clinical application of circulating tumor cells in breast cancer: overview of the current interventional trials. Cancer Metastasis Rev. *32*, 179–188.

Blann, A.D., Woywodt, A., Bertolini, F., Bull, T.M., Buyon, J.P., Clancy, R.M., Haubitz, M., Hebbel, R.P., Lip, G.Y.H., Mancuso, P., et al. (2005). Circulating endothelial cells. Biomarker of vascular disease. Thromb. Haemost. *93*, 228–235.

Bommarius, A.S., Blum, J.K., and Abrahamson, M.J. (2011). Status of protein engineering for biocatalysts: how to design an industrially useful biocatalyst. Curr. Opin. Chem. Biol. *15*, 194–200.

de Bono, J.S., Scher, H.I., Montgomery, R.B., Parker, C., Miller, M.C., Tissing, H., Doyle, G.V., Terstappen, L.W.W.M., Pienta, K.J., and Raghavan, D. (2008). Circulating tumor cells predict survival benefit from treatment in metastatic castration-

resistant prostate cancer. Clin. Cancer Res. Off. J. Am. Assoc. Cancer Res. *14*, 6302–6309.

Boruah, B.M., Liu, D., Ye, D., Gu, T., Jiang, C., Qu, M., Wright, E., Wang, W., He, W., Liu, C., et al. (2013). Single Domain Antibody Multimers Confer Protection against Rabies Infection. PLoS ONE *8*, e71383.

Brannigan, J.A., and Wilkinson, A.J. (2002). Protein engineering 20 years on. Nat. Rev. Mol. Cell Biol. *3*, 964–970.

Brizzard, B., and Chubet, R. (2001). Epitope tagging of recombinant proteins. Curr. Protoc. Neurosci. Editor. Board Jacqueline N Crawley Al *Chapter 5*, Unit 5.8.

Brustad, E.M., and Arnold, F.H. (2011). Optimizing Non-natural Protein Function with Directed Evolution. Curr. Opin. Chem. Biol. *15*, 201–210.

Budzik, J.M., Marraffini, L.A., Souda, P., Whitelegge, J.P., Faull, K.F., and Schneewind, O. (2008). Amide bonds assemble pili on the surface of bacilli. Proc. Natl. Acad. Sci. U. S. A. *105*, 10215–10220.

Busch, G.K., Tate, E.W., Gaffney, P.R.J., Rosivatz, E., Woscholski, R., and Leatherbarrow, R.J. (2008). Specific N-terminal protein labelling: use of FMDV 3Cproprotease and native chemical ligation. Chem. Commun. 3369–3371.

Cameron, M.D., Schmidt, E.E., Kerkvliet, N., Nadkarni, K.V., Morris, V.L., Groom, A.C., Chambers, A.F., and MacDonald, I.C. (2000). Temporal progression of metastasis in lung: cell survival, dormancy, and location dependence of metastatic inefficiency. Cancer Res. *60*, 2541–2546.

Carlson, J.C.T., Jena, S.S., Flenniken, M., Chou, T., Siegel, R.A., and Wagner, C.R. (2006). Chemically controlled self-assembly of protein nanorings. J. Am. Chem. Soc. *128*, 7630–7638.

Chaffer, C.L., and Weinberg, R.A. (2011). A Perspective on Cancer Cell Metastasis. Science *331*, 1559–1564.

Chattopadhaya, S., Abu Bakar, F.B., and Yao, S.Q. (2009). Use of intein-mediated protein ligation strategies for the fabrication of functional protein arrays. Methods Enzymol. *462*, 195–223.

Chen, R. (2001). Enzyme engineering: rational redesign versus directed evolution. Trends Biotechnol. *19*, 13–14.

Chen, I., Howarth, M., Lin, W., and Ting, A.Y. (2005). Site-specific labeling of cell surface proteins with biophysical probes using biotin ligase. Nat. Methods *2*, 99–104.

Chen, P., Huang, Y.-Y., Hoshino, K., and Zhang, J.X.J. (2015). Microscale magnetic field modulation for enhanced capture and distribution of rare circulating tumor cells. Sci. Rep. *5*, 8745.

Chen, W., Villa-Diaz, L.G., Sun, Y., Weng, S., Kim, J.K., Lam, R.H.W., Han, L., Fan, R., Krebsbach, P.H., and Fu, J. (2012). Nanotopography influences adhesion,

spreading, and self-renewal of human embryonic stem cells. ACS Nano *6*, 4094–4103.

Chen, W., Weng, S., Zhang, F., Allen, S., Li, X., Bao, L., Lam, R.H.W., Macoska, J.A., Merajver, S.D., and Fu, J. (2013). Nanoroughened Surfaces for Efficient Capture of Circulating Tumor Cells without Using Capture Antibodies. ACS Nano *7*, 566–575.

Chen, Y.-X., Triola, G., and Waldmann, H. (2011). Bioorthogonal Chemistry for Site-Specific Labeling and Surface Immobilization of Proteins. Acc. Chem. Res. *44*, 762–773.

Chiu, J., March, P.E., Lee, R., and Tillett, D. (2004). Site-directed, Ligase-Independent Mutagenesis (SLIM): a single-tube methodology approaching 100% efficiency in 4 h. Nucleic Acids Res. *32*, e174.

Chivers, C.E., Crozat, E., Chu, C., Moy, V.T., Sherratt, D.J., and Howarth, M. (2010). A streptavidin variant with slower biotin dissociation and increased mechanostability. Nat. Methods *7*, 391–393.

Chmura, A.J., Orton, M.S., and Meares, C.F. (2001). Antibodies with infinite affinity. Proc. Natl. Acad. Sci. U. S. A. *98*, 8480–8484.

Cho, H.-S., Mason, K., Ramyar, K.X., Stanley, A.M., Gabelli, S.B., Denney, D.W., and Leahy, D.J. (2003a). Structure of the extracellular region of HER2 alone and in complex with the Herceptin Fab. Nature *421*, 756–760.

Cho, H.-S., Mason, K., Ramyar, K.X., Stanley, A.M., Gabelli, S.B., Denney, D.W., and Leahy, D.J. (2003b). Structure of the extracellular region of HER2 alone and in complex with the Herceptin Fab. Nature *421*, 756–760.

Citri, A., and Yarden, Y. (2006). EGF–ERBB signalling: towards the systems level. Nat. Rev. Mol. Cell Biol. *7*, 505–516.

Clark, L.A., Boriack-Sjodin, P.A., Eldredge, J., Fitch, C., Friedman, B., Hanf, K.J.M., Jarpe, M., Liparoto, S.F., Li, Y., Lugovskoy, A., et al. (2006). Affinity enhancement of an in vivo matured therapeutic antibody using structure-based computational design. Protein Sci. Publ. Protein Soc. *15*, 949–960.

Clarke, C., and Davies, S. (2001). Immunomagnetic cell separation. Methods Mol. Med. *58*, 17–23.

Clarke, E.J., and Allan, V. (2002). Intermediate filaments: vimentin moves in. Curr. Biol. CB *12*, R596–R598.

Cobbold, M., Khan, N., Pourgheysari, B., Tauro, S., McDonald, D., Osman, H., Assenmacher, M., Billingham, L., Steward, C., Crawley, C., et al. (2005). Adoptive transfer of cytomegalovirus-specific CTL to stem cell transplant patients after selection by HLA–peptide tetramers. J. Exp. Med. *202*, 379–386.

Cooper, R.A. (1978). Influence of increased membrane cholesterol on membrane fluidity and cell function in human red blood cells. J. Supramol. Struct. *8*, 413–430.

Cuesta, Á.M., Sainz-Pastor, N., Bonet, J., Oliva, B., and Álvarez-Vallina, L. (2010). Multivalent antibodies: when design surpasses evolution. Trends Biotechnol. *28*, 355–362.

Dainiak, M.B., Kumar, A., Galaev, I.Y., and Mattiasson, B. (2007). Methods in cell separations. Adv. Biochem. Eng. Biotechnol. *106*, 1–18.

Daniels, D. L., Méndez, J., Benink, H., and Niles, A. (2014). Discovering Protein Interactions and Characterizing Protein Function Using HaloTag Technology. J. Vis. Exp. *89*.

Dassa, B., Amitai, G., Caspi, J., Schueler-Furman, O., and Pietrokovski, S. (2007). Trans Protein Splicing of Cyanobacterial Split Inteins in Endogenous and Exogenous Combinations. Biochemistry (Mosc.) *46*, 322–330.

Davies, D.R., and Cohen, G.H. (1996). Interactions of protein antigens with antibodies. Proc. Natl. Acad. Sci. U. S. A. *93*, 7–12.

Davis, M.M., Altman, J.D., and Newell, E.W. (2011). Interrogating the repertoire: broadening the scope of peptide–MHC multimer analysis. Nat. Rev. Immunol. *11*, 551–558.

Dawson, P.E., and Kent, S.B.H. (2000). Synthesis of Native Proteins by Chemical Ligation. Annu. Rev. Biochem. *69*, 923–960.

Dawson, P.E., Muir, T.W., Clark-Lewis, I., and Kent, S.B. (1994). Synthesis of proteins by native chemical ligation. Science *266*, 776–779.

Day, C.L., Seth, N.P., Lucas, M., Appel, H., Gauthier, L., Lauer, G.M., Robbins, G.K., Szczepiorkowski, Z.M., Casson, D.R., Chung, R.T., et al. (2003). Ex vivo analysis of human memory CD4 T cells specific for hepatitis C virus using MHC class II tetramers. J. Clin. Invest. *112*, 831–842.

Deng, G., Herrler, M., Burgess, D., Manna, E., Krag, D., and Burke, J.F. (2008). Enrichment with anti-cytokeratin alone or combined with anti-EpCAM antibodies significantly increases the sensitivity for circulating tumor cell detection in metastatic breast cancer patients. Breast Cancer Res. BCR *10*, R69.

Dennler, P., Chiotellis, A., Fischer, E., Brégeon, D., Belmant, C., Gauthier, L., Lhospice, F., Romagne, F., and Schibli, R. (2014). Transglutaminase-based chemo-enzymatic conjugation approach yields homogeneous antibody-drug conjugates. Bioconjug. Chem. *25*, 569–578.

Dharmasiri, U., Witek, M.A., Adams, A.A., and Soper, S.A. (2010). Microsystems for the Capture of Low-Abundance Cells. Annu. Rev. Anal. Chem. *3*, 409–431.

Di Ianni, M., Del Papa, B., Cecchini, D., Bonifacio, E., Moretti, L., Zei, T., Iacucci Ostini, R., Falzetti, F., Fontana, L., Tagliapietra, G., et al. (2009). Immunomagnetic isolation of CD4+CD25+FoxP3+ natural T regulatory lymphocytes for clinical applications. Clin. Exp. Immunol. *156*, 246–253.

Dimberg, L.Y., Anderson, C.K., Camidge, R., Behbakht, K., Thorburn, A., and Ford, H.L. (2013). On the TRAIL to successful cancer therapy? Predicting and counteracting resistance against TRAIL-based therapeutics. Oncogene *32*, 1341–1350.

Dragovich, T., and Campen, C. (2009). Anti-EGFR-Targeted Therapy for Esophageal and Gastric Cancers: An Evolving Concept. J. Oncol. *2009*, 804108.

Dufner, P., Jermutus, L., and Minter, R.R. (2006). Harnessing phage and ribosome display for antibody optimisation. Trends Biotechnol. *24*, 523–529.

Ehrick, J.D., Deo, S.K., Browning, T.W., Bachas, L.G., Madou, M.J., and Daunert, S. (2005). Genetically engineered protein in hydrogels tailors stimuli-responsive characteristics. Nat. Mater. *4*, 298–302.

Feldwisch, J., Tolmachev, V., Lendel, C., Herne, N., Sjöberg, A., Larsson, B., Rosik, D., Lindqvist, E., Fant, G., Höidén-Guthenberg, I., et al. (2010). Design of an optimized scaffold for affibody molecules. J. Mol. Biol. *398*, 232–247.

Fierer, J.O., Veggiani, G., and Howarth, M. (2014). SpyLigase peptide-peptide ligation polymerizes affibodies to enhance magnetic cancer cell capture. Proc. Natl. Acad. Sci. U. S. A. *111*, E1176–E1181.

Fischer-Durand, N., Salmain, M., Rudolf, B., Dai, L., Jugé, L., Guérineau, V., Laprévote, O., Vessières, A., and Jaouen, G. (2010). Site-specific conjugation of metal carbonyl dendrimer to antibody and its use as detection reagent in immunoassay. Anal. Biochem. *407*, 211–219.

Fox, J.D., and Waugh, D.S. (2003). Maltose-binding protein as a solubility enhancer. Methods Mol. Biol. Clifton NJ *205*, 99–117.

Friedlander, T.W., Ngo, V.T., Dong, H., Premasekharan, G., Weinberg, V., Doty, S., Zhao, Q., Gilbert, E.G., Ryan, C.J., Chen, W.-T., et al. (2014). Detection and characterization of invasive circulating tumor cells derived from men with metastatic castration-resistant prostate cancer. Int. J. Cancer *134*, 2284–2293.

Friedman, M., Orlova, A., Johansson, E., Eriksson, T.L.J., Höidén-Guthenberg, I., Tolmachev, V., Nilsson, F.Y., and Ståhl, S. (2008). Directed evolution to low nanomolar affinity of a tumor-targeting epidermal growth factor receptor-binding affibody molecule. J. Mol. Biol. *376*, 1388–1402.

Fuchs, C.S., Fakih, M., Schwartzberg, L., Cohn, A.L., Yee, L., Dreisbach, L., Kozloff, M.F., Hei, Y., Galimi, F., Pan, Y., et al. (2013). TRAIL receptor agonist conatumumab with modified FOLFOX6 plus bevacizumab for first-line treatment of metastatic colorectal cancer: A randomized phase 1b/2 trial. Cancer *119*, 4290–4298.

Gach, P.C., Attayek, P.J., Whittlesey, R.L., Yeh, J.J., and Allbritton, N.L. (2014). Micropallet arrays for the capture, isolation and culture of circulating tumor cells from whole blood of mice engrafted with primary human pancreatic adenocarcinoma. Biosens. Bioelectron. *54*, 476–483.

Gaipa, G., Dassi, M., Perseghin, P., Venturi, N., Corti, P., Bonanomi, S., Balduzzi, A., Longoni, D., Uderzo, C., Biondi, A., et al. (2003). Allogeneic bone marrow stem cell transplantation following CD34+ immunomagnetic enrichment in patients with inherited metabolic storage diseases. Bone Marrow Transplant. *31*, 857–860.

Galanzha, E.I., and Zharov, V.P. (2012). Photoacoustic flow cytometry. Methods San Diego Calif *57*, 280–296.

Galanzha, E.I., and Zharov, V.P. (2013). Circulating Tumor Cell Detection and Capture by Photoacoustic Flow Cytometry in Vivo and ex Vivo. Cancers *5*, 1691–1738.

Gautier, A., Juillerat, A., Heinis, C., Corrêa Jr., I.R., Kindermann, M., Beaufils, F., and Johnsson, K. (2008). An Engineered Protein Tag for Multiprotein Labeling in Living Cells. Chem. Biol. *15*, 128–136.

Geiger, T.R., and Peeper, D.S. (2009). Metastasis mechanisms. Biochim. Biophys. Acta BBA - Rev. Cancer *1796*, 293–308.

Gerstner, R.B., Carter, P., and Lowman, H.B. (2002). Sequence plasticity in the antigen-binding site of a therapeutic anti-HER2 antibody. J. Mol. Biol. *321*, 851–862.

Gires, O., and Stoecklein, N.H. (2014). Dynamic EpCAM expression on circulating and disseminating tumor cells: causes and consequences. Cell. Mol. Life Sci. CMLS *71*, 4393–4402.

Gorges, T.M., Tinhofer, I., Drosch, M., Röse, L., Zollner, T.M., Krahn, T., and von Ahsen, O. (2012). Circulating tumour cells escape from EpCAM-based detection due to epithelial-to-mesenchymal transition. BMC Cancer *12*, 178.

Graves, J.D., Kordich, J.J., Huang, T.-H., Piasecki, J., Bush, T.L., Sullivan, T., Foltz, I.N., Chang, W., Douangpanya, H., Dang, T., et al. (2014). Apo2L/TRAIL and the Death Receptor 5 Agonist Antibody AMG 655 Cooperate to Promote Receptor Clustering and Antitumor Activity. Cancer Cell *26*, 177–189.

Griffin, B.A., Adams, S.R., and Tsien, R.Y. (1998). Specific Covalent Labeling of Recombinant Protein Molecules Inside Live Cells. Science *281*, 269–272.

Griffin, M., Casadio, R., and Bergamini, C.M. (2002). Transglutaminases: Nature's biological glues. Biochem. J. *368*, 377–396.

Grover, P.K., Cummins, A.G., Price, T.J., Roberts-Thomson, I.C., and Hardingham, J.E. (2014). Circulating tumour cells: the evolving concept and the inadequacy of their enrichment by EpCAM-based methodology for basic and clinical cancer research. Ann. Oncol. Off. J. Eur. Soc. Med. Oncol. ESMO *25*, 1506–1516.

Gupta, V., Jafferji, I., Garza, M., Melnikova, V.O., Hasegawa, D.K., Pethig, R., and Davis, D.W. (2012). ApoStream™, a new dielectrophoretic device for antibody independent isolation and recovery of viable cancer cells from blood. Biomicrofluidics *6*.

Haanen, J.B., van Oijen, M.G., Tirion, F., Oomen, L.C., Kruisbeek, A.M., Vyth-Dreese, F.A., and Schumacher, T.N. (2000). In situ detection of virus- and tumor-specific T-cell immunity. Nat. Med. *6*, 1056–1060.

Hackeng, T.M., Griffin, J.H., and Dawson, P.E. (1999). Protein synthesis by native chemical ligation: Expanded scope by using straightforward methodology. Proc. Natl. Acad. Sci. U. S. A. *96*, 10068–10073.

Han, B.W., Layman, H., Rode, N.A., Conway, A., Schaffer, D.V., Boudreau, N., Jackson, W.M., and Healy, K.E. (2015). Multivalent conjugates of Sonic hedgehog ccelerate diabetic wound healing. Tissue Eng. Part A.

Hancock, S.M., Uprety, R., Deiters, A., and Chin, J.W. (2010). Expanding the Genetic Code of Yeast for Incorporation of Diverse Unnatural Amino Acids via a Pyrrolysyl-tRNA Synthetase/tRNA Pair. J. Am. Chem. Soc. *132*, 14819–14824.

Harouaka, R.A., Nisic, M., and Zheng, S.-Y. (2013). Circulating Tumor Cell Enrichment Based on Physical Properties. J. Lab. Autom. *18*, 455–468.

Hayes, D.F., Cristofanilli, M., Budd, G.T., Ellis, M.J., Stopeck, A., Miller, M.C., Matera, J., Allard, W.J., Doyle, G.V., and Terstappen, L.W.W.M. (2006). Circulating tumor cells at each follow-up time point during therapy of metastatic breast cancer patients predict progression-free and overall survival. Clin. Cancer Res. Off. J. Am. Assoc. Cancer Res. *12*, 4218–4224.

Hekimian, K., Stein, E.-L., Pachmann, U., and Pachmann, K. (2012). Demasking of epithelial cell adhesion molecule (EpCAM) on circulating epithelial tumor cells by Tween®20 treatment in breast cancer patients. Clin. Chem. Lab. Med. CCLM FESCC *50*, 701–708.

Hengen, P.N. (1995). Purification of His-Tag fusion proteins from Escherichia coli. Trends Biochem. Sci. *20*, 285–286.

Herbst, R.S. (2004). Review of epidermal growth factor receptor biology. Int. J. Radiat. Oncol. Biol. Phys. *59*, 21–26.

Higuchi, R., Krummel, B., and Saiki, R. (1988). A general method of in vitro preparation and specific mutagenesis of DNA fragments: study of protein and DNA interactions. Nucleic Acids Res. *16*, 7351–7367.

Holm, L., Moody, P., and Howarth, M. (2009). Electrophilic Affibodies Forming Covalent Bonds to Protein Targets. J. Biol. Chem. *284*, 32906–32913.

Hong, B., and Zu, Y. (2013). Detecting circulating tumor cells: current challenges and new trends. Theranostics *3*, 377–394.

Hong, W.Y., Jeon, S.H., Lee, E.S., and Cho, Y. (2014). An integrated multifunctional platform based on biotin-doped conducting polymer nanowires for cell capture, release, and electrochemical sensing. Biomaterials *35*, 9573–9580.

Hou, H.W., Warkiani, M.E., Khoo, B.L., Li, Z.R., Soo, R.A., Tan, D.S.-W., Lim, W.-T., Han, J., Bhagat, A.A.S., and Lim, C.T. (2013). Isolation and retrieval of circulating tumor cells using centrifugal forces. Sci. Rep. *3*, 1259.

Hou, J.-M., Krebs, M., Ward, T., Sloane, R., Priest, L., Hughes, A., Clack, G., Ranson, M., Blackhall, F., and Dive, C. (2011). Circulating Tumor Cells as a Window on Metastasis Biology in Lung Cancer. Am. J. Pathol. *178*, 989–996.

Hou, J.-M., Krebs, M.G., Lancashire, L., Sloane, R., Backen, A., Swain, R.K., Priest, L.J.C., Greystoke, A., Zhou, C., Morris, K., et al. (2012). Clinical significance and molecular characteristics of circulating tumor cells and circulating tumor microemboli in patients with small-cell lung cancer. J. Clin. Oncol. Off. J. Am. Soc. Clin. Oncol. *30*, 525–532.

Hu, B., Rochefort, H., and Goldkorn, A. (2013). Circulating Tumor Cells in Prostate Cancer. Cancers *5*, 1676–1690.

Huet, H.A., Growney, J.D., Johnson, J.A., Li, J., Bilic, S., Ostrom, L., Zafari, M., Kowal, C., Yang, G., Royo, A., et al. (2014). Multivalent nanobodies targeting death receptor 5 elicit superior tumor cell killing through efficient caspase induction. mAbs *6*, 1560–1570.

Huh, W.-K., Falvo, J.V., Gerke, L.C., Carroll, A.S., Howson, R.W., Weissman, J.S., and O'Shea, E.K. (2003). Global analysis of protein localization in budding yeast. Nature *425*, 686–691.

Hüsemann, Y., Geigl, J.B., Schubert, F., Musiani, P., Meyer, M., Burghart, E., Forni, G., Eils, R., Fehm, T., Riethmüller, G., et al. (2008). Systemic spread is an early step in breast cancer. Cancer Cell *13*, 58–68.

Hussain, A., Amoury, M., and Barth, S. (2013). SNAP-Tag Technology: A Powerful Tool for Site Specific Conjugation of Therapeutic and Imaging Agents. Curr. Pharm. Des. *19*, 5437–5442.

Hynes, N.E., and Stern, D.F. (1994). The biology of erbB-2/neu/HER-2 and its role in cancer. Biochim. Biophys. Acta *1198*, 165–184.

Ignatiadis, M., Kallergi, G., Ntoulia, M., Perraki, M., Apostolaki, S., Kafousi, M., Chlouverakis, G., Stathopoulos, E., Lianidou, E., Georgoulias, V., et al. (2008). Prognostic value of the molecular detection of circulating tumor cells using a multimarker reverse transcription-PCR assay for cytokeratin 19, mammaglobin A, and HER2 in early breast cancer. Clin. Cancer Res. Off. J. Am. Assoc. Cancer Res. *14*, 2593–2600.

Jain, J., Veggiani, G., and Howarth, M. (2013). Cholesterol loading and ultrastable protein interactions determine the level of tumor marker required for optimal isolation of cancer cells. Cancer Res. *73*, 2310–2321.

Jing, C., and Cornish, V.W. (2011). Chemical tags for labeling proteins inside living cells. Acc. Chem. Res. *44*, 784–792.

Jones, J.C., Settles, E.W., Brandt, C.R., and Schultz-Cherry, S. (2011). Virus aggregating peptide enhances the cell-mediated response to influenza virus vaccine. Vaccine *29*, 7696–7703.

Kalef, E., and Gitler, C. (1994). [43] Purification of vicinal dithiol-containing proteins by arsenical-based affinity chromatography. B.-M. in Enzymology, ed. (Academic Press), pp. 395–403.

Kallergi, G., Papadaki, M.A., Politaki, E., Mavroudis, D., Georgoulias, V., and Agelaki, S. (2011). Epithelial to mesenchymal transition markers expressed in circulating tumour cells of early and metastatic breast cancer patients. Breast Cancer Res. BCR *13*, R59.

Kaltenbach, M., Stein, V., and Hollfelder, F. (2011). SNAP dendrimers: multivalent protein display on dendrimer-like DNA for directed evolution. Chembiochem Eur. J. Chem. Biol. *12*, 2208–2216.

Kaluz, S., Kaluzová, M., and Pastorek, J. (1999). Inverse PCR-generated internally deleted constructs for direct characterization of promoter regulatory regions. BioTechniques *26*, 446–450.

Kang, H.J., and Baker, E.N. (2009). Intramolecular Isopeptide Bonds Give Thermodynamic and Proteolytic Stability to the Major Pilin Protein of Streptococcus pyogenes. J. Biol. Chem. *284*, 20729–20737.

Kang, H.J., and Baker, E.N. (2011). Intramolecular isopeptide bonds: protein crosslinks built for stress? Trends Biochem. Sci. *36*, 229–237.

Kang, H.J., Coulibaly, F., Clow, F., Proft, T., and Baker, E.N. (2007). Stabilizing isopeptide bonds revealed in gram-positive bacterial pilus structure. Science *318*, 1625–1628.

Kang, J.H., Krause, S., Tobin, H., Mammoto, A., Kanapathipillai, M., and Ingber, D.E. (2012). A combined micromagnetic-microfluidic device for rapid capture and culture of rare circulating tumor cells. Lab. Chip *12*, 2175–2181.

Kazane, S.A., Axup, J.Y., Kim, C.H., Ciobanu, M., Wold, E.D., Barluenga, S., Hutchins, B.A., Schultz, P.G., Winssinger, N., and Smider, V.V. (2013). Self-assembled antibody multimers through peptide nucleic acid conjugation. J. Am. Chem. Soc. *135*, 340–346.

Khan, M.S., Tsigani, T., Rashid, M., Rabouhans, J.S., Yu, D., Luong, T.V., Caplin, M., and Meyer, T. (2011). Circulating Tumor Cells and EpCAM Expression in Neuroendocrine Tumors. Clin. Cancer Res. *17*, 337–345.

Kiessling, L.L., Gestwicki, J.E., and Strong, L.E. (2000). Synthetic multivalent ligands in the exploration of cell-surface interactions. Curr. Opin. Chem. Biol. *4*, 696–703.

Kiessling, L.L., Gestwicki, J.E., and Strong, L.E. (2006). Synthetic multivalent ligands as probes of signal transduction. Angew. Chem. Int. Ed Engl. *45*, 2348–2368.

Kim, J.S., and Raines, R.T. (1993). Ribonuclease S-peptide as a carrier in fusion proteins. Protein Sci. Publ. Protein Soc. *2*, 348–356.

Kim, C.H., Axup, J.Y., Dubrovska, A., Kazane, S.A., Hutchins, B.A., Wold, E.D., Smider, V.V., and Schultz, P.G. (2012). Synthesis of Bispecific Antibodies using Genetically Encoded Unnatural Amino Acids. J. Am. Chem. Soc. *134*, 9918–9921.

King, N.P., Sheffler, W., Sawaya, M.R., Vollmar, B.S., Sumida, J.P., André, I., Gonen, T., Yeates, T.O., and Baker, D. (2012). Computational design of self-assembling protein nanomaterials with atomic level accuracy. Science *336*, 1171–1174.

Kolostova, K., Spicka, J., Matkowski, R., and Bobek, V. (2015). Isolation, primary culture, morphological and molecular characterization of circulating tumor cells in gynecological cancers. Am. J. Transl. Res. *7*, 1203–1213.

Krishnamurthy, V.M., Estroff, L.A., and Whitesides, G.M. (2006). Multivalency in Ligand Design. In Fragment-Based Approaches in Drug Discovery, W. Jahnke, and D.A. Erlanson, eds. (Wiley-VCH Verlag GmbH & Co. KGaA), pp. 11–53.

Krishnan, V., Gaspar, A.H., Ye, N., Mandlik, A., Ton-That, H., and Narayana, S.V.L. (2007). An IgG-like domain in the minor pilin GBS52 of Streptococcus agalactiae mediates lung epithelial cell adhesion. Struct. Lond. Engl. 1993 *15*, 893–903.

Książkiewicz, M., Markiewicz, A., and Zaczek, A.J. (2012). Epithelial-mesenchymal transition: a hallmark in metastasis formation linking circulating tumor cells and cancer stem cells. Pathobiol. J. Immunopathol. Mol. Cell. Biol. *79*, 195–208.

Kuhlman, B., Yang, H.Y., Boice, J.A., Fairman, R., and Raleigh, D.P. (1997). An exceptionally stable helix from the ribosomal protein L9: implications for protein folding and stability. J. Mol. Biol. *270*, 640–647.

Lacroix, M. (2006). Significance, detection and markers of disseminated breast cancer cells. Endocr. Relat. Cancer *13*, 1033–1067.

Laemmli, U.K. (1970). Cleavage of Structural Proteins during the Assembly of the Head of Bacteriophage T4. Nature *227*, 680–685.

Lang, K., and Chin, J.W. (2014). Cellular Incorporation of Unnatural Amino Acids and Bioorthogonal Labeling of Proteins. Chem. Rev. *114*, 4764–4806.

Lankiewicz, S., Zimmermann, S., Hollmann, C., Hillemann, T., and Greten, T.F. (2008). Circulating tumour cells as a predictive factor for response to systemic chemotherapy in patients with advanced colorectal cancer. Mol. Oncol. *2*, 349–355.

Leader, B., Baca, Q.J., and Golan, D.E. (2008). Protein therapeutics: a summary and pharmacological classification. Nat. Rev. Drug Discov. *7*, 21–39.

Leary, R.J., Kinde, I., Diehl, F., Schmidt, K., Clouser, C., Duncan, C., Antipova, A., Lee, C., McKernan, K., Vega, F.M.D.L., et al. (2010). Development of Personalized Tumor Biomarkers Using Massively Parallel Sequencing. Sci. Transl. Med. *2*, 20ra14–ra20ra14.

Lee, H.J., Oh, J.H., Oh, J.M., Park, J.-M., Lee, J.-G., Kim, M.S., Kim, Y.J., Kang, H.J., Jeong, J., Kim, S.I., et al. (2013). Efficient Isolation and Accurate In Situ Analysis of Circulating Tumor Cells Using Detachable Beads and a High-Pore-Density Filter. Angew. Chem. Int. Ed. *52*, 8337–8340.

Lee, J.H., Choi, H.K., Lee, S.Y., Lim, M.-W., and Chang, J.H. (2011). Enhancing immunoassay detection of antigens with multimeric protein Gs. Biosens. Bioelectron. *28*, 146–151.

Levary, D.A., Parthasarathy, R., Boder, E.T., and Ackerman, M.E. (2011). Protein-protein fusion catalyzed by sortase A. PloS One *6*, e18342.

Li, J., Lundberg, E., Vernet, E., Larsson, B., Höidén-Guthenberg, I., and Gräslund, T. (2010a). Selection of affibody molecules to the ligand-binding site of the insulin-like growth factor-1 receptor. Biotechnol. Appl. Biochem. *55*, 99–109.

Li, L., Fierer, J.O., Rapoport, T.A., and Howarth, M. (2014). Structural analysis and optimization of the covalent association between SpyCatcher and a peptide Tag. J. Mol. Biol. *426*, 309–317.

Li, Q., So, C.R., Fegan, A., Cody, V., Sarikaya, M., Vallera, D.A., and Wagner, C.R. (2010b). Chemically Self-Assembled Antibody Nanorings (CSANs): Design and Characterization of an Anti-CD3 IgM Biomimetic. J. Am. Chem. Soc. *132*, 17247–17257.

Li, W., Reátegui, E., Park, M.-H., Castleberry, S., Deng, J.Z., Hsu, B., Mayner, S., Jensen, A.E., Sequist, L.V., Maheswaran, S., et al. (2015). Biodegradable nano-films for capture and non-invasive release of circulating tumor cells. Biomaterials *65*, 93–102.

Li, Y.-M., Xu, S.-C., Li, J., Han, K.-Q., Pi, H.-F., Zheng, L., Zuo, G.-H., Huang, X.-B., Li, H.-Y., Zhao, H.-Z., et al. (2013). Epithelial-mesenchymal transition markers expressed in circulating tumor cells in hepatocellular carcinoma patients with different stages of disease. Cell Death Dis. *4*, e831.

Lim, S.H., Spring, K.J., de Souza, P., MacKenzie, S., and Bokey, L. (2015). Circulating tumour cells and circulating nucleic acids as a measure of tumour dissemination in non-metastatic colorectal cancer surgery. Eur. J. Surg. Oncol. J. Eur. Soc. Surg. Oncol. Br. Assoc. Surg. Oncol. *41*, 309–314.

Lin, H.K., Zheng, S., Williams, A.J., Balic, M., Groshen, S., Scher, H.I., Fleisher, M., Stadler, W., Datar, R.H., Tai, Y.-C., et al. (2010). Portable filter-based microdevice for detection and characterization of circulating tumor cells. Clin. Cancer Res. Off. J. Am. Assoc. Cancer Res. *16*, 5011–5018.

Ling, J.J., Policarpo, R.L., Rabideau, A.E., Liao, X., and Pentelute, B.L. (2012). Protein Thioester Synthesis Enabled by Sortase. J. Am. Chem. Soc. *134*, 10749–10752.

Litvinov, S.V., Velders, M.P., Bakker, H.A., Fleuren, G.J., and Warnaar, S.O. (1994). Ep-CAM: a human epithelial antigen is a homophilic cell-cell adhesion molecule. J. Cell Biol. *125*, 437–446.

Liu, Z., Fusi, A., Klopocki, E., Schmittel, A., Tinhofer, I., Nonnenmacher, A., and Keilholz, U. (2011). Negative enrichment by immunomagnetic nanobeads for unbiased characterization of circulating tumor cells from peripheral blood of cancer patients. J. Transl. Med. *9*, 70.

Liu, Z., Zhou, H., Wang, W., Tan, W., Fu, Y.-X., and Zhu, M. (2014). A novel method for synthetic vaccine construction based on protein assembly. Sci. Rep. *4*, 7266.

Lockless, S.W., and Muir, T.W. (2009). Traceless protein splicing utilizing evolved split inteins. Proc. Natl. Acad. Sci. U. S. A. *106*, 10999–11004.

Löfblom, J., Feldwisch, J., Tolmachev, V., Carlsson, J., Ståhl, S., and Frejd, F.Y. (2010). Affibody molecules: engineered proteins for therapeutic, diagnostic and biotechnological applications. FEBS Lett. *584*, 2670–2680.

London, N., Movshovitz-Attias, D., and Schueler-Furman, O. (2010). The structural basis of peptide-protein binding strategies. Struct. Lond. Engl. 1993 *18*, 188–199.

Lorand, L., and Graham, R.M. (2003). Transglutaminases: crosslinking enzymes with pleiotropic functions. Nat. Rev. Mol. Cell Biol. *4*, 140–156.

Los, G.V., Encell, L.P., McDougall, M.G., Hartzell, D.D., Karassina, N., Zimprich, C., Wood, M.G., Learish, R., Ohana, R.F., Urh, M., et al. (2008). HaloTag: A Novel Protein Labeling Technology for Cell Imaging and Protein Analysis. ACS Chem. Biol. *3*, 373–382.

Lu, N.-N., Xie, M., Wang, J., Lv, S.-W., Yi, J.-S., Dong, W.-G., and Huang, W.-H. (2015a). Biotin-triggered decomposable immunomagnetic beads for capture and release of circulating tumor cells. ACS Appl. Mater. Interfaces *7*, 8817–8826.

Lu, W., Qasim, M.A., and Kent, S.B.H. (1996). Comparative Total Syntheses of Turkey Ovomucoid Third Domain by Both Stepwise Solid Phase Peptide Synthesis and Native Chemical Ligation. J. Am. Chem. Soc. *118*, 8518–8523.

Lu, Y., Liang, H., Yu, T., Xie, J., Chen, S., Dong, H., Sinko, P.J., Lian, S., Xu, J., Wang, J., et al. (2015b). Isolation and characterization of living circulating tumor cells in patients by immunomagnetic negative enrichment coupled with flow cytometry. Cancer.

Lustberg, M.B., Balasubramanian, P., Miller, B., Garcia-Villa, A., Deighan, C., Wu, Y., Carothers, S., Berger, M., Ramaswamy, B., Macrae, E.R., et al. (2014). Heterogeneous atypical cell populations are present in blood of metastatic breast cancer patients. Breast Cancer Res. *16*, R23.

Maeda, Y., Yoshino, T., and Matsunaga, T. (2009). Novel nanocomposites consisting of in vivo-biotinylated bacterial magnetic particles and quantum dots for magnetic separation and fluorescent labeling of cancer cells. J. Mater. Chem. *19*, 6361.

Maetzel, D., Denzel, S., Mack, B., Canis, M., Went, P., Benk, M., Kieu, C., Papior, P., Baeuerle, P.A., Munz, M., et al. (2009). Nuclear signalling by tumour-associated antigen EpCAM. Nat. Cell Biol. *11*, 162–171.

Maheswaran, S., Sequist, L.V., Nagrath, S., Ulkus, L., Brannigan, B., Collura, C.V., Inserra, E., Diederichs, S., Iafrate, A.J., Bell, D.W., et al. (2008). Detection of Mutations in EGFR in Circulating Lung-Cancer Cells. N. Engl. J. Med. *359*, 366–377.

Maltez-da Costa, M., de la Escosura-Muñiz, A., Nogués, C., Barrios, L., Ibáñez, E., and Merkoçi, A. (2012). Simple Monitoring of Cancer Cells Using Nanoparticles. Nano Lett. *12*, 4164–4171.

Man, Y., Wang, Q., and Kemmner, W. (2011a). Currently Used Markers for CTC Isolation - Advantages, Limitations and Impact on Cancer Prognosis. J. Clin. Exp. Pathol. *01*.

Man, Y., Wang, Q., and Kemmner, W. (2011b). Currently Used Markers for CTC Isolation - Advantages, Limitations and Impact on Cancer Prognosis. J. Clin. Exp. Pathol. *01*.

Marraffini, L.A., DeDent, A.C., and Schneewind, O. (2006). Sortases and the Art of Anchoring Proteins to the Envelopes of Gram-Positive Bacteria. Microbiol. Mol. Biol. Rev. *70*, 192–221.

Martin, L.J., and Raines, R.T. (2010). Carpe Diubiquitin. Angew. Chem. Int. Ed Engl. *49*, 9042–9044.

Matsui, K., Boniface, J.J., Reay, P.A., Schild, H., Groth, B.F. de S., and Davis, M.M. (1991). Low affinity interaction of peptide-MHC complexes with T cell receptors. Science *254*, 1788–1791.

Mazzucchelli, S., Colombo, M., De Palma, C., Salvadè, A., Verderio, P., Coghi, M.D., Clementi, E., Tortora, P., Corsi, F., and Prosperi, D. (2010). Single-Domain Protein A-Engineered Magnetic Nanoparticles: Toward a Universal Strategy to Site-Specific Labeling of Antibodies for Targeted Detection of Tumor Cells. ACS Nano *4*, 5693–5702.

McCann, A.H., Dervan, P.A., O'Regan, M., Codd, M.B., Gullick, W.J., Tobin, B.M., and Carney, D.N. (1991). Prognostic significance of c-erbB-2 and estrogen receptor status in human breast cancer. Cancer Res. *51*, 3296–3303.

McCloskey, K.E., Comella, K., Chalmers, J.J., Margel, S., and Zborowski, M. (2001). Mobility measurements of immunomagnetically labeled cells allow quantitation of secondary antibody binding amplification. Biotechnol. Bioeng. *75*, 642–655.

McCloskey, K.E., Chalmers, J.J., and Zborowski, M. (2003a). Magnetic cell separation: characterization of magnetophoretic mobility. Anal. Chem. *75*, 6868–6874.

McCloskey, K.E., Moore, L.R., Hoyos, M., Rodriguez, A., Chalmers, J.J., and Zborowski, M. (2003b). Magnetophoretic cell sorting is a function of antibody binding capacity. Biotechnol. Prog. *19*, 899–907.

Merrifield, R.B. (1963). Solid Phase Peptide Synthesis. I. The Synthesis of a Tetrapeptide. J. Am. Chem. Soc. *85*, 2149–2154.

Millner, L.M., Linder, M.W., and Valdes, R. (2013). Circulating Tumor Cells: A Review of Present Methods and the Need to Identify Heterogeneous Phenotypes. Ann. Clin. Lab. Sci. *43*, 295–304.

Mills, K.V., Johnson, M.A., and Perler, F.B. (2014). Protein Splicing: How Inteins Escape from Precursor Proteins. J. Biol. Chem. *289*, 14498–14505.

Modica, J.A., Skarpathiotis, S., and Mrksich, M. (2012). Modular Assembly of Protein Building Blocks To Create Precisely Defined Megamolecules. ChemBioChem *13*, 2331–2334.

Mogensen, T.H. (2009). Pathogen Recognition and Inflammatory Signaling in Innate Immune Defenses. Clin. Microbiol. Rev. *22*, 240–273.

Moss, J.A. (2001). Guide for Resin and Linker Selection in Solid-Phase Peptide Synthesis. In Current Protocols in Protein Science, (John Wiley & Sons, Inc.),.

Myung, J.H., Gajjar, K.A., Saric, J., Eddington, D.T., and Hong, S. (2011). Dendrimer-mediated Multivalent Binding for Enhanced Capture of Tumor Cells. Angew. Chem. Int. Ed Engl. *50*, 11769–11772.

Myung, J.H., Gajjar, K.A., Chen, J., Molokie, R.E., and Hong, S. (2014). Differential Detection of Tumor Cells Using a Combination of Cell Rolling, Multivalent Binding, and Multiple Antibodies. Anal. Chem. *86*, 6088–6094.

Nagrath, S., Sequist, L.V., Maheswaran, S., Bell, D.W., Irimia, D., Ulkus, L., Smith, M.R., Kwak, E.L., Digumarthy, S., Muzikansky, A., et al. (2007). Isolation of rare circulating tumour cells in cancer patients by microchip technology. Nature *450*, 1235–1239.

Nagy, P., Vereb, G., Sebestyén, Z., Horváth, G., Lockett, S.J., Damjanovich, S., Park, J.W., Jovin, T.M., and Szöllosi, J. (2002). Lipid rafts and the local density of ErbB proteins influence the biological role of homo- and heteroassociations of ErbB2. J. Cell Sci. *115*, 4251–4262.

Naumov, G.N., MacDonald, I.C., Weinmeister, P.M., Kerkvliet, N., Nadkarni, K.V., Wilson, S.M., Morris, V.L., Groom, A.C., and Chambers, A.F. (2002). Persistence of solitary mammary carcinoma cells in a secondary site: a possible contributor to dormancy. Cancer Res. *62*, 2162–2168.

Nelson, A.L., Ries, J., Bagnoli, F., Dahlberg, S., Fälker, S., Rounioja, S., Tschöp, J., Morfeldt, E., Ferlenghi, I., Hilleringmann, M., et al. (2007). RrgA is a pilus-associated adhesin in Streptococcus pneumoniae. Mol. Microbiol. *66*, 329–340.

Nettleship, J.E., Ren, J., Rahman, N., Berrow, N.S., Hatherley, D., Barclay, A.N., and Owens, R.J. (2008). A pipeline for the production of antibody fragments for structural studies using transient expression in HEK 293T cells. Protein Expr. Purif. *62*, 83–89.

Nguyen, P.Q., Botyanszki, Z., Tay, P.K.R., and Joshi, N.S. (2014). Programmable biofilm-based materials from engineered curli nanofibres. Nat. Commun. *5*.

Normanno, N., De Luca, A., Bianco, C., Strizzi, L., Mancino, M., Maiello, M.R., Carotenuto, A., De Feo, G., Caponigro, F., and Salomon, D.S. (2006). Epidermal growth factor receptor (EGFR) signaling in cancer. Gene *366*, 2–16.

Ntouroupi, T.G., Ashraf, S.Q., McGregor, S.B., Turney, B.W., Seppo, A., Kim, Y., Wang, X., Kilpatrick, M.W., Tsipouras, P., Tafas, T., et al. (2008). Detection of circulating tumour cells in peripheral blood with an automated scanning fluorescence microscope. Br. J. Cancer *99*, 789–795.

Nuraje, N., Banerjee, I.A., MacCuspie, R.I., Yu, L., and Matsui, H. (2004). Biological bottom-up assembly of antibody nanotubes on patterned antigen arrays. J. Am. Chem. Soc. *126*, 8088–8089.

Orlova, A., Magnusson, M., Eriksson, T.L.J., Nilsson, M., Larsson, B., Höidén-Guthenberg, I., Widström, C., Carlsson, J., Tolmachev, V., Ståhl, S., et al. (2006). Tumor imaging using a picomolar affinity HER2 binding affibody molecule. Cancer Res. *66*, 4339–4348.

Orr, G., Hu, D., Ozçelik, S., Opresko, L.K., Wiley, H.S., and Colson, S.D. (2005). Cholesterol dictates the freedom of EGF receptors and HER2 in the plane of the membrane. Biophys. J. *89*, 1362–1373.

Ozawa, T. (2006). Designing split reporter proteins for analytical tools. Anal. Chim. Acta *556*, 58–68.

Ozkumur, E., Shah, A.M., Ciciliano, J.C., Emmink, B.L., Miyamoto, D.T., Brachtel, E., Yu, M., Chen, P., Morgan, B., Trautwein, J., et al. (2013). Inertial Focusing for Tumor Antigen–Dependent and –Independent Sorting of Rare Circulating Tumor Cells. Sci. Transl. Med. *5*, 179ra47–ra179ra47.

Pähler, A., Hendrickson, W.A., Kolks, M.A., Argaraña, C.E., and Cantor, C.R. (1987). Characterization and crystallization of core streptavidin. J. Biol. Chem. *262*, 13933–13937.

Panchapakesan, B., Caprara, R., Velasco, V., Loomis, J., King, B., Xu, P., Burkhead, T., Sethu, P., Stallons, L.J., McGregor, W.G., et al. (2010). Micro- and nanotechnology approaches for capturing circulating tumor cells. Cancer Nanotechnol. *1*, 3–11.

Pantel, K., and Alix-Panabières, C. (2010). Circulating tumour cells in cancer patients: challenges and perspectives. Trends Mol. Med. *16*, 398–406.

Pantel, K., and Alix-Panabières, C. (2013). Real-time liquid biopsy in cancer patients: fact or fiction? Cancer Res. *73*, 6384–6388.

Pantel, K., Alix-Panabières, C., and Riethdorf, S. (2009). Cancer micrometastases. Nat. Rev. Clin. Oncol. *6*, 339–351.

Payne, R.E., Yagüe, E., Slade, M.J., Apostolopoulos, C., Jiao, L.R., Ward, B., Coombes, R.C., and Stebbing, J. (2009). Measurements of EGFR expression on circulating tumor cells are reproducible over time in metastatic breast cancer patients. Pharmacogenomics *10*, 51–57.

Perseghin, P., Gaipa, G., Dassi, M., Belotti, D., Pogliani, E.M., Pioltelli, P., Balduzzi, A., Rovelli, A., Uderzo, C., and Biondi, A. (2005). CD34+ stem cell recovery after positive selection of “overloaded” immunomagnetic columns. Stem Cells Dev. *14*, 740–743.

Pohl, H.A., and Crane, J.S. (1971). Dielectrophoresis of Cells. Biophys. J. *11*, 711–727.

Polyak, M.J., Ayer, L.M., Szczepek, A.J., and Deans, J.P. (2003). A cholesterol-dependent CD20 epitope detected by the FMC7 antibody. Leukemia *17*, 1384–1389.

Popp, M.W., Antos, J.M., Grotenbreg, G.M., Spooner, E., and Ploegh, H.L. (2007). Sortagging: a versatile method for protein labeling. Nat. Chem. Biol. *3*, 707–708.

Popp, M.W., Dougan, S.K., Chuang, T.-Y., Spooner, E., and Ploegh, H.L. (2011). Sortase-catalyzed transformations that improve the properties of cytokines. Proc. Natl. Acad. Sci. *108*, 3169–3174.

Preiner, J., Kodera, N., Tang, J., Ebner, A., Brameshuber, M., Blaas, D., Gelbmann, N., Gruber, H.J., Ando, T., and Hinterdorfer, P. (2014). IgGs are made for walking on bacterial and viral surfaces. Nat. Commun. *5*, 4394.

Prescher, J.A., and Bertozzi, C.R. (2005). Chemistry in living systems. Nat. Chem. Biol. *1*, 13–21.

Raab, A., Han, W., Badt, D., Smith-Gill, S.J., Lindsay, S.M., Schindler, H., and Hinterdorfer, P. (1999). Antibody recognition imaging by force microscopy. Nat. Biotechnol. *17*, 901–905.

Rashidian, M., Dozier, J.K., and Distefano, M.D. (2013). Chemoenzymatic Labeling of Proteins: Techniques and Approaches. Bioconjug. Chem. *24*, 1277–1294.

Ravikumar, Y., Nadarajan, S.P., Hyeon Yoo, T., Lee, C., and Yun, H. (2015). Unnatural amino acid mutagenesis-based enzyme engineering. Trends Biotechnol. *33*, 462–470.

Riethdorf, S., Fritsche, H., Müller, V., Rau, T., Schindlbeck, C., Rack, B., Janni, W., Coith, C., Beck, K., Jänicke, F., et al. (2007). Detection of Circulating Tumor Cells in Peripheral Blood of Patients with Metastatic Breast Cancer: A Validation Study of the CellSearch System. Clin. Cancer Res. *13*, 920–928.

Ritzefeld, M. (2014). Sortagging: A Robust and Efficient Chemoenzymatic Ligation Strategy. Chem. – Eur. J. *20*, 8516–8529.

Saleh, L., and Perler, F.B. (2006). Protein splicing In Cis and In Trans. Chem. Rec. *6*, 183–193.

Saltz, L., Badarinath, S., Dakhil, S., Bienvenu, B., Harker, W.G., Birchfield, G., Tokaz, L.K., Barrera, D., Conkling, P.R., O'Rourke, M.A., et al. (2012). Phase III trial of cetuximab, bevacizumab, and 5-fluorouracil/leucovorin vs. FOLFOX-bevacizumab in colorectal cancer. Clin. Colorectal Cancer *11*, 101–111.

Saphire, E.O., Stanfield, R.L., Crispin, M.D.M., Parren, P.W.H.I., Rudd, P.M., Dwek, R.A., Burton, D.R., and Wilson, I.A. (2002). Contrasting IgG structures reveal extreme asymmetry and flexibility. J. Mol. Biol. *319*, 9–18.

Sarioglu, A.F., Aceto, N., Kojic, N., Donaldson, M.C., Zeinali, M., Hamza, B., Engstrom, A., Zhu, H., Sundaresan, T.K., Miyamoto, D.T., et al. (2015). A microfluidic device for label-free, physical capture of circulating tumor cell clusters. Nat. Methods *12*, 685–691.

Savitzky, A., and Golay, M.J.E. (1964). Smoothing and Differentiation of Data by Simplified Least Squares Procedures. Anal. Chem. *36*, 1627–1639.

Schmidt, M.M., and Wittrup, K.D. (2009). A modeling analysis of the effects of molecular size and binding affinity on tumor targeting. Mol. Cancer Ther. *8*, 2861–2871.

Schmidt, T.G., and Skerra, A. (2007). The Strep-tag system for one-step purification and high-affinity detection or capturing of proteins. Nat. Protoc. *2*, 1528–1535.

Schoene, C., Fierer, J.O., Bennett, S.P., and Howarth, M. (2014). SpyTag/SpyCatcher Cyclization Confers Resilience to Boiling on a Mesophilic Enzyme. Angew. Chem. Int. Ed. *53*, 6101–6104.

Schulze, K., Gasch, C., Staufer, K., Nashan, B., Lohse, A.W., Pantel, K., Riethdorf, S., and Wege, H. (2013). Presence of EpCAM-positive circulating tumor cells as biomarker for systemic disease strongly correlates to survival in patients with hepatocellular carcinoma. Int. J. Cancer J. Int. Cancer *133*, 2165–2171.

Shah, N.H., and Muir, T.W. (2011). Split Inteins: Nature's Protein Ligases. Isr. J. Chem. *51*, 854–861.

Shahneh, F.Z. (2013). Sensitive antibody-based CTCs detection from peripheral blood. Hum. Antibodies *22*, 51–54.

Shekhawat, S.S., and Ghosh, I. (2011). Split-protein systems: beyond binary protein-protein interactions. Curr. Opin. Chem. Biol. *15*, 789–797.

Sheng, W., Chen, T., Tan, W., and Fan, Z.H. (2013). Multivalent DNA Nanospheres for Enhanced Capture of Cancer Cells in Microfluidic Devices. ACS Nano *7*, 7067–7076.

Shih, W., and Yamada, S. (2012). N-cadherin-mediated cell-cell adhesion promotes cell migration in a three-dimensional matrix. J. Cell Sci. jcs.103861.

Siebold, C., and Erni, B. (2002). Intein-mediated cyclization of a soluble and a membrane protein in vivo: function and stability. Biophys. Chem. *96*, 163–171.

Sieuwerts, A.M., Kraan, J., Bolt-de Vries, J., van der Spoel, P., Mostert, B., Martens, J.W.M., Gratama, J.-W., Sleijfer, S., and Foekens, J.A. (2009). Molecular characterization of circulating tumor cells in large quantities of contaminating leukocytes by a multiplex real-time PCR. Breast Cancer Res. Treat. *118*, 455–468.

Sievers, F., Wilm, A., Dineen, D., Gibson, T.J., Karplus, K., Li, W., Lopez, R., McWilliam, H., Remmert, M., Söding, J., et al. (2011). Fast, scalable generation of high-quality protein multiple sequence alignments using Clustal Omega. Mol. Syst. Biol. *7*, 539.

Siezen, R.J., and Leunissen, J.A. (1997). Subtilases: the superfamily of subtilisin-like serine proteases. Protein Sci. Publ. Protein Soc. *6*, 501–523.

Silpe, J.E., Sumit, M., Thomas, T.P., Huang, B., Kotlyar, A., van Dongen, M.A., Banaszak Holl, M.M., Orr, B.G., and Choi, S.K. (2013). Avidity modulation of folate-targeted multivalent dendrimers for evaluating biophysical models of cancer targeting nanoparticles. ACS Chem. Biol. *8*, 2063–2071.

Simons, K., and Gerl, M.J. (2010). Revitalizing membrane rafts: new tools and insights. Nat. Rev. Mol. Cell Biol. *11*, 688–699.

Siontorou, C.G. (2013). Nanobodies as novel agents for disease diagnosis and therapy. Int. J. Nanomedicine *8*, 4215–4227.

Sletten, E.M., and Bertozzi, C.R. (2009). Bioorthogonal Chemistry: Fishing for Selectivity in a Sea of Functionality. Angew. Chem. Int. Ed. *48*, 6974–6998.

Smerage, J.B., Barlow, W.E., Hortobagyi, G.N., Winer, E.P., Leyland-Jones, B., Srkalovic, G., Tejwani, S., Schott, A.F., O'Rourke, M.A., Lew, D.L., et al. (2014). Circulating tumor cells and response to chemotherapy in metastatic breast cancer: SWOG S0500. J. Clin. Oncol. Off. J. Am. Soc. Clin. Oncol. *32*, 3483–3489.

Smith, I.O., Liu, X.H., Smith, L.A., and Ma, P.X. (2009). Nanostructured polymer scaffolds for tissue engineering and regenerative medicine. Wiley Interdiscip. Rev. Nanomed. Nanobiotechnol. *1*, 226–236.

Soerjomataram, I., Lortet-Tieulent, J., Parkin, D.M., Ferlay, J., Mathers, C., Forman, D., and Bray, F. (2012). Global burden of cancer in 2008: a systematic analysis of disability-adjusted life-years in 12 world regions. Lancet Lond. Engl. *380*, 1840–1850.

Sollier, E., Go, D.E., Che, J., Gossett, D.R., O'Byrne, S., Weaver, W.M., Kummer, N., Rettig, M., Goldman, J., Nickols, N., et al. (2014). Size-selective collection of circulating tumor cells using Vortex technology. Lab. Chip *14*, 63–77.

Spirig, T., Weiner, E.M., and Clubb, R.T. (2011). Sortase enzymes in Gram-positive bacteria. Mol. Microbiol. *82*, 1044–1059.

Stanton, S.G., Kantor, A.B., Petrossian, A., and Owicki, J.C. (1984). Location and dynamics of a membrane-bound fluorescent hapten. A spectroscopic study. Biochim. Biophys. Acta *776*, 228–236.

Stebbing, J., Payne, R., Reise, J., Frampton, A.E., Avery, M., Woodley, L., Di Leo, A., Pestrin, M., Krell, J., and Coombes, R.C. (2013). The efficacy of lapatinib in metastatic breast cancer with HER2 non-amplified primary tumors and EGFR positive circulating tumor cells: a proof-of-concept study. PloS One *8*, e62543.

Stott, S.L., Hsu, C.-H., Tsukrov, D.I., Yu, M., Miyamoto, D.T., Waltman, B.A., Rothenberg, S.M., Shah, A.M., Smas, M.E., Korir, G.K., et al. (2010). Isolation of circulating tumor cells using a microvortex-generating herringbone-chip. Proc. Natl. Acad. Sci. U. S. A. *107*, 18392–18397.

Stroffekova, K., Proenza, C., and Beam, K.G. (2001). The protein-labeling reagent FLASH-EDT2 binds not only to CCXXCC motifs but also non-specifically to endogenous cysteine-rich proteins. Pflüg. Arch. Eur. J. Physiol. *442*, 859–866.

Sun, F., Zhang, W.-B., Mahdavi, A., Arnold, F.H., and Tirrell, D.A. (2014). Synthesis of bioactive protein hydrogels by genetically encoded SpyTag-SpyCatcher chemistry. Proc. Natl. Acad. Sci. *111*, 11269–11274.

Sun, W., Yang, J., and Liu, X.-Q. (2004). Synthetic two-piece and three-piece split inteins for protein trans-splicing. J. Biol. Chem. *279*, 35281–35286.

Sun, Y.-F., Yang, X.-R., Zhou, J., Qiu, S.-J., Fan, J., and Xu, Y. (2011). Circulating tumor cells: advances in detection methods, biological issues, and clinical relevance. J. Cancer Res. Clin. Oncol. *137*, 1151–1173.

Swee, L.K., Lourido, S., Bell, G.W., Ingram, J.R., and Ploegh, H.L. (2015). One-Step Enzymatic Modification of the Cell Surface Redirects Cellular Cytotoxicity and Parasite Tropism. ACS Chem. Biol. *10*, 460–465.

Symersky, J., Patti, J.M., Carson, M., House-Pompeo, K., Teale, M., Moore, D., Jin, L., Schneider, A., DeLucas, L.J., Höök, M., et al. (1997). Structure of the collagen-binding domain from a Staphylococcus aureus adhesin. Nat. Struct. Biol. *4*, 833–838.

Tang, L., Zhao, S., Liu, W., Parchim, N.F., Huang, J., Tang, Y., Gan, P., and Zhong, M. (2013). Diagnostic accuracy of circulating tumor cells detection in gastric cancer: systematic review and meta-analysis. BMC Cancer *13*, 314.

Telmer, P.G., and Shilton, B.H. (2003). Insights into the conformational equilibria of maltose-binding protein by analysis of high affinity mutants. J. Biol. Chem. *278*, 34555–34567.

Terpe, K. (2003). Overview of tag protein fusions: from molecular and biochemical fundamentals to commercial systems. Appl. Microbiol. Biotechnol. *60*, 523–533.

Thapa, P., Zhang, R.-Y., Menon, V., and Bingham, J.-P. (2014). Native Chemical Ligation: A Boon to Peptide Chemistry. Molecules *19*, 14461–14483.

Thiery, J.P., Acloque, H., Huang, R.Y.J., and Nieto, M.A. (2009). Epithelial-Mesenchymal Transitions in Development and Disease. Cell *139*, 871–890.

Thompson, E.W., and Haviv, I. (2011). The social aspects of EMT-MET plasticity. Nat. Med. *17*, 1048–1049.

Thorn, K.S., Naber, N., Matuska, M., Vale, R.D., and Cooke, R. (2000). A novel method of affinity-purifying proteins using a bis-arsenical fluorescein. Protein Sci. Publ. Protein Soc. *9*, 213–217.

Torre, L.A., Bray, F., Siegel, R.L., Ferlay, J., Lortet-Tieulent, J., and Jemal, A. (2015). Global cancer statistics, 2012. CA. Cancer J. Clin. *65*, 87–108.

Toss, A., Mu, Z., Fernandez, S., and Cristofanilli, M. (2014). CTC enumeration and characterization: moving toward personalized medicine. Ann. Transl. Med. *2*.

Trzpis, M., McLaughlin, P.M.J., de Leij, L.M.F.H., and Harmsen, M.C. (2007). Epithelial Cell Adhesion Molecule: More than a Carcinoma Marker and Adhesion Molecule. Am. J. Pathol. *171*, 386–395.

Tsukiji, S., and Nagamune, T. (2009). Sortase-Mediated Ligation: A Gift from Gram-Positive Bacteria to Protein Engineering. ChemBioChem *10*, 787–798.

Vamvaca, K., Vögeli, B., Kast, P., Pervushin, K., and Hilvert, D. (2004). An enzymatic molten globule: Efficient coupling of folding and catalysis. Proc. Natl. Acad. Sci. U. S. A. *101*, 12860–12864.

Veggiani, G., and de Marco, A. (2011). Improved quantitative and qualitative production of single-domain intrabodies mediated by the co-expression of Erv1p sulfhydryl oxidase. Protein Expr. Purif. *79*, 111–114.

Voss, S., and Skerra, A. (1997). Mutagenesis of a flexible loop in streptavidin leads to higher affinity for the Strep-tag II peptide and improved performance in recombinant protein purification. Protein Eng. *10*, 975–982.

Walker, I.H., Hsieh, P., and Riggs, P.D. (2010). Mutations in maltose-binding protein that alter affinity and solubility properties. Appl. Microbiol. Biotechnol. *88*, 187–197.

Wang, J., Huang, J., Wang, K., Xu, J., Huang, J., and Zhang, T. (2013a). Prognostic significance of circulating tumor cells in non-small-cell lung cancer patients: a meta-analysis. PloS One *8*, e78070.

Wang, L., Brock, A., Herberich, B., and Schultz, P.G. (2001). Expanding the Genetic Code of Escherichia coli. Science *292*, 498–500.

Wang, L., Liu, X., Zhu, X., Wang, L., Wang, W., Liu, C., Cui, H., Sun, M., and Gao, B. (2013b). Generation of single-domain antibody multimers with three different self-associating peptides. Protein Eng. Des. Sel. *26*, 417–423.

Wang, S., Wan, Y., and Liu, Y. (2014). Effects of nanopillar array diameter and spacing on cancer cell capture and cell behaviors. Nanoscale *6*, 12482–12489.

Wängler, C., Moldenhauer, G., Eisenhut, M., Haberkorn, U., and Mier, W. (2008). Antibody-dendrimer conjugates: the number, not the size of the dendrimers, determines the immunoreactivity. Bioconjug. Chem. *19*, 813–820.

Weigelt, B., Peterse, J.L., and van't Veer, L.J. (2005). Breast cancer metastasis: markers and models. Nat. Rev. Cancer *5*, 591–602.

Wikoff, W.R., Liljas, L., Duda, R.L., Tsuruta, H., Hendrix, R.W., and Johnson, J.E. (2000). Topologically linked protein rings in the bacteriophage HK97 capsid. Science *289*, 2129–2133.

Wildes, D., and Wells, J.A. (2010). Sampling the N-terminal proteome of human blood. Proc. Natl. Acad. Sci. *107*, 4561–4566.

Williamson, D.J., Fascione, M.A., Webb, M.E., and Turnbull, W.B. (2012). Efficient N-terminal labeling of proteins by use of sortase. Angew. Chem. Int. Ed Engl. *51*, 9377–9380.

Williamson, D.J., Webb, M.E., and Turnbull, W.B. (2014). Depsipeptide substrates for sortase-mediated N-terminal protein ligation. Nat. Protoc. *9*, 253–262.

Wilson, N.S., Yang, B., Yang, A., Loeser, S., Marsters, S., Lawrence, D., Li, Y., Pitti, R., Totpal, K., Yee, S., et al. (2011). An Fcγ Receptor-Dependent Mechanism Drives Antibody-Mediated Target-Receptor Signaling in Cancer Cells. Cancer Cell *19*, 101–113.

Wittekind, C., and Neid, M. (2005). Cancer Invasion and Metastasis. Oncology *69*, 14–16.

Xie, M., Lu, N.-N., Cheng, S.-B., Wang, X.-Y., Wang, M., Guo, S., Wen, C.-Y., Hu, J., Pang, D.-W., and Huang, W.-H. (2014). Engineered decomposable multifunctional nanobioprobes for capture and release of rare cancer cells. Anal. Chem. *86*, 4618–4626.

Yancey, P.H. (2004). Compatible and counteracting solutes: protecting cells from the Dead Sea to the deep sea. Sci. Prog. *87*, 1–24.

Yarden, Y. (2001). Biology of HER2 and Its Importance in Breast Cancer. Oncology *61*, 1–13.

Yeagle, P.L. (1985). Cholesterol and the cell membrane. Biochim. Biophys. Acta *822*, 267–287.

Yoon, H.J., Kim, T.H., Zhang, Z., Azizi, E., Pham, T.M., Paoletti, C., Lin, J., Ramnath, N., Wicha, M.S., Hayes, D.F., et al. (2013). Sensitive capture of circulating tumour cells by functionalized graphene oxide nanosheets. Nat. Nanotechnol. *8*, 735–741.

Yu, Y., and Lutz, S. (2011). Circular permutation: a different way to engineer enzyme structure and function. Trends Biotechnol. *29*, 18–25.

Yu, M., Stott, S., Toner, M., Maheswaran, S., and Haber, D.A. (2011a). Circulating tumor cells: approaches to isolation and characterization. J. Cell Biol. *192*, 373–382.

Yu, M., Stott, S., Toner, M., Maheswaran, S., and Haber, D.A. (2011b). Circulating tumor cells: approaches to isolation and characterization. J. Cell Biol. *192*, 373–382.

Yu, M., Bardia, A., Wittner, B.S., Stott, S.L., Smas, M.E., Ting, D.T., Isakoff, S.J., Ciciliano, J.C., Wells, M.N., Shah, A.M., et al. (2013). Circulating Breast Tumor Cells Exhibit Dynamic Changes in Epithelial and Mesenchymal Composition. Science *339*, 580–584.

Yu, M., Bardia, A., Aceto, N., Bersani, F., Madden, M.W., Donaldson, M.C., Desai, R., Zhu, H., Comaills, V., Zheng, Z., et al. (2014). Ex vivo culture of circulating breast tumor cells for individualized testing of drug susceptibility. Science *345*, 216–220.

Zaher, H.S., and Green, R. (2009). Fidelity at the molecular level: lessons from protein synthesis. Cell *136*, 746–762.

Zakeri, B., and Howarth, M. (2010). Spontaneous Intermolecular Amide Bond Formation between Side Chains for Irreversible Peptide Targeting. J. Am. Chem. Soc. *132*, 4526–4527.

Zakeri, B., Fierer, J.O., Celik, E., Chittock, E.C., Schwarz-Linek, U., Moy, V.T., and Howarth, M. (2012). Peptide tag forming a rapid covalent bond to a protein, through engineering a bacterial adhesin. Proc. Natl. Acad. Sci. *109*, E690–E697.

Zeisberg, M., and Neilson, E.G. (2009). Biomarkers for epithelial-mesenchymal transitions. J. Clin. Invest. *119*, 1429–1437.

Zemskov, E.A., Mikhailenko, I., Smith, E.P., and Belkin, A.M. (2012). Tissue Transglutaminase Promotes PDGF/PDGFR-mediated Signaling and Responses in Vascular Smooth Muscle Cells. J. Cell. Physiol. *227*, 2089–2096.

Zhang, L., Ridgway, L.D., Wetzel, M.A., Ngo, J., Yin, W., Kumar, D., Goodman, J.C., Groves, M.D., and Marchetti, D. (2013a). The identification and characterization of breast cancer CTCs competent for brain metastasis. Sci. Transl. Med. *5*.

Zhang, W., Kai, K., Choi, D.S., Iwamoto, T., Nguyen, Y.H., Wong, H., Landis, M.D., Ueno, N.T., Chang, J., and Qin, L. (2012a). Microfluidics separation reveals the stem-cell-like deformability of tumor-initiating cells. Proc. Natl. Acad. Sci. U. S. A. *109*, 18707–18712.

Zhang, W., Luo, Q., Miao, L., Hou, C., Bai, Y., Dong, Z., Xu, J., and Liu, J. (2012b). Self-assembly of glutathione S-transferase into nanowires. Nanoscale *4*, 5847–5851.

Zhang, W.-B., Sun, F., Tirrell, D.A., and Arnold, F.H. (2013b). Controlling macromolecular topology with genetically encoded SpyTag-SpyCatcher chemistry. J. Am. Chem. Soc. *135*, 13988–13997.

Zhao, C., Hellman, L.M., Zhan, X., Bowman, W.S., Whiteheart, S.W., and Fried, M.G. (2010). Hexahistidine-tag-specific optical probes for analyses of proteins and their interactions. Anal. Biochem. *399*, 237–245.

Zhao, L., Lu, Y.-T., Li, F., Wu, K., Hou, S., Yu, J., Shen, Q., Wu, D., Song, M., OuYang, W.-H., et al. (2013). High-Purity Prostate Circulating Tumor Cell Isolation by

a Polymer Nanofiber-Embedded Microchip for Whole Exome Sequencing. Adv. Mater. Deerfield Beach Fla *25*, 2897–2902.

Zhao, W., Cui, C.H., Bose, S., Guo, D., Shen, C., Wong, W.P., Halvorsen, K., Farokhzad, O.C., Teo, G.S.L., Phillips, J.A., et al. (2012). Bioinspired multivalent DNA network for capture and release of cells. Proc. Natl. Acad. Sci. *109*, 19626–19631.

Zhao, Y., Yan, Q., Long, X., Chen, X., and Wang, Y. (2008). Vimentin affects the mobility and invasiveness of prostate cancer cells. Cell Biochem. Funct. *26*, 571–577.

Zhu, X., Wang, L., Liu, R., Flutter, B., Li, S., Ding, J., Tao, H., Liu, C., Sun, M., and Gao, B. (2010). COMBODY: one-domain antibody multimer with improved avidity. Immunol. Cell Biol. *88*, 667–675.

Zidovetzki, R., and Levitan, I. (2007). Use of cyclodextrins to manipulate plasma membrane cholesterol content: evidence, misconceptions and control strategies. Biochim. Biophys. Acta *1768*, 1311–1324.

Zieglschmid, V., Hollmann, C., Mannel, J., Albert, W., Jaeschke-Melli, S., Eckstein, B., Hillemann, T., Greten, T.F., Gross, E., and Böcher, O. (2007). Tumor-associated gene expression in disseminated tumor cells correlates with disease progression and tumor stage in colorectal cancer. Anticancer Res. *27*, 1823–1832.

Appendix

A. Sequence alignments

Sequences alignments of the main proteins used in this thesis were performed using the Clustal Omega online tool (Sievers et al., 2011).

A.1 Sequence alignment of CnaB2 domain, SpyCatcher and SpyLigase

```
CnaB2           MSYYHHHHHHDYDIPTTENLYFQGAMVDTLSGLSSEQGQSGDMTIEEDSATHIKFSKRDI
SpyCatcher      MSYYHHHHHHDYDIPTTENLYFQGAMVDTLSGLSSEQGQSGDMTIEEDSATHIKFSKRDE
SpyLigase       MSYYHHHHHHDYD-----------------------GQSG------------------

CnaB2           DGKELAGATMELRDSSGKTISTWISDGQVKDFYLMPGKYTFVETAAPDGYEVATAITFTV
SpyCatcher      DGKELAGATMELRDSSGKTISTWISDGQVKDFYLYPGKYTFVETAAPDGYEVATAITFTV
SpyLigase       DGKELAGATMELRDSSGKTISTWISDGQVKDFYLYPGKYTFVETAAPDGYEVATAITFTV

CnaB2           NEQGQVTVNGKATKGDAHIVMVDA-------
SpyCatcher      NEQGQVTVNGKATKGDAHI------------
SpyLigase       NEQGQVTVNGKATKGGSGGSGGSGEDSATHI
```

KTag Mutated residues to make SpyCatcher

SpyTag Circular permutation of SpyLigase

A.2 Sequence alignment of affibody tailored with KTag and SpyTag

```
KTag-AffiEGFR-SpyTag    MGATHIKFSKRDGSGASMTGGQQMGRDPGVDNKFNKEMWAAWEEIRNLPNLNGWQMTAF
KTag-AffiHER2-SpyTag    MGATHIKFSKRDGSGASMTGGQQMGRDPGVDNKFNKEMRNAYWEIALLPNLNNQQKRAF
KTag-AffiHER2-SpyTag_2  MGATHIKFSKRDGSGASMTGGQQMGRDPGVDNKFNKEMRNAYWEIALLPNLTNQQKRAF

KTag-AffiEGFR-SpyTag    IASLVDDPSQSANLLAEAKKLNDAQAPKGLEHHHHHHGSGAHIVMVDAYKPTK
KTag-AffiHER2-SpyTag    IRSLYDDPSQSANLLAEAKKLNDAQAPKGLEHHHHHHGSGAHIVMVDAYKPTK
KTag-AffiHER2-SpyTag_2  IRKLYDDPSQSANLLAEAKKLNDAQAPKGLEHHHHHHGSGAHIVMVDAYKPTK
```

KTag Residues involved in antigen binding

Mutated residues to reduce IgG binding SpyTag

A.3 Sequence alignment of RrgA D4 domain, RrgACatcher and SnoopCatcher

```
RrgA D4 domain    ---KEKKLGDIEFIKVNKNDKKPLRGAVFSLQKQHPDYPDIYGAIDQNGTYQNVRTGEDG
RrgACatcher       MGSSHHHHHHSSGLVPRGSHMKPLRGAVFSLQKQHPDYPDIYGAIDQNGTYQNVRTGEDG
SnoopCatcher      MGSSHHHHHHSSGLVPRGSHMKPLRGAVFSLQKQHPDYPDIYGAIDQNGTYQNVRTGEDG

RrgA D4 domain    KLTFKNLSDGKYRLFENSEPAGYKPVQNKPIVAFQIVNGEVRDVTSIVPQDIPAGYEFTN
RrgACatcher       KLTFKNLSDGKYRLFENSEPAGYKPVQNKPIVAFQIVNGEVRDVTSIVPQDIPAGYEFTN
SnoopCatcher      KLTFKNLSDGKYRLFENSEPAGYKPVQNKPIVAFQIVNGEVRDVTSIVPQDIPATYEFTN

RrgA D4 domain    DKHYITNEPIPPKREYPRTGGIGMLPFYLIGCMMMGGVLLYTRKHP
RrgACatcher       DKHYITNEPIPPK-----------------------------------
SnoopCatcher      GKHYITNEPIPPK-----------------------------------
```

SnoopTag Residues mutated to make SnoopCatcher

A.4 Sequence alignment of used BiCatcher variants

```
BiCatcher                MSYYHHHHHHDYDIPTTENLYFQGAMVDTLSGLSSEQGQSGDMTIEEDSATHIKFSKRDE
BiCatcher long linker    MSYYHHHHHHDYDIPTTENLYFQGAMVDTLSGLSSEQGQSGDMTIEEDSATHIKFSKRDE
BiCatcher helical linker MSYYHHHHHHDYD----------------------------------SATHIKFSKRDE

BiCatcher                DGKELAGATMELRDSSGKTISTWISDGQVKDFYLYPGKYTFVETAAPDGYEVATAITFTV
BiCatcher long linker    DGKELAGATMELRDSSGKTISTWISDGQVKDFYLYPGKYTFVETAAPDGYEVATAITFTV
BiCatcher helical linker DGKELAGATMELRDSSGKTISTWISDGQVKDFYLYPGKYTFVETAAPDGYEVATAITFTV

BiCatcher                NEQGQVTVNGKATKGDAHIGSGSSG-------------------------LV-PRGSHMK
BiCatcher long linker    NEQGQVTVNGKATKGDAHIGSGESE-------------------------SGGEGGSHMK
BiCatcher helical linker NEQGQVTVNGKATKGDAHIGSPANLKALEAQKQKEQRQAAEELANAKKLKEQLEKGSHMK

BiCatcher                PLRGAVFSLQKQHPDYPDIYGAIDQNGTYQNVRTGEDGKLTFKNLSDGKYRLFENSEPAG
BiCatcher long linker    PLRGAVFSLQKQHPDYPDIYGAIDQNGTYQNVRTGEDGKLTFKNLSDGKYRLFENSEPAG
BiCatcher helical linker PLRGAVFSLQKQHPDYPDIYGAIDQNGTYQNVRTGEDGKLTFKNLSDGKYRLFENSEPAG

BiCatcher                YKPVQNKPIVAFQIVNGEVRDVTSIVPQDIPATYEFTNGKHYITNEPIPPK
BiCatcher long linker    YKPVQNKPIVAFQIVNGEVRDVTSIVPQDIPATYEFTNGKHYITNEPIPPK
BiCatcher helical linker YKPVQNKPIVAFQIVNGEVRDVTSIVPQDIPATYEFTNGKHYITNEPIPPK
```

SpyCatcher Linkers SnoopCatcher Mutations to make SnoopCatcher

A.5 Sequence alignment of affibody tailored with SnoopTag and SpyTag

```
SnoopTag-AffiEGFR-SpyTag      MGSSHHHHHHSSGLVPRGSHMGKLGDIEFIKVNKGS----------------------G
SnoopTag-AffiIGF1R-SpyTag     MGSSHHHHHHSSGLVPRGSHMGKLGDIEFIKVNKGS----------------------G
SnoopTag-AffiHER2-SpyTag      MGSSHHHHHHSSGLVPRGSHMGKLGDIEFIKVNKGS----------------------G
SnoopTag-SpyTag-AffiHER2x3    MGSSHHHHHHSSGLVPRGSHMGKLGDIEFIKVNKGSGGSGEGSGAHIVMVDAYKPTKGSG

SnoopTag-AffiEGFR-SpyTag      ESGSGASMTGGQQMGRDPGVDNKFNKEMWAAWEEIRNLPNLNGWQMTAFIASLVDDPSQS
SnoopTag-AffiIGF1R-SpyTag     ESGSGASMTGGQQMGRDPGVDNKFNKEGFYAAIEILALPNLNRKQSTAFISSLEDDPSQS
SnoopTag-AffiHER2-SpyTag      ESGSGASMTGGQQMGRDPGVDNKFNKEMRNAYWEIALLPNLNNQQKRAFIRSLYDDPSQS
SnoopTag-SpyTag-AffiHER2x3    ESGSGASMTGGQQMGRDPGVDNKFNKEMRNAYWEIALLPNLNNQQKRAFIRSLYDDPSQS

SnoopTag-AffiEGFR-SpyTag      ANLLAEAKKLNDAQAPKGLEGSGE---GSGAHIVMVDAYKPTK-----------------
SnoopTag-AffiIGF1R-SpyTag     ANLLAEAKKLNDAQAPKGLEGSGE---GSGAHIVMVDAYKPTK-----------------
SnoopTag-AffiHER2-SpyTag      ANLLAEAKKLNDAQAPKGLEGSGE---GSGAHIVMVDAYKPTK-----------------
SnoopTag-SpyTag-AffiHER2x3    ANLLAEAKKLNDAQAPKGLEGSGGSGEGSGASMTGGQQMGRDPGVDNKFNKEMRNAYWEI

SnoopTag-AffiEGFR-SpyTag      ------------------------------------------------------------
SnoopTag-AffiIGF1R-SpyTag     ------------------------------------------------------------
SnoopTag-AffiHER2-SpyTag      ------------------------------------------------------------
SnoopTag-SpyTag-AffiHER2x3    ALLPNLNNQQKRAFIRSLYDDPSQSANLLAEAKKLNDAQAPKGLEGSGGSGEGSGASMTG

SnoopTag-AffiEGFR-SpyTag      ------------------------------------------------------------
SnoopTag-AffiIGF1R-SpyTag     ------------------------------------------------------------
SnoopTag-AffiHER2-SpyTag      ------------------------------------------------------------
SnoopTag-SpyTag-AffiHER2x3    GQQMGRDPGVDNKFNKEMRNAYWEIALLPNLNNQQKRAFIRSLYDDPSQSANLLAEAKKL

SnoopTag-AffiEGFR-SpyTag      ----------
SnoopTag-AffiIGF1R-SpyTag     ----------
SnoopTag-AffiHER2-SpyTag      ----------
SnoopTag-SpyTag-AffiHER2x3    NDAQAPKGLE
```

SnoopTag Residues involved in antigen binding SpyTag

B. Reprints of publications arising from this thesis